Order number: 42244

UNIVERSITY LILLE 1, SCIENCES AND TECHNOLOGIES

Doctoral School **ED SMRE**

Laboratory: **Unity of Catalysis and Solid State Chemistry**

THESIS

defended by

Anita BOROWIEC

In order to become a Doctor of the University Lille 1, Sciences and Technology

Academic **Field Molecules and Condensed Matter**

Speciality **Heterogeneous catalysis**

New acrolein production route starting from alcohols mixtures over FeMo-based catalysts

Thesis supervised by: **Mickaël CAPRON** Director

Franck DUMEIGNIL Co-Director

Thesis planned to be defended the 7th of December 2016 before the Committee Members:

Referees	Karine DE OLIVEIRA VIGIER	Associate professor at the University of Poitiers
	Jean-Marc MILLET	Research Director (CNRS) at IRCELYON
Examiners	Pascal ROUSSEL	Research Director (CNRS) at UCCS
	Nathalie TANCHOUX	Associate professor at ICG Montpellier
	Aline AUROUX	Research Director (CNRS) at IRCELYON
	Jean-François DEVAUX	Senior Research Scientist, ARKEMA

Order number: 42244

UNIVERSITÉ LILLE 1, SCIENCES ET TECHNOLOGIES

École doctorale **ED SMRE**

Unité de recherche **Unité de Catalyse et Chimie du Solide**

THÈSE

présentée par

Anita BOROWIEC

En vue de l'obtention du grade de docteur de l'Université Lille 1, Sciences et Technologies

Discipline **Molécules et Matière Condensée**

Spécialité **Catalyse hétérogène**

Une nouvelle méthode de production d'acroléine à partir d'un mélange d'alcools en utilisant un catalyseur de type FeMo.

Thèse dirigée par: **Mickaël CAPRON** Directeur

Franck DUMEIGNIL Co-Directeur

La soutenance de la thèse est prévue le 7 Décembre 2016 devant le jury composé de :

Rapporteurs	Karine DE OLIVEIRA VIGIER	Maître de Conférences à l'Université de Poitiers
	Jean-Marc MILLET	Directeur de Recherches (CNRS) à l'IRCELYON
Examinateurs	Pascal ROUSSEL	Directeur de Recherches (CNRS) à l'UCCS
	Nathalie TANCHOUX	Maître de Conférences à ICG Montpellier
	Aline AUROUX	Directeur de Recherches (CNRS) à l'IRCELYON
	Jean-François DEVAUX	Chercheur Sénior, ARKEMA

Acknowledgment

I would like to thank everyone who supported me during this 3 years and without whom this thesis could not have been fulfilled.

Firstly, I wish to thank ADEME (The French Environment and Energy Management Agency) for financing this work within the framework of the Investissements d'Avenir program ("Investment for the Future"). I am grateful as well to BioMA+ project consortium partners for all helpful discussions during our meetings.

Afterwards, I would like to thank Mickaël Capron, my thesis director for giving me the opportunity to work with him and for everything he made for me. He was always ready to discuss (even small) problems and he was encouraging me in moments of doubt with smile and good mood. I wish to thank as well my co-director, Franck Dumeignil for each very valuable discussion, precious remarks and for his constant motivation during this PhD period.

I would like to thank all jury members and particularly two refeeres Karine de Oliveira Vigier and Jean-Marc Millet for having accepted to judge this thesis.

I gratefully acknowledge also Elżbieta Skrzyńska for being my guardian angel at the very beginning.

Equally, this work would have not been possible without the precious help of Jérémy Faye who introduced me all laboratory mysteries and was the big support in GC problems I have encountered during these three years.

Subsequently, I wish to thank the interns I have co-supervised : Loïc Jouenne and Georgiana Bucataru for their involvement at work.

I would like to gratefully acknowledge persons who have kindly made various catalysts analysis for me and have given their time to explain me all of techniques, namely Jean-Charles Morin, Olivier Gardoll, Pardis Simon, Martine Trentesaux, Maxence Vanderwalle, Anne-Sophie Mamede and Laurence Burylo. I thank as well Muriel Bigan, Marie Colmont and Pascal Fongerland for all helpful discussions.

Likewise, I wish to thank all my office-mates: Mengdie Cai, Claudia Travera, Juliana Aparicio and Maha Ammoury for joyful work atmosphere. The special thanks goes to Cathy Brabant, for being so friendly and supportive during these three years. I would like

to thanks as well all members of UCCS-C3 laboratory, for every smile, small chat and joke that made my days brighter. Merci!

Next, I thank my project colleague – Aleksandra Lilić for all interesting discussions (not only scientific) and constant motivation she gave me.

I am grateful to all my friends in Poland: Daria Czechowicz, Jakub Fudyma, Klaudia Świder, Łukasz Suślik, Wojciech Stryjewski, Katarzyna Mendela for supporting me all that time. Special thanks goes to Iwona Wójcik and Krystyna Martyna for being absolutely always there despite 1500 km between us. I am lucky to have you in my life!

I would have achieved nothing without My Family. Firstly, I thank my brothers: Mariusz and Piotr as well as my sister in law Sabina for helping me every time I have needed. I am grateful to My Parents, for their unconditional love, the support and the effort they have put in my education. I am who I am and I am where I am only thanks to them.

Finally, I would like to thank Sylvain. Your love and smile were the everyday support and motivation for me. Thank you for all further and closer journeys that have opened my eyes and for every simple moment that we have passed together. I am grateful to have you on my side.

Abstract

Acrolein is the simplest unsaturated aldehyde, which - due to its high reactivity - finds applications as an intermediate in the chemical industry (*e.g.*, for acrylic acid and methionine production). Recently, a worldwide demand increase of acrolein derivatives was observed, which is expected to continuously grow within the next years. However, nowadays acrolein is commercially obtained by propylene oxidation, where the raw material comes from fossil resources.

This work proposes a new method of acrolein production starting from renewable feedstock – methanol and ethanol mixture. This reaction was approached by reaction conditions optimization (*i.e.* Design of Experiment method do decrease the number of catalytic tests and save time), $FeMoO_x$ modifications (*e.g.* various Mo/Fe ratios, calcination temperature, and basic elements addition) and a second catalyst utilization (e.g. single commercial oxides and silica-based materials) in order to balance the acid base properties.

Key words: Acrolein, Partial oxidation, FeMo catalysts, Heterogeneous catalysis, Biomass valorization

Resumé

L'acroléine est le plus simple des aldéhydes insaturés, qui - en raison de sa réactivité élevée - trouve des applications comme produit intermédiaire dans l'industrie chimique (par exemple pour la synthèse d'acide acrylique et la production de méthionine (i.e. acide aminé essentiel)). Récemment, on a observé une augmentation de la demande mondiale de produits dérivés de l'acroléine, qui devrait croître de façon continue au cours des prochaines années. De nos jours, l'acroléine est obtenue par oxydation du propylène, et donc ce procédé est basé sur des ressources fossiles qui ne cessent de décroitre.

Ce travail propose une nouvelle méthode de production d'acroléine à partir de matières premières renouvelables – un mélange d'alcools formé de méthanol et d'éthanol. Cette réaction a été étudiée et optimisée en travaillant sur : les conditions de réaction *via* l'établissement d'un plan d'expériences afin de minimiser le nombre de tests catalytiques à réaliser, les modifications de la formulation catalytique FeMoOx (i.e. différents rapports Mo / Fe, température de calcination, et l'ajout d'éléments basiques (e.g. La, Ce) pendant la synthèse) et enfin l'utilisation d'un second catalyseur pour balancer les propriétés acides-bases nécessaires à l'obtention de notre molécule cible.

Mots clés: Acroléine, Oxydation partielle, Catalyseur FeMo, Catalyse Hétérogène, Valorisation de la biomasse

Symbols, acronyms and abbreviations

ADEME	Agence de l'Environnement et de la Maîtrise de l'Energie
AHM	Ammonium molybdate tetrahydrate
AIBN	α,α'-azoisobutyronitrile
BET	Brunauer, Emmett, Teller nitrogen adsorption-desorption
CB	Carbon balance
CNRS	Centre national de la recherche scientifique
DME	Dimethyl ether
DoE	Design of Experiments
DTA	Double totoidal energy analyser
e.g.	For example
ED SMRE	Ecole Doctorale – Sciences de la Matière, du Rayonnement et de l'Environnement
EtOH	Ethanol
Eq.	Equation
FID	Flame Ionization Detector
GBE	Global Bioenergies
GC-MS	Gas chromatograph with mass spectrometer
GHSV	Gas hourly space velocity
H	Enthalpy
HPA	Heteropoly acids
i.e.	That is
IBN	Isobutene
ICG	Institut Charles Gerhardt
IR	Infrared
IRCELyon	Insitut de recherches sur la catalyse et l'environnement Lyon
k	Factor number
LEIS	Low energy ion scattering
MA	Methacrylic acid
MetOH	Methanol
n	Number of experiments
n_0	Number of experiments in the centre of the studied domain
n_{AC}	Acrolein number of moles
n_{CO2}	Carbon dioxide number of moles
n_{DME}	Dimethyl ether number of moles
$n_{EtOH,in}$	Ethanol inlet number of moles
$n_{EtOH,out}$	Ethanol outlet number of moles
n_{MetCHO}	Acetaldehyde number of moles
$n_{Methoxyethane}$	Methoxyethane number of moles
$n_{MetOH,in}$	Methanol inlet number of moles
$n_{MetOH,out}$	Methanol outlet number of moles
NAP	Near Ambient Pressure
S_{AC}	Acrolein selectivity
S_{CO2}	Carbon dioxide selectivity

S_{DME}	Dimethyl ether selectivity
S_{Formol}	Formaldehyde selectivity
S_{MetCHO}	Acetaldehyde selectivity
$S_{Methoxyethane}$	Methoxyethane selectivity
SSA	Specific surface area
T	Temperature
TGA-DSC	Differential thermal analysis and thermogravimetric analysis
TPD	Temperature programmed desorption
U.S.	United States
UCCS	Unité de Catalyse et Chimie du Solide
wt.	Weight
X_{EtOH}	Ethanol conversion
X_{MetOH}	Methanol conversion
XPS	X-ray photoelectron spectroscopy
XRD	X-ray diffraction
XRF	X-ray fluorescence
Y_{AC}	Acrolein yield
Y_{ACpot}	Potential acrolein yield
Y_{CO2}	Carbon dioxide yield
Y_{DME}	Dimethyl ether yield
Y_{Formol}	Formaldehyde yield
Y_{MetCHO}	Acetaldehyde yield
$Y_{Methoxyethane}$	Methoxyethane yield

Table of contents

Introduction

Background Energy consumption increases with human development. From early nineteenth century to present days, it has increased almost 13 times. The majority of our energy comes from fossil resources and it is predicted that the oil reserves can still satisfy the world needs for only the next 53 years. Further, the price of fuel is subjected to many more or less unpredictable fluctuations and strongly depends on the geopolitical situation (Figure I).

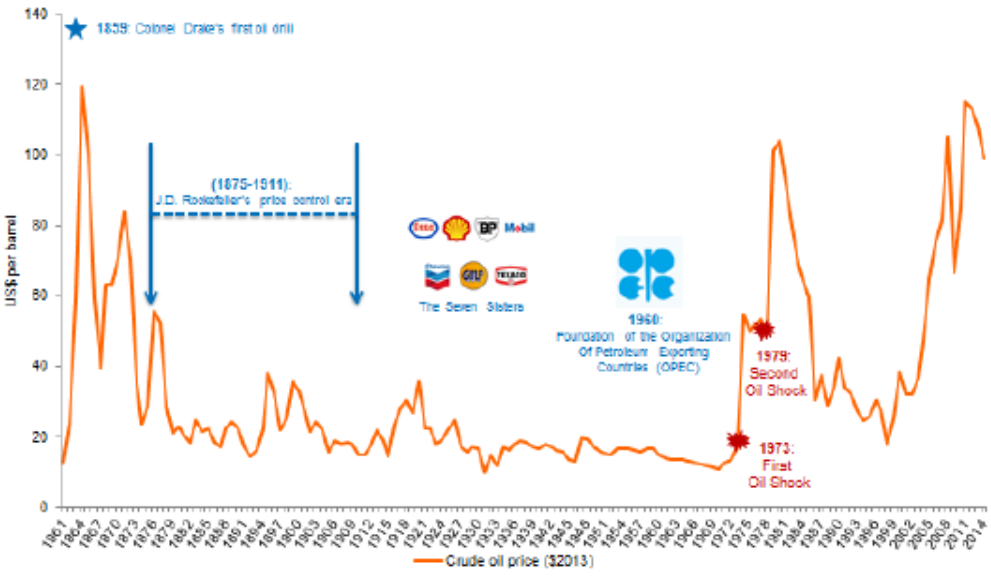

Figure I. Price variation over the years [1].

Thus, a lot of research groups are working on alternative ways. Accordingly, biomass feedstock seems to be a good substitute for petrochemical resources because of carbon neutrality – if the processes along the value chain are correctly designed. This renewable resource potentially enables producing molecules traditionally obtained in the refineries such as alkanes, alkynes, aldehydes, acetals etc. in and environmental friendly way even if the most of the designed processes economics is still an issue regarding the very

competitive market of petro-sourced compounds. In any case, biomass utilisation in the chemical industry will undoubtedly increase over the years (Figure II).

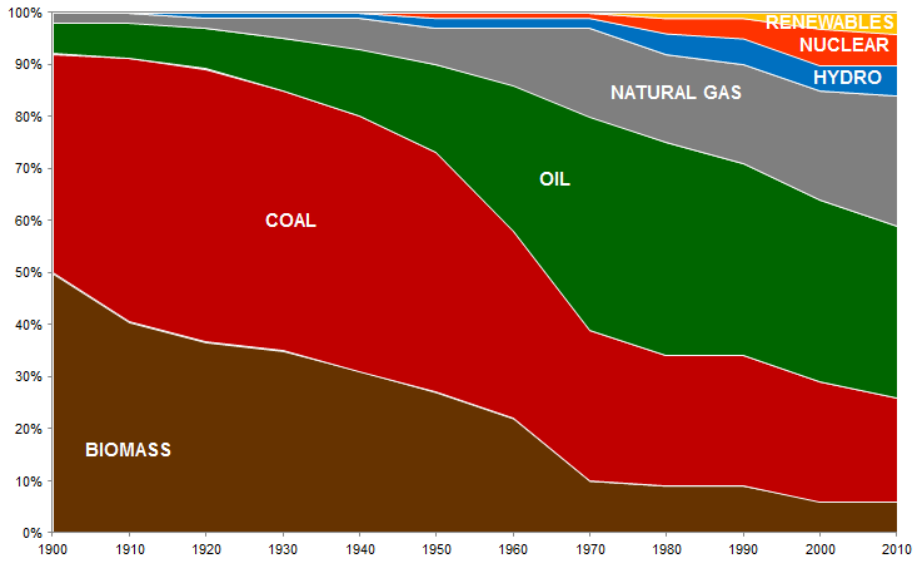

Figure II. Share of the different energy sources consumption over the last century [2].

The present PhD thesis work is a part of the BioMA+ project, which received the financial support of ADEME within the framework of the French governmental program of Investments for the Future. In addition to UCCS, three more partners were involved in this project: Global Bioenergies (Coordinator, Evry, France), Arkema (Colombes, France) and IRCELYON (Lyon, France). The main goal of BioMA+ was to transform vegetal resources in methacrylic acid (MA) through a sequence of two connected processes, namely sugars direct fermentation to *iso*butene (*i.e.*, IBN) followed by its catalytic oxidation to MA. The world market of this compound is indeed estimated at 300 to 400,000 tons, with a Western Europe total production of 80-85,000 tons (2012)[3].

The *iso*butene used in methacrylic acid production is obtained nowadays from petrochemical processes (*i.e.*, fluid catalytic cracking) in the quantity of 15 million tons per year. The novel way of production proposed by Global Bioenergies is based on an enzymatic fermentation process of sugars. First generation sugars were first used, but, because of the competition with food/feed applications, GBE subsequently also studied second generation sugars. The isobutene stream produced by fermentation has a different composition compared to that issued from a petro refinery. Indeed, some fermentation impurities as well as CO_2, acetone and water are present in the streams. Therefore, a

specific purification step is desired. As a potential solution, hydration of isobutene to *tert*-butanol can be envisioned not only because of the impurities (as the efficient purification method), but also because transportation of IBN can be much facilitated (liquefied gas compound *vs.* gaseous compound). The final product – methacrylic acid, would then be obtained by oxidation of the corresponding alcohol in the gas phase. To this respect, we performed experiments on isobutene hydration, with a specific focus on the on impurities influence.

The second part of our project consisted on the research in the domain of acrylics chemistry, *e.g.*, acrolein production based on renewable resources. The new method developed herein is based on methanol and ethanol as the feedstock [4]. The first step of this direct conversion of methanol and ethanol to acrolein consists on the oxidation of the alcohols to their corresponding aldehydes, which are coupled to acrolein by aldol condensation in the second step. It is well known that oxidation of alcohols occurs over redox sites (*i.e.*, in the case of alcohols mostly over combinations of molybdenum, vanadium, tungsten and copper) catalysts and that aldol condensation of aldehydes typically occurs over basic or acid materials (*e.g.*, over zeolites impregnated with basic oxides). In the mentioned work [4], these two stages occurs over single $FeMoO_x$ catalyst giving important acrolein quantities. Thus, this material became the base for our studies.

Thesis objectives The work reported herein describes our realizations within the frame of the second part of the BioMA+ project – namely methanol and ethanol direct conversion to acrolein. The main established goal was a 70% of acrolein yield. This objective was approached by reaction conditions optimization (*e.g.*, Design of Experiment method), $FeMoO_x$ modifications (*e.g.*, by varying the Mo/Fe ratio, the catalysts calcination temperature, and by addition of basic functions) and by the use of a second catalyst to promote conversion of unreacted intermediate aldehydes (*e.g.*, basic oxides and silica-based basic materials).

Thesis structure The present thesis is divided into five chapters. The first one (Chapter 1) contains the bibliographic study concentrated on the acrolein applications, its main production methods and the description of early works concerning the acrolein production process we have developed. Afterwards, in the second part (Chapter 2), the catalysts synthesis and characterization procedures are described, with a specific part explaining the Designed of Experiment method we used to optimize the reaction conditions. In the

same chapter, the procedures for the catalytic tests of methanol and ethanol oxidation to acrolein are presented in details. Afterwards, in Chapter 3, the study based on the use of the iron molybdate type catalyst is presented. After determining the optimal conditions on a native formulation, the influence of the calcination temperature and of the Mo/Fe ratio on the acrolein yield is studied. Further, the results of the modification of iron molybdates with La and Ce are presented. Chapter 4 is focusing on the tandem of catalysts strategy. Catalytic performance of systems containing couples $FeMoO_x$ and commercial basic oxides or synthesized silica basic catalysts is presented. In the last part of the thesis, the general discussion and conclusions are given with project perspectives for the future.

References

[1] BP Statistical Review of World Energy, 2014

[2] Exxon Energy Outlook, 2013

[3] Arkema data

[4] PCT Patent WO2014068213, assigned to Arkema France, Priority date Oct 17,2013

Chapter 1. Bibliography

Acrolein is the simplest unsaturated aldehyde, which - due to its high reactivity - finds applications as an intermediate in the chemical industry (*e.g.*, for acrylic acid and methionine production). Recently, a worldwide demand increase of acrolein derivatives was observed, which is expected to continuously grow within the next years. However, nowadays acrolein is commercially obtained by propylene oxidation, which is based on fossil resources. The biggest issues of this method are a limited feedstock availability and more and more stringent environmental requirements. Thus, some alternative processes are actively researched. For instance, so far, the most productive reaction based on renewable resources is glycerol dehydration. Unfortunately, the volatility of the substrate price associated to some technical issues (*e.g.*, coking of the catalysts) are not in favor of its industrial application in a short-term perspective. As a new option, it has been previously shown that it is possible to obtain acrolein from a mixture of methanol and ethanol [1], which is at the base of further results presented herein.

1.1. Acrolein manufacturing.

As aforementioned, acrolein is an important compound on the chemical market. It is a highly toxic chemical, which is in the liquid state at room temperature. Acrolein's main characteristic properties are presented in Table 1.1.

Table 1.1. Main properties of acrolein [2]

Property	Value
Molecular formula	C_3H_4O
Molecular weight [g/mol]	56.06
Boiling point [°C]	52.69
Vapor pressure* [kPa]	29.3
Solubility in water* [% by wt]	20.6
Liquid density* [kg/L]	0.8412
Flash point [°C]	-18
Flammability limits in air (upper/lower) [°C]	31/2.8
Autoignition temperature in air [°C]	234

* at 20°C, atmospheric pressure

In the followings, we briefly present the acrolein's applications before giving insights on the various ways it can be synthesized from fossil and renewable resources. Then, we detail the ethanol-methanol reaction pathway developed herein.

1.1.1. Acrolein applications.

On the chemicals market, acrolein derivatives have a significant role, which is growing every year. The most common products are schematically summarized on Figure 1.1, which actually underlines the acrolein applications diversity.

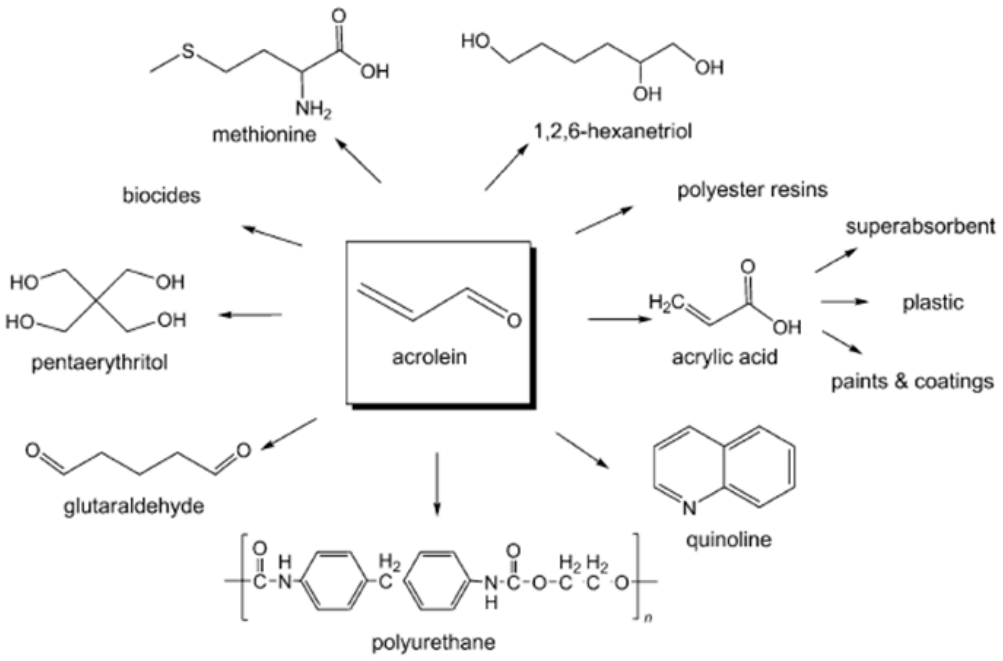

Figure 1.1. Chemicals derived from acrolein [2].

The most important compound is acrylic acid obtained by acrolein oxidation (Eq. 1.1 hereafter). *Inter alia*, this compound and its esters find applications as monomers/additives for a wide variety of polymers. Acrylate esters are used to improve polymeric material's unfavorable qualities such as: color stability, low temperature flexibility, good weatherability and others. Moreover, they are used in functional acrylates oligomers production, which are components of inks, adhesives and radiation curable coatings. Acrylic acid can be transformed into polyacrylic acid or copolymers, which are applied as superabsorbents, detergents, dispersants and flocculants. In everyday's life, we can find them in diapers and hygiene products [3,4,5].

$$CH_2 = CHCHO + \frac{1}{2}O_2 \rightarrow CH_2 = CHCOOH \qquad (1.1)$$

The acrylates industry is particularly developed in the United States and in Western Europe. Figure 1.2 shows the breakdown of acrylic acid uses in the case of U.S. [5].

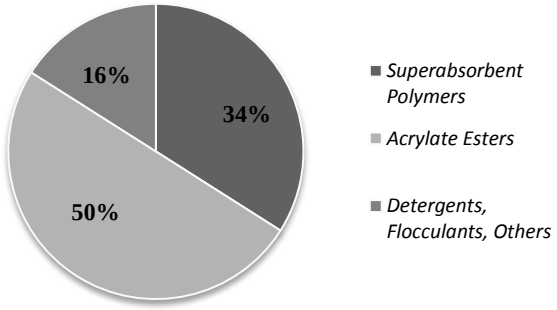

Figure 1.2. U.S. acrylic acid consumption [5].

The second important acrolein derivative is methionine, which is synthesized in the presence of methyl mercaptan (*i.e.*, CH_3SH). The involved reaction is schematically represented in Figure 1.3 [6,7]. Methionine is an essential compound for human and animals. Its deficiency may lead to serious consequences. Therefore, in some cases a supplementation by chemically synthetized methionine is necessary [8]. As a consequence, for year 2000 its worldwide capacity was estimated at 570,000 t [2] and is still growing due to the population increase.

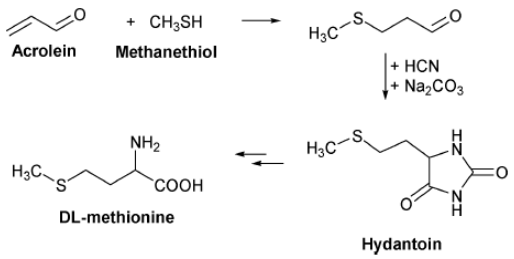

Figure 1.3. Methionine production by the acrolein pathway [7].

Under some conditions (*e.g.*, heating, exposure to light or non-basic catalysts) acrolein can polymerize. The as-obtained polymers find various applications in the industry depending on their properties [8]. Moreover, they can be subsequently transformed into other molecules such as 1,2,6-hexanetriol obtained from acrolein dimer [9]. This liquid polyol has several interesting properties such as a high boiling point, a good stability, while being non-toxic. It finds application in pharmaceutical preparations and in the plastic industry [10].

The other well-known derivate is glutaraldehyde industrially obtained by Diels-Alder reaction of acrolein and methyl vinyl ether, before final hydrolysis. This compound finds

its main uses in leather tanning, as a biocide for industrial water treatment and in oilfield applications. Glutaraldehyde can be also used as a disinfectant and sterilizer for hospital equipment [8]. Acrolein is also used in the Skraup reaction in order to produce quinoline in the presence of acid catalysts [11]. In the past, this molecule was used as a medicine against malaria. Nowadays, quinoline finds applications in pharmaceuticals, cosmetics and foods. Furthermore, it is used in the production of dyes and as a solvent for resins and terpenes [12,13].

Acrolein and its polymers find also direct applications as additives to products used against bacteria and microorganisms that contaminate products in petrochemical industry. They protect also pipelines from corrosion and they are used to disinfect, decontaminate and sterilize materials [8,14,15].

1.1.2. Production methods based on fossil resources.

Figure 1.4 shows the various acrolein production pathways proposed so far. The blue square focuses on propylene oxidation, which is the current mainstream industrial production process and the green square corresponds to bio-based glycerol dehydration, which has been largely studied in the recent years as a biosourced alternative.

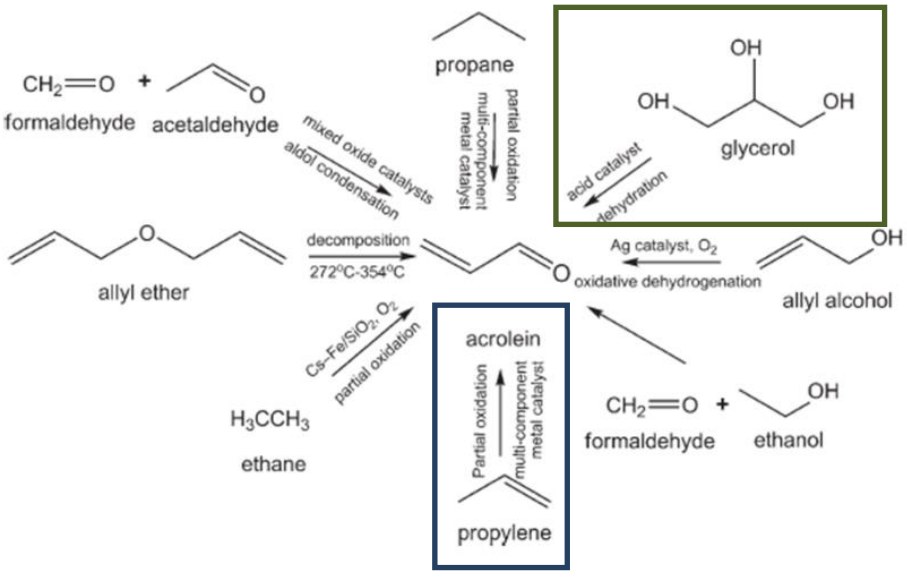

Figure 1.4. Different acrolein production methods [16].

In the followings, we first describe the fossil routes.

Acrolein production by propylene oxidation

Propylene gas-phase oxidation (Eq. 1.2) [17] was developed in the 1940's and has become the main method for acrolein production. In 1948, this process was commercialized by Shell using copper oxide supported on silicon carbide as a catalyst. At the beginning, propylene conversion was quite low (about 15%). Researches were performed on the catalyst improvement and on the optimization of reaction conditions. In 1957, Standard Oil of Ohio (Sohio) discovered bismuth molybdate catalysts, which gave a high selectivity to acrolein at high propylene conversions (>90%).

$$CH_2 = CHCH_3 + O_2 \rightarrow CH_2 = CHCHO + H_2O \qquad \Delta H = -368\, kJ/mol \quad (1.2)$$

Nowadays, based on the previous discoveries, we can conclude that the most efficient materials are multicomponent metal systems consisting of Mo, Bi, Fe, Ni and/or Co, K and some additives P, B, W or Sb. In Table 1.2, the various efficient industrial catalysts for selective propene oxidation are presented.

Table 1.2. Industrial catalysts for propylene selective oxidation [8]

Catalyst	T [°C]	Propene Conv. [%]	AC Yield [%]	ACA Yield [%]	Company	Ref.
$Mo_{12}Fe_3Bi_{0.75}Co_8Ox$ +Sb, K	350	87	84.5	1.4	-	[18]
$Mo_{12}Fe_2Bi_{1.5}Co_{4.4}K_{0.06}Ox$	320	99	89.6	1.6	LG Chem	[19]
$Mo_{12}Fe_{2.4}Bi_{1.08}Co_{9.6}Al_{1.48}V_{0.056}Ag_{0.1764}Pd_{0.0019}K_{0.064}O_x$	342	97	95.6	-	Sabic	[20]
$Mo_{12}Fe_{2.94}Bi_{0.8}Ci_7Si_{1.52}K_{0.08}O_x$	318	95	87.1	4.1	BASF	[21]
$Mo_{12}Fe_{1.3}Bi_{1.3}Co_6Ni_{2.0}Si_{2.0}K_{0.08}O_x$	310	98.2	92.4*		Nippon Shoukubai	[22]
$Mo_{12}Fe_{1.8}Bi_{1.7}Ni_{2.8}Co_{5.2}K_{0.1}O_x$	346	97	84.8	7.4	Nippon Kayaku	[23]
$Mo_{12}Fe_{0.6}Bi_{1.0}Co_{3.3}Ni_{3.3}B_{0.2}K_{0.1}Na_{0.1}Si_{24}O_x$	315	98.5	90.1	4.2	Mitsubishi	[24]

* sum $Y_{AC}+Y_{ACA}$

Typically, propylene conversion reaches up to 99% and acrolein yield is *ca.* 80-90%. For this reaction, the main by-product is acrylic acid (up to a yield of 10%). Moreover, acetaldehyde, acetic acid, CO and CO_2 are also produced in small quantities. In industrial plants, propylene oxidation occurs at 300-400°C in a multitubular fixed-bed reactor. The reaction is highly exothermic, and therefore a molten bath is used in order to control heat dissipation [2,8]. A scheme of a typical process flowsheet is presented in Figure 1.5.

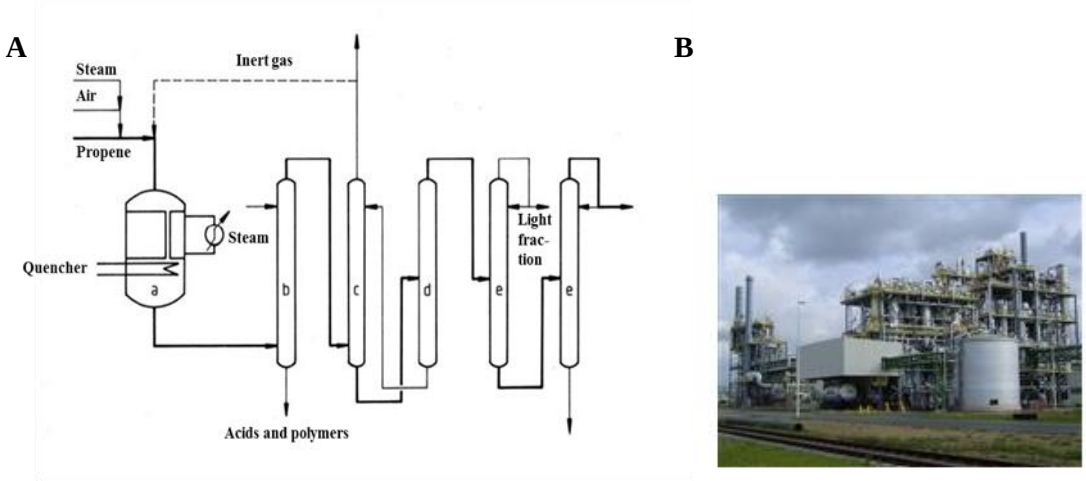

Figure 1.5. A: Typical process flowsheet for acrolein manufacture from propene (a-oxidation reactor, b-scrubber, c-adsorber, d-desorber, e-fractionators); B: Evonik acrolein plant in Antwerpen (Belgium) [8, 25].

Despite the fact that propylene oxidation has already been extensively studied, there is still a certain research interest in the development and the improvement of this reaction. Clearly, the different methods of catalysts preparation, the catalysts composition, the reaction conditions and the engineering solutions have an influence on the process performances. Therefore, many studies have been published recently on such aspects. The reaction is performed over various catalysts, namely, *e.g.*, co-precipitated Fe-Sb-Ti [26], supported V_2O_5 oxides [27,28] or assembled Bi_2WO_6 nanoflakes with surface dispersed molybdenum species [29]. Generally, the catalytic performance is evaluated in a fixed-bed reactor system, in which a high selectivity to acrolein is obtained (up to 90%). Polkovnikova *et al.* [30] examined the influence of several factors on propylene oxidation using copper supported catalyst (*e.g.*, the concentration of steam, the temperature, the contact time). It was reported that using a higher reaction temperature, the production of carbon dioxide increases, that the acrolein production is optimal at 380°C. It was discovered as well that the propylene-oxygen ratio should be kept between 5.6:1 to 4:1 to

favor the acrolein production. Finally, it was found that the acrolein yield depends also on the steam concentration and is limited by the flammability diagram.

Acrolein production by condensation of acetaldehyde and formaldehyde

Industrially, acrolein has also been produced by the vapor phase cross-condensation of acetaldehyde and formaldehyde. This reaction is one of stage in the process studied in this thesis. This technology was established by Degussa in 1942 [2,31] and was further replaced by propylene oxidation. It is well-known that aldol condensation can occur over both acid and basic catalysts. Figure 1.6 the presents possible reaction scenarios depending on the used materials (acidic or basic).

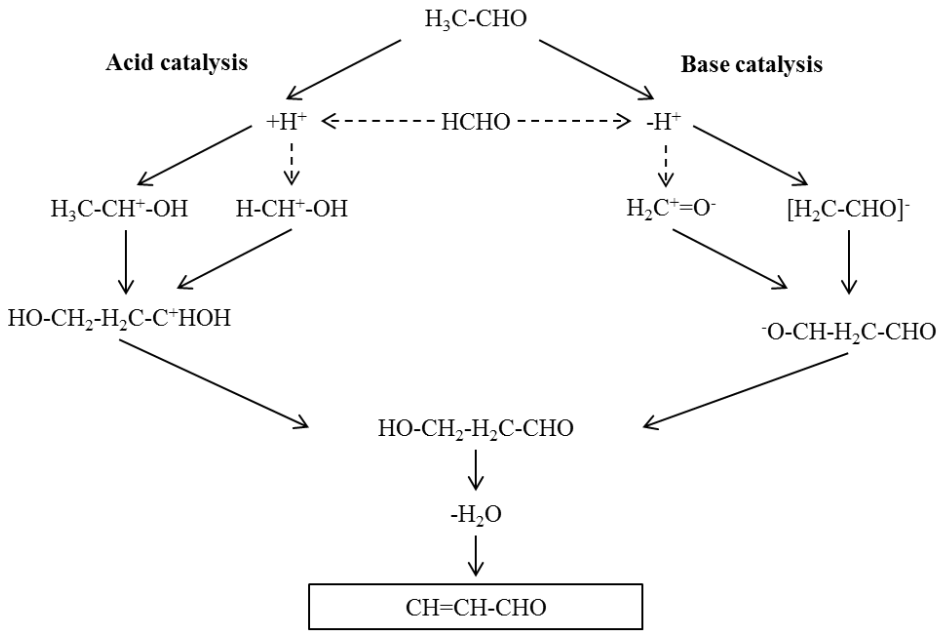

Figure 1.6. Possible pathways of acetaldehyde and formaldehyde condensation [32].

During the reaction, acetaldehyde can react in two different ways (Figure 1.7): by cross-condensation with formaldehyde giving acrolein or by self-condensation with another acetaldehyde molecule forming crotonaldehyde. The pathway direction depends on the nature and the strength of the actives sites.

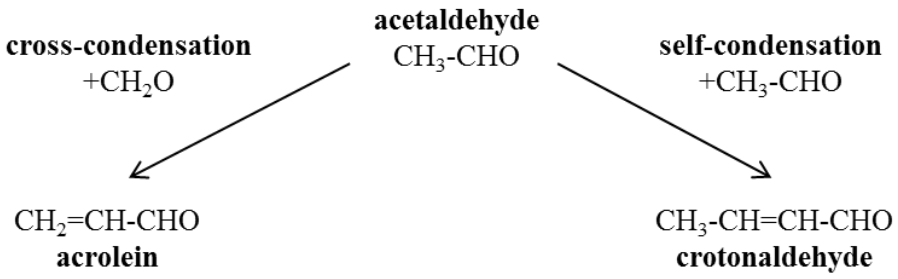

Figure 1.7. Acetaldehyde reactions during aldol condensation with formaldehyde [32].

Azzouz et *al.* [32] explains that acid catalysts provokes acetaldehyde to act as carbonyl and methylene intermediates. This is possible because of the difference in electron density on the oxygen compared to formaldehyde, which behaves as a carbonyl species. Therefore, in the case of acid catalysts, acetaldehyde and its enol are competitive substrates preferring both cross- and self-condensation. In contrast, for basic materials, it is formaldehyde that acts in the role of the competitive. The same behavior is presented by a small number of non-active acetaldehyde molecules. Accordingly, the selectivity to acrolein appears to be favorable in that case. However, some researchers have reported [33] that the most efficient catalyst should be bifunctional owning both acid (to activate acetaldehyde) and basic properties (to activate formaldehyde). Therefore, the efficient cross-condensation is difficult to achieve and numerous studies were published.

Table 1.3 presents a catalysts review for the aforementioned reaction. Generally, catalytic tests were performed in fixed-bed micro-reactors at different temperatures and under moderate pressure (*i.e.*, 1-2 bar). Moreover, the acetaldehyde/formaldehyde ratio was chosen between 1 and 2. The first group of catalysts was supported oxides developed by Dumitriu *et al.* [34,35]. Different supports were examined such as ZSM-5, Y-faujasite, volcanic tuff, Al_2O_3 and SiO_2 with various oxides (*e.g.*, ZnO, MgO, MoO_3, B_2O_3, P_2O_5, Na_2O, K_2O and Al_2O_3). The best results were reported for MgO supported on ZSM-5, which confirms that the effective cross-condensation to acrolein needs a given balance between both acid and basic sites. For the ZSM-5 support, the conversion to acrolein increases in the following order: $MgO>MoO_3>ZnO>B_2O_3>P_2O_5$. Authors reported as well that it is favorable to use an excess of formaldehyde compared to acetaldehyde. The next catalysts type was natural montmorillonite-rich materials exchanged with cations such as Na^+, Cs^+, Mg^{2+}, Ni^{2+}, La^{3+} and UO_2^{2+} studied by Azzouz *et al.* [32]. The best acrolein selectivity was obtained for catalysts containing Na^+, Cs^+ and Mg^{2+}, namely

basic elements that provide the needed balance with acid support sites. These observations are compatible with those reported by Dimitriu. Ai [33], who tested numerous catalysts – single, binary oxides and phosphates. From all the presented results (Table 1.3), the highest acrolein yield was reported for the Mn-P catalyst (86%). Ai also examined the influence of the reaction temperature and of the contact time on the acrolein yield (Table 1.4) using Ni-P. Finally, it was found that the highest acrolein yield (*i.e.*, 86%) can be obtained at 320°C with a contact time of 10 s. This study opens perspectives for this new kind of materials.

Table 1.3. Catalysts review for acetaldehyde and formaldehyde aldol condensation [32,33,36]

Catalyst	Temperature [°C]	Pressure [Bar]	Acetaldehyde / Formaldehyde Ratio	Acetaldehyde Conversion [%]	Acrolein Yield [%]	Acrolein Selectivity [%]	Ref.
NaY	275	2.5	1	19	2	9	[36]
NaMor				14	1	8	
NaZSM-5				41	11	26	
NaH(48)Y				71	11	16	
NaH(65)Y				42	3	8	
HMor (Si/Al=10)				55	2	3	
HZSM-5				30	1	3	
HY				32	1	4	
Native tuff				27	6	22	
MgO/ZSM-5 (4/100)	400	-	1	50	23	47	[32]
MoO_3	320	1	2	15	14	93	[33]
Mo-V (8:2)				30	30	100	
Mo-Ti (9:1)				57	15	26	
Mo-Sn (9:1)				54	8	15	
Mo-Fe (7:3)				32	29	91	
Mo-Fe (3:7)				58	49	84	
Mo-Bi (5:5)				45	21	47	
WO_3				38	35	92	
W-P (9:1)				Low	Low	Low	
W-Fe (5:5)				73	67	92	
W-Fe (7:3)				62	60	97	
W-Sn (5:5)				55	50	91	
W-Ti (6:4)				50	28	56	
W-V (8:2)				22	20	91	
V_2O_5				60	28	47	

Table 1.3. Catalysts review for acetaldehyde and formaldehyde aldol condensation [32,33,36]

Catalyst	Temperature [°C]	Pressure [Bar]	Acetaldehyde / Formaldehyde Ratio	Acetaldehyde Conversion [%]	Acrolein Yield [%]	Acrolein Selectivity [%]	Ref.
V-P (1:1.06	320	1	2	87	79	91	[33]
V-Ti-P (1:2:5.5)				89	63	71	
TiO_2				89	37	42	
Ti-W (9:1)				67	60	40	
SnO_2				56	56	100	
Sn-Mo (7:3)				61	13	21	
Sn-W (7:3)				57	50	88	
Sn-P (7:3)				60	60	100	
Fe_2O_3				68	42	62	
Fe-W				79	66	83	
Fe-P (8:2)				68	65	96	
Co-P (1:0.67)				77	75	97	
Ni-P (5:5)				79	66	84	
Mn-P (6:4)				86	86	100	

Table 1.4. Temperature effect on acrolein selectivity (Ni-P catalyst, Acetaldehyde / Formaldehyde /MetOH / Water / Nitrogen feed rate = 13/26/5.6/71/350 mmol/h) [33].

T (°C)	Contact time (s)	Acetaldehyde Conversion (%)	Acrolein Yield (%)	Selectivity to acrolein (%)
250	27	89	79	88
280	13	91	85	93
300	13	94	85	90
320	10	91	86	94
360	6	84	81	96
	10	92	71	77

Acrolein production by condensation of formaldehyde and ethanol

In the literature, it is reported by Ai *et al.* [36] that acrolein can be formed by formaldehyde reaction with ethanol. This method is based on the same principles as those previously described for formaldehyde and acetaldehyde aldol-condensation. The following equation (Eq. 1.3) describes this process:

$$CH_3CH_2OH + 2HCHO \rightarrow CH_2CHCHO + CH_3OH + H_2O \quad (1.3)$$

The reaction comprises two steps. First, ethanol reacts with formaldehyde to form acetaldehyde and methanol. Afterwards, the unreacted HCHO forms acrolein by aldol condensation with acetaldehyde. Ai has developed metal oxides supported on silica gel and metal phosphates to perform this reaction. The best results were obtained using nickel phosphate and tungsten, zinc, nickel and magnesium oxides supported on silica. The catalytic performances were evaluated in a continuous flow system with a constant formaldehyde/ethanol ratio of 2. The highest measured acrolein yield was 52% for nickel phosphate at 320°C. In his research, Ai reported that the acrolein yield increases with increasing the electronegativity value of the alkaline/alkaline earth metal contained in the active phase (*i.e.*, Mg>Ca>Li>K). Table 1.5. presents a selection of the most efficient catalysts. It has to be noticed that, in all cases, the formaldehyde conversion reached 100%.

Table 1.5. Best catalysts for formaldehyde and ethanol condensation (T = 280°C, EtOH / Formaldehyde / MetOH / Water / Nitrogen feed rates = 13.5/27/5.9/74/350 mmol/h) [36].

Catalyst	Ethanol conversion [%]	Yield [mol-%]			
		Acrolein	Acetaldehyde	Methanol	CO_2
Si-W	87	41	30	88	3
Si-Ti	59	31	18	90	6
Si-Sn	58	30	25	98	12
Si-Ni	70	36	32	120	14
Si-Zn	57	43	10	100	17
Si-Mg	58	40	6	92	11
Co-P	54	37	11	87	8
Ni-P (1:0.67)	73	51	18	122	6
Ni-P (1:0.9)	62	42	16	83	1

Acrolein production by ethane partial oxidation

Another method of acrolein production is ethane partial oxidation studied by Zhao *et al.* [37,38,39,40]. These authors developed several catalysts and the so-called "best results", summarized in Table 1.6, were obtained for Cs-V/SiO_2, V/SiO_2 and Cs-Bi/SiO_2 in a fixed-bed reactor at 475°C. The inlet composition was fixed at 75% of ethane and 25% of oxygen. In all cases, the ethane conversion was obviously very low, which disqualifies this process for industrial application.

Table 1.6. Best catalysts review for ethane oxidation (75% Ethane, 25% Oxygen, 475°C) [37,38,39,40].

Catalyst	Ethane conversion [%]	Yield [%]					Ref
		Acetaldehyde	Acrolein	Formaldehyde	Ethylene	CO_x	
Cs-V/SiO_2	2.8	8.4	4.1	0.5	1.8	13.2	[37]
V/SiO_2	2.4	4	7.2	1.6	0.04	8.8	[38]
Cs-Bi/SiO_2	8.5	13	5.7	1	7.3	57.8	[39]
Cs-Fe/SiO_2	6.8	0.4	1.1	0.5	0.4	4.4	[40]

Zhao *et al.* [38] suggested possible ethane oxidation pathways. They have considered three different scenarios of acrolein formation: a cross-aldol condensation between acetaldehyde and formaldehyde (formed from acetaldehyde), the cracking of C4 aldehydes (formed by acetaldehyde self-condensation) and the oxidation of propane and propylene. The second possibility was ruled out because of the C4 aldehyde absence in the outlet streams. The other rejected scenario is propane and propene oxidation. It is reported that this reaction should form a significant acetone quantity and this compound was not detected by Zhao *et al.* Therefore, the cross-aldol condensation seems to be the best explanation. The mechanism proposed by the authors is presented in Figure 1.8.

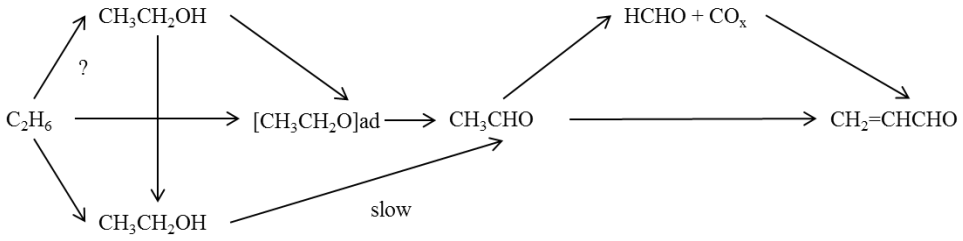

Figure 1.8. Possible ethane oxidation pathway to acrolein [38].

Allyl alcohol oxidative dehydrogenation to acrolein

It was discovered in 1995, that acrolein can be obtained by allyl alcohol oxidative dehydrogenation. Hutchings and Lee [41] developed different Y zeolites to obtain the highest acrolein yield as possible. The catalytic tests were performed using a microreactor working in the gas phase. It was remarked that the acrolein formation is favorable using the ion-exchanged zeolites containing Brønsted acid sites needed to initiate the dehydrogenation reaction, which is illustrated in Figure 1.9. The best results were obtained with CsHY, over which acrolein was the main product. Hutchings and Lee also examined the influence of the temperature. A temperature increase improved the acrolein selectivity (up to 76.9% with 20% of allyl alcohol conversion). It was reported that for ion-exchanged zeolites (*e.g.*, NaHY, LiHY and KHY), the catalyst deactivation associated with coke formation increased the acrolein selectivity.

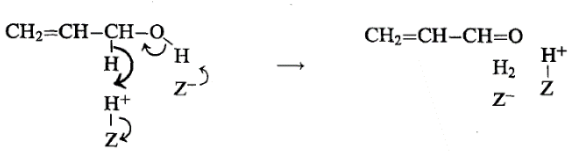

Figure 1.9. Proposed mechanism of acrolein production by oxidative dehydrogenation of allyl alcohol [41].

Propane partial oxidation to acrolein

Another method of acrolein production consists on propane partial oxidation. This reaction was studied using different catalysts containing molybdenum. Typically, catalytic tests were performed in a quartz tubular fixed-bed reactor at high temperatures (up to 520°C) and under atmospheric pressure. Zhang *et al.* [42,43] concentrated their work on Ce-doped Ag-Mo-P-O catalysts. These authors reported the highest acrolein selectivity of 28.7% with a propane conversion of 15.3% (at 500°C). The other detected products were propylene (up to 25.7% of selectivity), propionaldehyde, acetone, acetaldehyde and CO_x. Following that, Kim *et al.* [44] synthetized metal oxides catalysts – magnesium vanadates, vanadia bismuth molybdates and vanadia antimony. They observed that the most performant material is Ag-Bi-V-Mo-O giving an acrolein selectivity of 63.5% with a propane conversion of 13.1% (at 500°C). Propylene, CO, CO_2 and C_2-hydrocarbons were observed as by-products. In order to fully understand the reaction, the mechanism was studied by Zhang *et al.* based on a $Ce_{0.1}Ag_{0.3}Mo_{0.5}P_{0.3}O_x$ catalyst. Three possible propane oxidation pathways were considered (Figure 1.10). Besides acrolein, small quantities of propionaldehyde and acetone were detected among the products. This suggests that during the reaction, pathways I and III actually occur. However, yields of compounds mentioned before (i.e., propionaldehyde and acetone) are low compared to acrolein, which confirms that the second route, *via* propylene, is the main one.

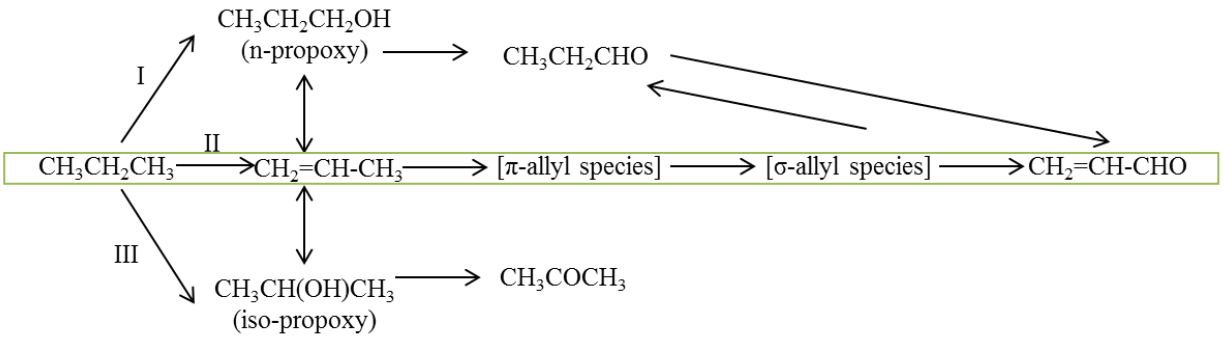

Figure 1.10. Possible pathways of propane oxidation [42].

1.1.3. Production methods based on renewable resources.

The most developed method of acrolein production based on renewable resources is glycerol acid-catalyzed dehydration, performed either in the gas or the liquid phase using different types of catalysts (Figure 1.11).

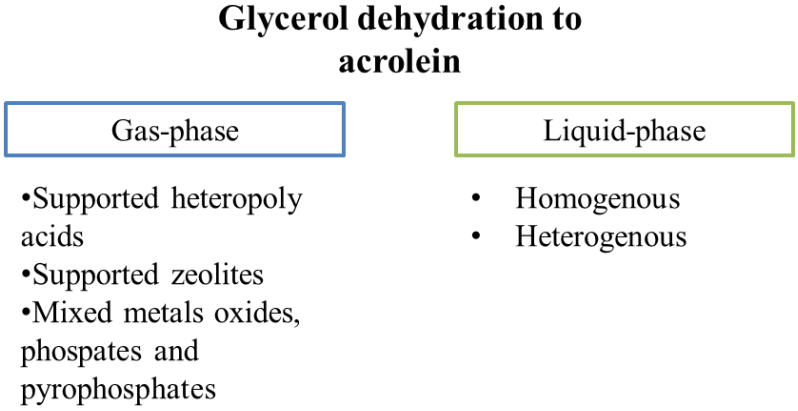

Figure 1.11. Glycerol dehydration ways and catalysts used [31].

Recently, glycerol appears in excess on the market because of a growing Biodiesel production from triglycerides, wherein it is formed as a by-product. Notwithstanding, its price is not stable and it makes this method of acrolein production possible to complement traditional propylene oxidation depending on the economic situation [3].

Gas phase dehydration of glycerol to acrolein

The glycerol dehydration (Figure 1.12) in the gas phase typically occurs in the temperature range of 260-350°C using a vaporized aqueous glycerol solution. The first group of catalysts for this reaction are heteropoly acids (HPAs). These materials are characterized by a good stability against humidity and air, a low toxicity, a high solubility

in polar solvents and a good corrosivity resistance. That is why HAPs have driven the interest of a lot of research groups. For example, Katryniok et *al.* [7] studied silicotungstic acid catalysts supported on SBA-15, Dubois et *al.* [45] examined the application of phosphotungstic (PW) and silicotungstic (SiW) salts substituted by various metals (*e.g.*, Cs, Rb, Ca, Bi, Zr, La). Notwithstanding, the best ever reported results were published by Alhanash *et al*. [46]. These authors have performed the glycerol dehydration using a well-known CsPW catalytic formulation. They have obtained 98% of acrolein yield. The chosen heteropoly salt possesses strong Brønsted acid sites, which improves the reaction efficiency and a high tolerance to water. However, the catalytic activity decreased after the first few hours, due to coke formation without impairing acrolein selectivity (up to 98% of selectivity).

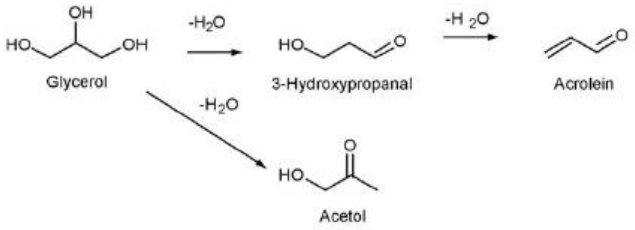

Figure 1.12. Schematic route of glycerol dehydration over acid catalysts [46].

The second group of catalysts used for the acrolein synthesis from glycerol are zeolites. These materials are largely used in the chemical industry, and they were found performant for the considered reaction by several researchers. The published studies report that the factor which is the most important for zeolites in the glycerol dehydration is their total acidity. This parameter can be controlled by three ways: the Si/Al ratio variation, applying transition metal oxides and catalysts surface modifications. The most commonly used materials reported in the literature are micro- and meso-porous ZSM-5 [47,48], ferrierites [49] and *β*-zeolites [47,50]. The highest reported acrolein yield was found with sulfonic-functionalized mesoporous silicas (SBA-15) [51] with 92.6% of acrolein selectivity at total glycerol conversion. The authors underlined the importance of open structure for this catalytic system in term of coke deposition. Therefore, it can be concluded that for this catalyst type, a large pores width is an important factor.

The last group of catalysts for the gas phase glycerol dehydration of glycerol is constituted by mixed metal oxides, phosphates and pyrophosphates. Various materials were reported by researchers, *i.e.*, niobium oxides (Nb_2O_5) [52], acid binary metal oxides (SnO_2-TiO_2, SnO_2-ZrO_2, TiO_2-Al_2O_3) [53] or cerium-doped $FePO_4$ [54]. Generally, for

these catalysts, the acrolein selectivity does not exceed 82% at a temperature up to 500°C. One of the exceptions are iron phosphates ($Fe_x(PO_4)_y$) reported by Deleplanque et *al.* [55]. These authors found after 5 h of reaction that the acrolein yield reached 92% with 100% glycerol conversion. The main observed catalyst disadvantage was its deactivation within 25 h caused by coke deposition. However, this phenomenon can be reduced by addition of oxygen in the inlet mixture.

Liquid phase dehydration of glycerol to acrolein

The liquid phase dehydration of glycerol was patented in 1934 by the Shell Company [56]. In their studies, they used strong mineral acids as catalysts and they obtained approximately 50% of acrolein yield. Afterwards, Ramayya et *al.* [57] tried to use supercritical water reforming reaction (SCWR) to develop this process. They decided that acid homogenous catalyst (H_2SO_4) will be used to perform the tests. The reaction occurred at 350°C in a batch reactor under supercritical water conditions. As a result, the best acrolein yield was 86% with a glycerol conversion of 55%. The main disadvantage of this process was the difficulty to separate the products from the catalyst. Yue *et al.* [58] used nano-copper over ZSM-5 (Cu/ZSM-5) as a catalyst. The reaction was performed in a stainless steel autoclave. In that case, the acrolein yield was higher than for the previous one and reached 91.2% with 100% of glycerol conversion at 250°C. However, the liquid phase glycerol dehydration is not ready to industrialize because of difficult and costly plant maintain, caused, *e.g.*, by reactors corrosion.

1.2.New acrolein production method from methanol and ethanol mixtures.

As aforementioned, acrolein is industrially obtained only based on fossil resources (namely by propylene oxidation). Until now, the only well-studied method based on renewable resources is the glycerol dehydration pathway described before. Unfortunately, the total production cost is not competitive compared to propylene oxidation, which prevents its industrialization. Recently, it was reported that acrolein can be formed *via* methanol and ethanol coupling oxidation [1]. Both alcohols can be produced from biomass with a low price, which lets as hope the possibility of large scale utilization. In

this section, methanol and ethanol manufacturing methods are presented as well as the catalyst used for the new acrolein synthesis reaction.

1.2.1. Methanol and ethanol production.

Methanol production

Worldwide production of methanol reaches almost 110 Mt and is in majority consumed in the formaldehyde industry [59]. Methanol was first produced in 1661 by Sir Robert Boyle through the rectification of crude wood vinegar over milk of lime. Afterwards, other reactions, such as the oxidation of hydrocarbons or the Fisher-Tropsch synthesis (*e.g.*, as by-product), were used, but they have lost their importance with time. Currently, the industrial methanol manufacturing is based on catalytic conversion of synthesis gas. This process consists of three steps [60]:

- Production of syngas;
- Synthesis of methanol;
- Processing of crude methanol.

The synthesis can be performed applying three different pressure levels: low-pressure methanol process (5-10 MPa), medium-pressure methanol process (10-25 MPa) and high-pressure methanol process (25-30 MPa). Schematically, the process is shown in Figure 1.13.

A **B**

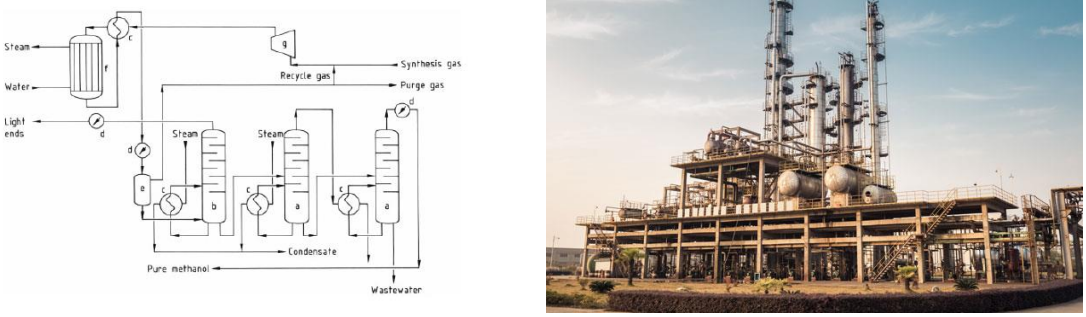

Figure 1.13. A: Process scheme for the Lurgi low pressure methanol synthesis process B: Methanol production plant in the USA [60,61].

The thermodynamics of this process can be described by the following reactions:

$$CO + 2H_2 \leftrightarrow CH_3OH \qquad \Delta H_{300K} = -90.77\ kJ/mol \quad (1.4)$$

$$CO_2 + 3H_2 \leftrightarrow CH_3OH + H_2O \qquad \Delta H_{300K} = -49.16\ kJ/mol \quad (1.5)$$

These reactions are exothermic and they are accompanied by a decrease in volume [60]. Because of the released heat, a tubular reactor with cooling by boiling water is applied. However, the endothermic reaction (Eq. 1.6) of carbon dioxide and hydrogen must be also included:

$$CO_2 + H_2 \leftrightarrow CO + H_2O \qquad \Delta H_{300K} = 41.21\ kJ/mol \quad (1.6)$$

The first industrial catalyst system consisted of ZnO-Cr_2O_3. Nowadays, after many modifications, the standard catalysts used for methanol production are based on Cu-ZnO-Al_2O_3 or Cr_2O_3 systems with different additives. In

Table 1.7, a summary of typical copper-containing catalysts is presented [60].

This technology is not the only current method of methanol production. Figure 1.14 presents an overview of the major processes from different carbon sources. It can be remarked, that it is possible to obtain CH_3OH from different biosources, *e.g.*, biogas, wastes and biomass. These methods are not only answering a worldwide trend of green chemistry but also have economic advantages. Shamsul *et al.* [62] reported that the cost difference between biomass and petrochemical methanol production reaches 300 €/ton in favour of biobased methanol.

Table 1.7. Summary of typical copper-containing catalysts for the low-pressure methanol synthesis [60].

Manufacturer	Component	Content [atom%]	Reference
IFP	Cu	25-80	[63]
	Zn	10-50	
	Al	4-25	
Sud Chemie	Cu	65-75	[64]
	Zn	18-23	
	Al	8-12	
Shell	Cu	71	[65]
	Zn	24	
	rare earth oxide	5	
ICI	Cu	61	[66]
	Zn	30	
	Al	9	
BASF	Cu	65-75	[67]
	Zn	20-30	
	Al	5-10	
Du Pont	Cu	50	[68]
	Zn	19	
	Al	31	
United Catalysis	Cu	62	[68]
	Zn	21	
	Al	17	
Haldor Topsøe	Cu	37	[68]
	Zn	15	
	Cr	48	

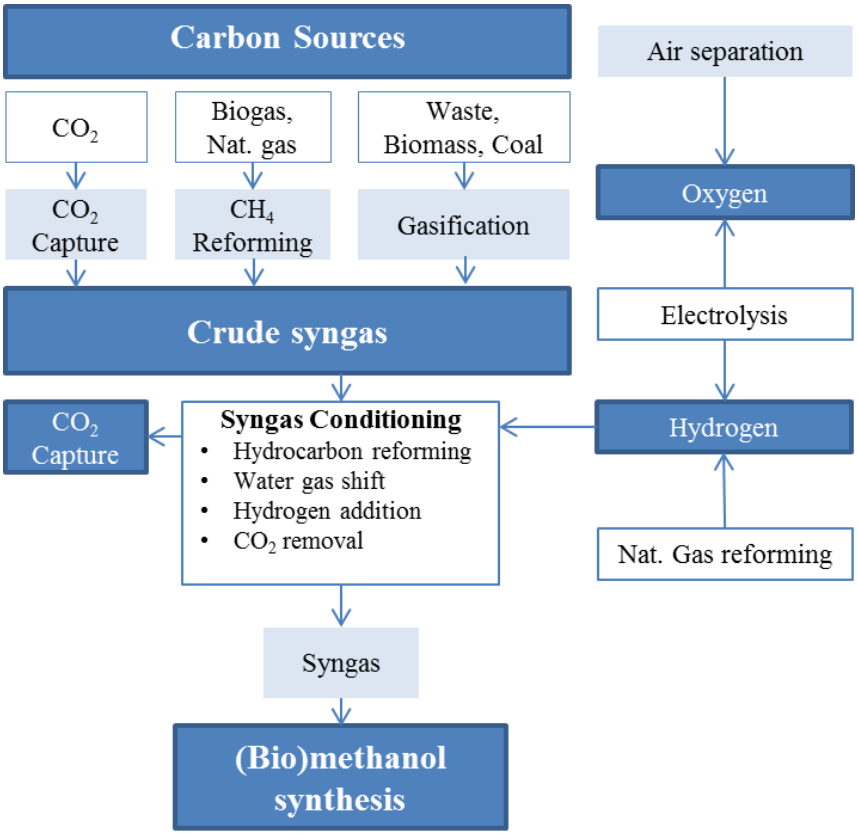

Figure 1.14. Overview of the major methanol production processes from different carbon sources [69].

Several methods of the so-called 'bio-methanol' production are known [62]: pyrolysis, gasification, biosynthesis, electrosynthesis and photo electrochemical processes. The first one is found as the easiest adaptable one in the large scale while gasification is the most cost-effective. The feedstock for the methanol production can come from organic wastes, municipal solid wastes, sewage sludges or primary and secondary agriculture wastes. Despite numerous studies, for now the 'bio-methanol' production is not productive enough to rival with traditional method. Notwithstanding, in the long term, it can gain some importance.

Ethanol production

The first industrial ethanol production method was developed in 1930 by the Carbide and Chemical Corporation. This process was based on two stages. First, ethylene was adsorbed in sulfuric acid followed by hydrolytic cleavage of the formed diethyl sulfide [70]. In 1948, the Shell company industrialized direct hydration of ethylene, and this method is used till today, with a big industrial importance. The thermodynamic equilibrium is presented hereafter [70]:

$$C_2H_{4(g)} + H_2O_{(g)} \leftrightarrow C_2H_5OH_{(g)} \qquad \Delta H = -43.4kJ (1.7)$$

Nowadays, in the industry, ethylene and deionized water are used in the ratio 1:0.3-1:0.8, heated at 250-300°C under a 6-8 MPa pressure [70]. Schematically, this process is presented in Figure 1.15 There are many catalysts patented and published for ethylene hydration. In the industry, only phosphoric acid catalysts supported on, *e.g.*, silica gel, opoka (Volga sandstone) or bentonite are used [70,71,72,73].

A **B**

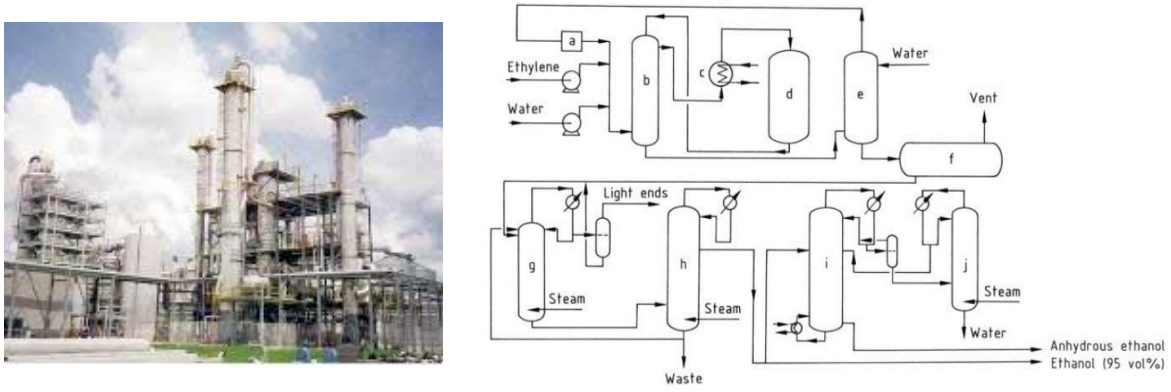

Figure 1.15. A: Ethanol production plant in York (USA), B: Scheme of synthesis of ethanol by direct hydration [70,74].

The obtained product is an azeotrope mixture containing 95% of ethanol. That is why an azeotropic distillation unit is necessary (notified as 'g' in Figure 1.15B). An extractive distillation column is chosen to perform purification. Ethylene hydration is not the only method used nowadays. This molecule can be also obtained from renewable sources by fermentation using yeasts. This method of ethanol production has numerous advantages such as a high selectivity, a low byproduct accumulation, a high ethanol yield, a low pH among others [70]. There are many factors that influence the productivity of the fermentation process. The first of them is the substrate concentration, which has to be between 14 and 18 wt.%. The concentration cannot be too high because of plasmolysis (*i.e.*, a water loss by cell in a hypertonic solution) [75]. The other important factor is the oxygen concentration. Depending on the microorganism's type, ethanol is produced under aerobic or anaerobic conditions. For the first group, the optimized level of oxygen is necessary for high ethanol productivity. pH and temperature have a strong influence also. In the industry, the standard pH value is between 4 and 6 with a temperature around 40°C [70]. We can classify raw materials for ethanol production in two main groups: fermentable carbohydrates for a direct use and organic materials (as starch) that must be

pretreated before the fermentation. Substrates come from three main sources: agriculture, forest and industrial byproducts [70].

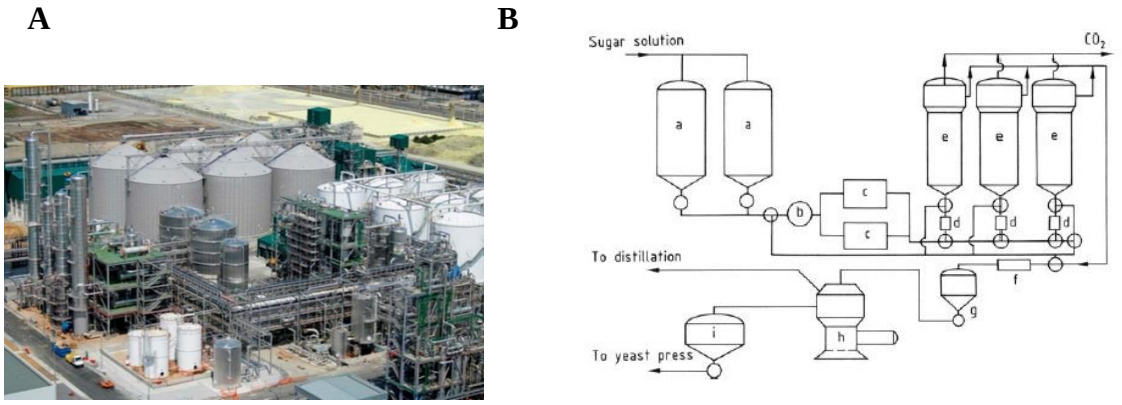

Figure 1.16. A: Bioethanol production plant in Pau (France) B: Commercial ethanol tower fermentation system (APV Company) [70,76,77].

From an engineering point of view, bioethanol production through fermentation process can be performed in different modes: Most of the processes occur in a batch system, where possible final ethanol concentration can reach 10-16% [78]. Nowadays, on the market, more than 60% of bioethanol are produced in the USA, India and Brazil. Those are countries with a climate adapted for the growth of the needed crops [70]. Figure 1.16 presents an example of bioethanol production plant and a schematic flow diagram for ethanol tower fermentation system used nowadays.

1.2.2. Catalyst choice for methanol and ethanol oxidative coupling.

In Dubois *et al.* patent application [1] acrolein formation from methanol and ethanol can be described schematically as follows (Figure 1.17): First, methanol and ethanol are partially oxidized to formaldehyde and acetaldehyde. Then, the aldol condensation between both aldehydes occurs. Dubois *et al.* [1] have carried out this reaction over iron molybdate mixed oxides. Thus, this catalyst was chosen as the reference formulation for the present study.

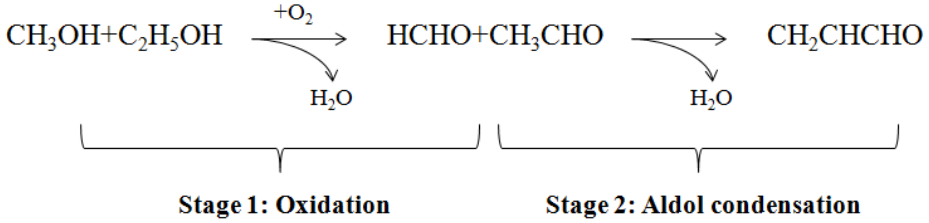

Figure 1.17. New acrolein method production.

The $FeMoO_x$ formulation is mostly used in the industry for methanol oxidation to formaldehyde. In 1931, this catalyst has been synthesized for the first time by Adkins and Paterson [79]. Since that, in the early 50's, this material was developed and became the most widely used formulation for formaldehyde production, which brought a lot of advantages compared to conventional silver catalysts [79,80,81]:

- High selectivity to formaldehyde at low methanol concentration- formaldehyde yield over 90%,
- Resistance for poisoning,
- Longer catalyst life,
- Lower reaction temperature compared to silver-based catalysts,
- Lower probability of explosion because of the lower methanol concentration.

Generally, non-supported MoO_3-$Fe_2(MoO_4)_3$ catalysts are synthesized by an aqueous phase co-precipitation method, with subsequent washing, drying and calcination (300-600°C) steps. It was reported by Pernicone [80] that the precipitation is influenced by several parameters (*i.e.*, pH, precursors …) and that the catalyst specific surface area strongly depends on the Mo solution concentration. During the catalyst characterization, the author found that $FeMoO_x$ owns the acid sites on the surface confirmed by TPD-NH_3 measurement [80,82].

Regarding methanol oxidation, other author, Trifirò *et al.* [83] proposed that during the oxidation this compound is chemisorbed and alkoxide complex may be formed (Figure 1.18).

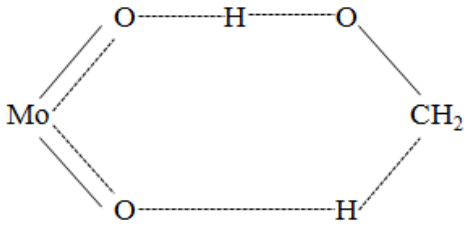

Figure 1.18. Adsorption complex on FeMoO*x* catalyst during methanol oxidation [83].

Even if the role of molybdenum ions is well defined, the Fe^{3+} ions function is difficult to determine. For example, it was found that pure MoO_3 activation energy is equal to that of MoO_3-$Fe_2(MoO_4)_3$ and that trivalent cations have a promoting effect [80]. However, Trifirò [83] has tried to propose the redox mechanism that takes place on the catalyst surface:

$$Mo^{5+} + Fe^{3+} \rightarrow Mo^{6+} + Fe^{2+} \quad (1.8)$$

It was remarked as well that gaseous oxygen oxidizes the Fe^{2+} ions. Following that, Pernicone [80] described the kinetic mechanism of methanol oxidation over $FeMoO_x$. It was reported that there are several factors influencing the reaction efficiency: water acting as an inhibitor, reactor type, the partial pressure of both reactants (*e.g.*, the reaction rate increases when increasing pressure) and the methanol partial pressure (*e.g.*, in the presence of water, higher pressure causes higher reaction rate). Based on these observations, the following mechanism was proposed:

1. Dissociative methanol chemisorption (Eq. 1.9)

$$CH_3OH + \square + O^{2-} \rightarrow (CH_3O - \square)^- + OH^- \quad (1.9)$$

2. Catalyst reduction with chemisorbed formaldehyde formation (Eq. 1.10)

$$(CH_3O - \square)^- + O^{2-} \rightarrow (CH_2O - \square)^{2-} + OH^- \quad (1.10)$$

3. Water desorption (Eq. 1.11)

$$2OH^- \leftrightarrow H_2O + O^{2-} + \square \quad (1.11)$$

4. Formaldehyde desorption (Eq. 1.12)

$$(CH_2O - \square)^{2-} \rightarrow CH_2O + \quad ^{2-} \qquad (1.12)$$

5. Catalyst reoxidation (Eq. 1.13)

$$0.5O_2 + \quad ^{2-} \rightarrow O^{2-} \qquad (1.13)$$

1.3. Conclusions.

As it was presented above, acrolein finds many applications in the chemical industry. Particularly important use is the acrylic acid and methionine productions. The demand for these compounds is growing every year due to the worldwide population increase. Consequently, this tendency requires an increase in the acrolein production. Till now, there are several well known synthesis method based on petrochemical or renewable resources. One of them is the acetaldehyde and formaldehyde aldol condensation. It was reported that the highest acrolein yield obtained via this reaction has reached 86% for Mn-P and Ni-P catalyst [36] which have the balance between acid and basic sites on the surface. This propriety was found the most preferable for acrolein formation [32]. However, only propylene oxidation is used in the industrial scale. In order to fulfill a growing acrolein demand and to answer more and more stringent environmental requirements, new production methods are actively studied.

Recently, Dubois *et al.* [1] proposed the oxidative coupling of methanol and ethanol to acrolein. This process is based on two reaction steps:

- Methanol and ethanol oxidation to formaldehyde and acetaldehyde, performed usually over redox catalysts [79].
- Formaldehyde and acetaldehyde aldol condensation, performed with basic or acid materials [33].

It was indeed shown that $FeMoO_x$ catalysts are able to directly convert methanol-ethanol streams to acrolein. This can be probably related to the property, mentioned by Pernicone [80], of a surface Lewis acidity linked to the presence of Mo^{6+} species. $FeMoO_x$-based formulations were thus used in the present study in order to better understand their behavior during methanol and ethanol oxidation with the purpose of back-optimization to yield better performances. Based on the literature review presented above, it was decided to perform catalysts modification by La and Ce addition, which were assumed to create

basicity in $FeMoO_x$ catalysts to balace acid sites and promote the second step (aldol condensation) of the considered process. Continuing this approach, it was decided to add the second catalyst into the catalytic bed. These material were typically basic (*i.e.*, commercial oxides: MgO, CaO and BaO) as well as acido-basic (*i.e.*, silica based synthesized through sol-gel method [84]) chosen based on literature review presented previously.

1.4.References.

[1] PCT Patent WO2014068213, assigned to Arkema France, Priority date Oct 17, 2013

[2] *Etzkorn, W. G.* 2009. Acrolein and Derivatives. Kirk-Othmer Encyclopedia of Chemical Technology. 1–29

[3] *Ohara, T., Sato, T., Shimizu, N., Prescher, G., Schwind, H., Weiberg, O., Marten, K. and Greim, H.* 2011. Acrylic Acid and Derivatives. Ullmann's Encyclopedia of Industrial Chemistry

[4] *Bauer, W.* 2003. Acrylic Acid and Derivatives. Kirk-Othmer Encyclopedia of Chemical Technology

[5] Arkema data

[6] *Drauz, K., Grayson, I., Kleemann, A., Krimmer, H.-P., Leuchtenberger, W. and Weckbecker*, C. 2007. Amino Acids. Ullmann's Encyclopedia of Industrial Chemistry

[7] *B. Katryniok et al.* Green Chemistry 12 (2010) 1922-1925

[8] *Arntz, D., Fischer, A., Höpp, M., Jacobi, S., Sauer, J., Ohara, T., Sato, T., Shimizu, N. and Schwind, H.* 2007. Acrolein and Methacrolein. Ullmann's Encyclopedia of Industrial Chemistry

[9] *Richard R. Whetstone, Seaver A. Ballard*, Shell Development Company U.S. Patent 2,768,213 (Oct. 23, 1956)

[10] Sigma-Aldrich Technical Bulletin AL-128, Product No. T6,620-6

[11] *Ravil I. Khusnutdinov et al.*, Journal of Organometalic Chemistry 768 (2014) 75-114

[12] *Ginelle A. Ramann, Bryan J. Cowen*, Tetrahedron Letters 56 (2015) 6436-6439

[13] *H. Saggadi et al.*, RSC Advances 4(2014) 21456-21464

[14] *Peter Werle et al.* U.S. Patent 6,060,571 (May 9, 2000)

[15] *A. Turkiewicz, J. Brzeszcz, P. Kapusta,* The application of biocides in the oil and gas industry, Oil & Gas Institute, 2013, Krakow

[16] *Liu L. et al.* ChemSusChem 5 (2012) 1162-1180

[17] *K. Weissermel, H-J. Arpe*, Industrial Organic Chemistry, 287-288, John Wiley&Sons, 2003

[18] *D.P. Shashikin et al*., Kinetics and Catalysis 46 (2005) 545-549

[19] *J.-H. Kang et al.,* LG Chem. Ltd, WO 2005079980

[20] *Kh. Karim et al.,* U.S. Patent 6,143,928

[21] *H. Arnold et al*., BASF AG, EP 1005908 1998

[22] *T. Kimura et al.*, Nippon Shokubai Kagaku Kogyo Co. Ltd, EP 1055455

[23] *K. Wada et al.*, Nippon Kayaku Co. Ltd, EP 807465 1997

[24] *N. Kanuka, I. Teshigahara*, Mitsubishi Chem. Corp., U.S. Patent 2005,159,620

[25] http://corporate.evonik.be/region/belgium/en/Pages/default.aspx , verified 10 June 2016

[26] *Carbucicchio et al.* Journal of Catalysis 107 (1987) 307-316

[27] *Zhao et al.* Journal of Catalysis 257 (2008) 181-189

[28] *Zhao et al.* Catalysis Today 118 (2006) 332-343

[29] *Cui et al.* Applied Catalysis A: General, 482 (2014) 179-188

[30] *Polkovnikova et al.* Scientific Research Institute of Synthetic Alcohols and Organic Products (12 November 1962)

[31] *A. Talebian-Kiakalaieh et al*. Renewable and Sustainable Energy Reviews 40 (2014) 28-59

[32] *A. Azzouz et al.* Applied Catalysis A: General 241 (2003) 1-13

[33] *M. Ai*, Bulletin of the Chemical Society of Japan 64 (1991) 1346-1350

[34] *E. Dumitriu et al.* Journal of Molecular Catalysis 79 (1993) 175-185

[35] *E. Dumitriu et al.* Journal of Catalysis 147 (1994) 133-139

[36] *M. Ai*, Applied Catalysis, 77 (1991) 123-132

[37] *Z. Zhao et al.* Applied Catalysis A: General 196 (2000) 37-42

[38] *Z. Zhao et al.* Journal of Catalysis 190 (2000) 215-227

[39] *Z. Zhao, T. Kobayashi*, Applied Catalysis A: General 207 (2001) 139-149

[40] *K. Nakagawa et al.* Catalysis Letters 63 (1999) 79-82

[41] *G.J. Hutching, D.F. Lee* Catalysis Letters 34 (1995) 115-127

[42] *X. Zhang et al.* Applied Catalysis A : General 353 (2009) 24-31

[43] *X. Zhang et al.* Catalysis Letters 97 (2003) Nos. 3-4

[44]*Y-C. Kim et al.* Applied Caralysis 70 (1991) 175-187

[45] *JL. Dubois et al.* (Arkema), WO 2009127889 A1

[46] *A. Alhanash et al.* Applied Catalysis A: General 378 (2010) 11-18

[47] *JL. Dubois et al.*, WO087083, 2006a

[48] *CJ. Zhou et al.,* Studies in Surface Science and Catalysis 165 (2007) 527-530

[49] *YT. Kim et al.,* Applied Catalysis A : General 393 (2011) 275-287

[50] *A. Witsuthammakul, T Sooknoi*, Applied Catalysis A: General 413-414 (2012) 109-116

[51] *Lourenço et al.* Catalysis Communications 19 (2012) 105-109

[52] *SH. Chai et al.*, Journal of Catalysis 250 (2007) 342-349

[53] *LZ. Tao et al.*, Catalysis Today 158 (2010) 310-316

[54] *G. Patience et al.*, Chemical Engineering & Technology 35(9) (2012) 1699-1706

[55] *J. Deleplanque et al.* Catalysis Today 157 (2010) 351-358

[56] *H. Groll, G. Hearne* (Shell), US patent 2042224, 1936

[57] *S. Ramayya et al.* Fuel 66 (1987) 1364

[58] *CJ. Yue et al.* Journal of the Taiwan Institute of Chemical Engineers 45(2014) 1443-1448

[59] Chemical Market Associates Inc. (CMAI): World Methanol Consumption-At a glance, Barcelona 2010

[60] *Ott, J., Gronemann, V., Pontzen, F., Fiedler, E., Grossmann, G., Kersebohm, D. B., Weiss, G. and Witte, C.* 2012. Methanol. Ullmann's Encyclopedia of Industrial Chemistry

[61] http://www.rsc.org/chemistryworld/2016/01/us-shale-methanol-boom-exports-china , verified 10 June 2016

[62] *N.S. Shamsul et al.* Renevable and Sustainable Energy Reviews 33 (2014) 578-588

[63] *P. Courty et al.* (IFP) EP 0152314, 1987

[64] *M. Schneider, K. Kochloefl, J.Ladebeck* (Sud Chemie), EP 0125689, 1987

[65] *E.F. Magoon* (Shell) US 3709919, 1973

[66] *J. Gallagher, Y.H. Kiold* (ICI), GB 1159035, 1965

[67] *F.J. Brocker et al.* (BASF), DE 2846614, 1978

[68] *R.H. Hoppener, E.B.M. Doesburg, J.J.F. Scholten*, Applied Catalysis 25 (1986) 109–194

[69] http://www.iaffairscanada.com/2015/renewable-energy- in-a- nutshell-bio- methanol, verified 10 June 2016

[70] *Kosaric, N., Duvnjak, Z., Farkas, A., Sahm, H., Bringer-Meyer, S., Goebel, O. and Mayer, D.* 2001. Ethanol. Ullmann's Encyclopedia of Industrial Chemistry

[71] National Distillers & Chemical Co., DE-OS 2015536, 1970

[72] *G. G. Eremeeva, V. M. Dronkin, G. I.Gagarina,Neftepererab*. Neftakhim (Moscow)1979, no. 16, 19– 20

[73] *K. W. Toptschijewa, S. M. Rachowskaja, I. K.Kutschkajewa,*Neftekhimiya 3(1963) 271

[74] http://www.greener-industry.org.uk, verified 10 June 2016

[75] *A. H. Rose, J. S. Harrison* The Yeasts, Academic Press, London 3 (1970) 306

[76] R. N. Greenshields, E. L. Smith, Process Biochemistry 9(1974) no. 3, 11 – 17, 28

[77] http://diseprosa.com/en/, verified 10 June 2016

[78] *D. Rose* Process Biochemistry 3 (1976) 10 – 12, 36

[79] *H. Adkins,W.R. Peterson* Journal of the American Chemical Society 53 (1931) 1513

[80] *N. Pernicone* Journal of the Less-Common Metals 36 (1974) 289-297

[81] N. *Pernicone et al.* Journal of Catalysis 14 (1969) 293-302

[82] *K. Thavornprasert et al.*, Applied Catalysis B : Envirenmental 145 (2014) 126-135

[83] *F. Trifirò, I. Pasquon*, La Chimica e l'Industria (Milan), 53 (1971) 577

[84] *A. Douy* Journal of European Ceramic Society 7 (1991) 397-403

Chapter 2. Catalyst preparation and experimental techniques

2.1.Catalysts synthesis

In this study, based on previous research involving our group [1], iron molybdate catalysts were chosen to realize the direct conversion of methanol and ethanol mixtures to acrolein. They were synthetized by a coprecipitation method presented by Pericone *et al.* [2,3]. In the following subsections, the detailed preparation method of these materials are presented. First, the improvement of the acrolein yield was attempted by addition of lanthanum and cerium in the initial $FeMoO_x$ formula. Afterwards, a second catalyst was added to the catalytic bed. Two types of material were considered: silica-powders containing alkaline earth metals (*i.e.*, Mg, Ca and Ba) and commercial oxides (*i.e.*, MgO, CaO and BaO). The former were synthetized by a sol-gel method based on the work of Douy [4]. The detailed procedure is presented in a following subsection as well.

2.1.1. Iron molybdate mixed oxides catalysts prepared by coprecipitation

Iron molybdate catalysts were prepared by a coprecipitation method based on a procedure described by Pernicone *et al.* [2,3]. Aqueous solutions of ammonium molybdate tetrahydrate $(NH_4)_6Mo_7O_{24}\cdot 4H_2O$ (AHM, Fluka, 99%) and iron (III) chloride hexahydrate $FeCl_3\cdot 6H_2O$ (Sigma-Aldrich, 97%) were prepared to obtain theoretical Mo/Fe molar ratios of 1.5, 2.0 and 2.5 (Table 2.1).

Table 2.1. Precursors quantities used for the synthesis of Fe-Mo catalysts.

Catalyst	Desired Mo/Fe ratio	Precursors [g]		Water volume [mL]	
		AHM	$FeCl_3$	AHM	$FeCl_3$
FeMo	1.5	10	10.185	250	75
FeMo	2.0	10	7.577	250	75
FeMo	2.5	10	6.110	250	75

The AHM solution (with an initial pH of 5) was acidified with concentrated HCl to decrease the pH to 1. These two solutions were independently stirred vigorously using a magnetic stirrer and heated to a temperature between 50-60 °C. Then, the solution of iron chloride was added slowly and continuously to the AHM solution using a burette, and a yellow precipitate was obtained. The solution agitation was kept for 1 h and followed by several hours of decantation. In order to remove chloride, the obtained precipitate was washed several times with distilled water, left for decantation before being recovered. This action was repeated till undesired species (Cl^-) content in the supernatant part of the solution was less than 2000 ppm. For this purpose, the estimation was made by comparison with the response of a reference solution prepared by dissolving 3.297 g of NaCl in 1 L of distilled water. The estimation tests were performed by placing 5 mL of the recovered supernatant solution and 5 mL of the reference in two test tubes. Then, 2 mL of the calibrated $AgNO_3$ solution acidified with nitric acid were added in each tube. The intensity of the white precipitate was visually checked. If the catalyst solution gave a response more marked than that of the reference solution, the washing step was repeated. It was important to keep the Cl^- concentration in the recovered solution at a level lower than 2000 ppm in order to avoid *e.g.*, a decrease in catalyst acidity. Following that, when satisfactory results were obtained, the recovered purified precipitate was filtered and dried in an oven at 120 °C for 4 hours. The obtained material was crushed in a mortar with 1 wt.% of stearic acid $C_{17}H_{35}COOH$ (Sigma-Aldrich, 98.5%) and pelletized using a press (3 tons), before sieving to obtain 2-3 mm particles, which were subsequently calcined under air (0.3 mL/min) at 350, 400 and 450 °C according to the profiles presented in Figure 2.1. In this study, homemade iron molybdate catalysts were named as follows: FeMoX(Y°C), where *X* is the Mo/Fe ratio (*e.g.*, 1.5, 2.0 or 2.5) and *Y* is the calcination temperature (*e.g.*, 350, 400 and 450 °C).

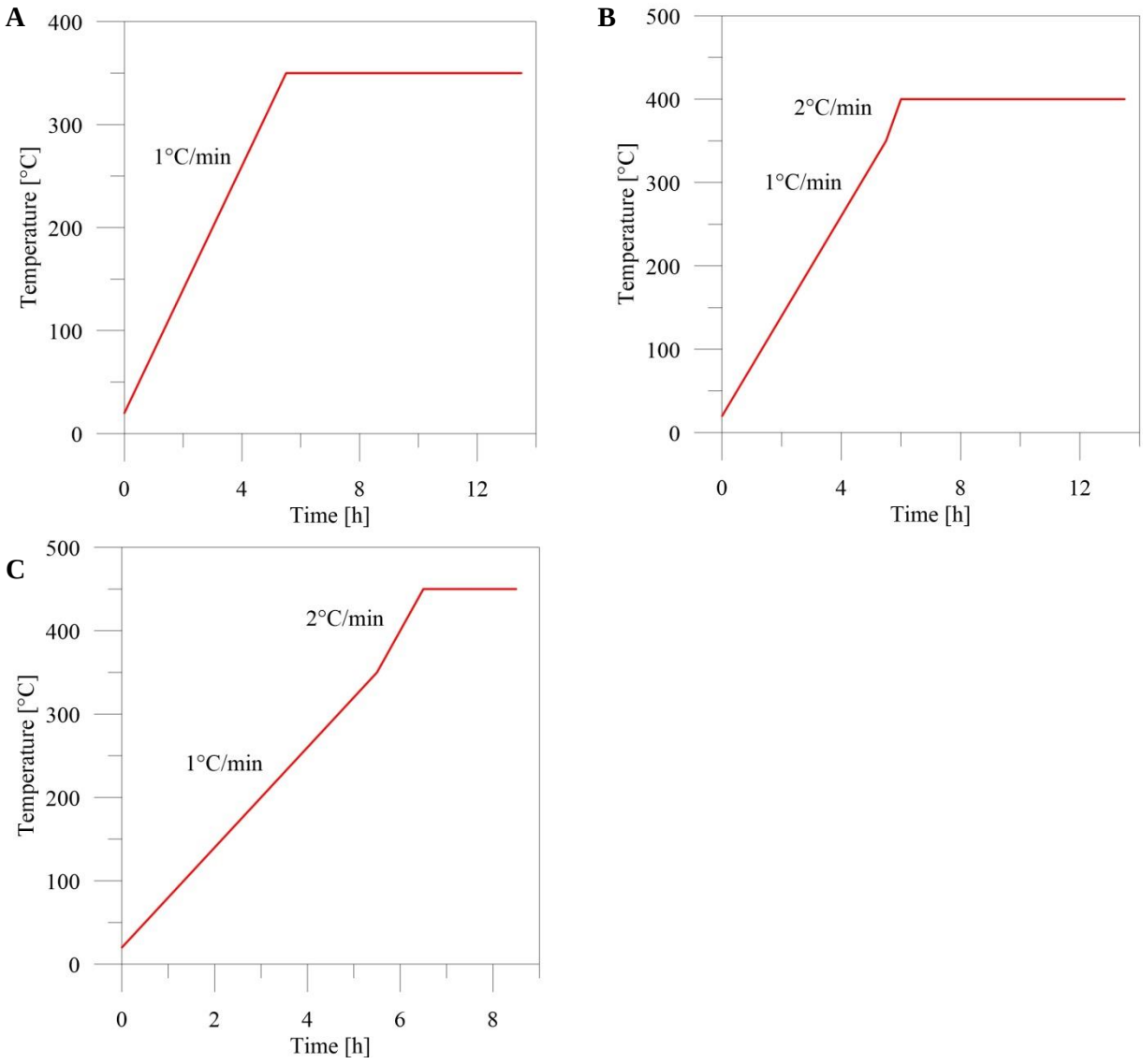

Figure 2.1. Calcination profiles for iron molybdate catalysts. A: 350 °C, B: 400 °C, C: 450 °C.

2.1.2. Iron molybdate mixed oxides catalysts modified with lanthanum and cerium.

The modified iron molybdate catalysts were also prepared using the aforementioned coprecipation method. An aqueous solution of ammonium molybdate tetrahydrate $(NH_4)_6Mo_7O_{24}\cdot 4H_2O$ (AHM, Fluka, 99%) was prepared and heated to a temperature between 50- 60 °C. Fe and Ce or La precursor solutions were prepared by dissolving separately in water iron (III) chloride hexahydrate $FeCl_3\cdot 6H_2O$ (Sigma-Aldrich, 97%), lanthanum (III) nitrate hexahydrate $La(NO_3)_3\cdot 6H_2O$ (Aldrich, 99.99%) and cerium (III) nitrate hexahydrate $Ce(NO_3)_3\cdot 6H_2O$ (Aldrich, 99.99%). The iron precursor quantity was set according to the desired Mo/Fe molar ratio (1.5, 2.0 or 2.5). Ce and La solutions were

prepared to obtain a 10 mol.% content relative to iron. The solutions were kept under heating at the same temperature as that of the molybdate precursor solution. The AHM solution (initial pH = 5) was acidified with concentrated HCl to decrease the pH to 1. Afterwards, the lanthanum or the cerium solution was added dropwise to the dissolved iron chloride solution. This mixture was introduced to the AHM solution by the means of a burette, and a yellow precipitate was obtained. The following preparation steps were the same as those of the unmodified FeMo catalysts. The detailed precursors quantities are presented in Table 2.2. We recall here the aforementioned nomenclature: FeMoLa(Ce)X(Y°C), where *X* is the Mo/Fe ratio and *Y* is the calcination temperature.

Table 2.2. Precursors quantities used for the synthesis of the modified Fe-Mo catalysts.

Catalyst	Mo/Fe ratio	Precursor [g]				Water volume [mL]			
		AHM	$FeCl_3$	$La(NO_3)_3$	$Ce(NO_3)_3$	AHM	$FeCl_3$	$La(NO_3)_3$	$Ce(NO_3)_3$
FeMoLa	1.5	10	9.167	1.584	-	250	75	75	-
FeMoLa	2.0	10	6.617	1.178	-	250	75	75	-
FeMoLa	2.5	10	5.499	0.951	-	250	75	75	-
FeMoCe	1.5	10	9.167	-	1.604	250	75	-	75
FeMoCe	2.0	10	6.617	-	1.198	250	75	-	75
FeMoCe	2.5	10	5.499	-	0.963	250	75	-	75

2.1.3. Silica-based catalysts prepared by a sol-gel method.

The silica-based catalysts were prepared by a sol-gel method proposed by Douy [4]. Aqueous solutions were prepared by dissolving magnesium nitrate hexahydrate $Mg(NO_3)_2 \cdot 6H_2O$ (Sigma-Aldrich, 99%), calcium nitrate tetrahydrate $Ca(NO_3)_2 \cdot 4H_2O$ (Sigma-Aldrich, 98%) or barium nitrate $Ba(NO_3)_2$ (Aldrich, 99.99%) in 50 mL of water. Afterwards, citric acid $HOC(COOH)(CH_2COOH)_2$ (Sigma-Aldrich, 99.5%) was added in the quantity of one mole equivalent by nitrate mole. The next step was the addition of ammonia to adjust the pH at 2.3, which is the value found for primary nitrates solutions. 50 mL of a tetraethylorthosilicate (TEOS, Aldrich, 99.99%) 0.3 M solution were prepared and added to a nitrate solution under vigorous stirring. Then, in this freshly prepared 100 mL of solution, 6 g of acrylamide $CH_2=CHCONH_2$ (Sigma-Aldrich, 98%) and 0.8 g of *N,N'*-methylenediacrylamide $(H_2C=CHCONH)_2CH_2$ (Sigma-Aldrich, 99%) were dissolved. The final solution was heated to 80 °C under magnetic stirring. As soon as this

temperature was reached, 0.1 g of α,α'-azoisobutyronitrile (AIBN, Aldrich, 98%) previously dissolved in hot ethanol (1 mL) was added. The gelation occurred after 1 to 2 min. The as-obtained transparent gel was then dried at 120 °C overnight. The calcination procedure presented in Figure 2.2 consisted in two steps. First, a stationary calcination was performed at 350 °C for 1 h, this temperature being reached at a heating rate of 1 °C/min. Afterwards, calcination under air (0.3 mL/min) was performed at 750 °C after a two-step heating (3 °C/min to 700 °C with a 5 h plateau and 1 °C/min to 750 °C with a 1 h plateau).

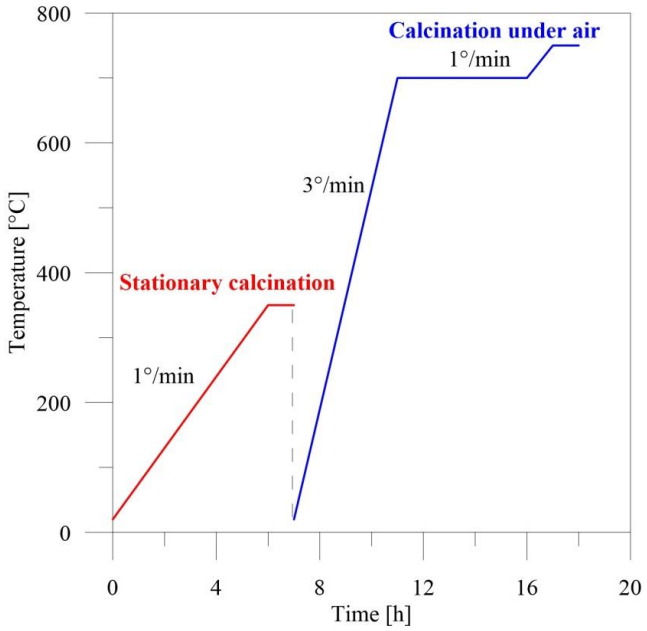

Figure 2.2. Calcination profiles for silica-based catalysts.

2.1.4. MgO, CaO and BaO simple oxides.

The single oxides catalysts were prepared by calcination of commercial products. The following starting materials were used: MgO (Aldrich, 99.99%), CaO (Aldrich, 99.99%) and BaO (Aldrich, 97%). They were calcined under air (0.3 mL/min) at 350°C during 1 h.

2.2.Characterization methods.

In order to better understand the properties of the synthetized catalysts, several characterization methods were used. The experimental procedures and apparatus are described below.

2.2.1. Nitrogen adsorption-desorption (BET).

The specific surface area was calculated using the single-point BET method (Brunauer, Emmett, Teller) [5] based on nitrogen adsorption and desorption. The calcined samples were analyzed with a Micrometrics Flowsorb II Surface Area Analyzer using nitrogen flow (70 mL/min). 200 mg of catalyst were placed in a glass chamber and outgassed at 150 °C during 20 min in order to remove the surface impurities. Afterwards, the vessel was put into liquid nitrogen to perform the adsorption/desorption procedure followed by a TCD signal.

2.2.2. Differential thermal analysis and thermogravimetric analysis (TGA-DSC).

Thermogravimetric analysis (TGA) and differential scanning calorimetric analysis (DSC) were performed on a TA Instruments SDT-Q600 apparatus. Alumina was used as the reference. The analysis was performed under air flow (100 mL/min) on non-calcined samples. In the case of iron molybdate catalysts, about 15 mg of sample were used. The temperature was increased at a rate of 5 °/min up to 600 °C. In the case of the silica-based catalysts, the parameters were the same except the maximal temperature, which was set at 800 °C. Furthermore, the primary amount of catalysts was reduced to 8 mg because of the lower material density.

2.2.3. X-ray diffraction (XRD).

Notably in order to verify the calcination temperature influence on the final structure of the solids, non-calcined iron molybdate catalysts were analyzed by temperature-programmed X-ray diffraction using a Brüker D8 apparatus (Brüker AXS, Cu-$K_{\alpha 1}$ λ = 1.5406 Å) to follow the temperature of phases crystallization. The analysis was performed under air flow from 50 °C to 500 °C with a heating rate of 10 °/min. The diffractograms were recorded each 25 °C for 2θ values in the 10° to 60° range, using a 0.02° step and a 0.5 s integration time.

For silica-based catalysts, the XRD recording at room temperature was performed with the same apparatus. In that case, the calcined samples are analyzed, and the diffractograms were recorded between 5° and 90° with the same 0.02° step and the same

0.5 s integration time. The results interpretation was made based on the database from the Joint Committee on Powder Diffraction Standards (JCPDS) with the help of the EVA X-ray diffraction analyses software.

2.2.4. X-ray photoelectron spectroscopy (XPS).

Three different kinds of XPS-based experiments were performed:

- *Catalyst surface analysis under vacuum*. Calcined samples were analyzed using a Kratos Axis (Figure 2.3) spectrometer apparatus with an alumina Kα radiation (1486.6 eV) under vacuum (to examine the catalyst surface composition). All the results were treated using the CasaXPS software, and the surface composition was determined from the various peaks (*i.e.*, Mo 3d, Fe 2p…) recorded at a 40 eV pass energy. The reference was taken for the C 1s level binding energy for C-(C, H) bonds fixed at 285 eV.

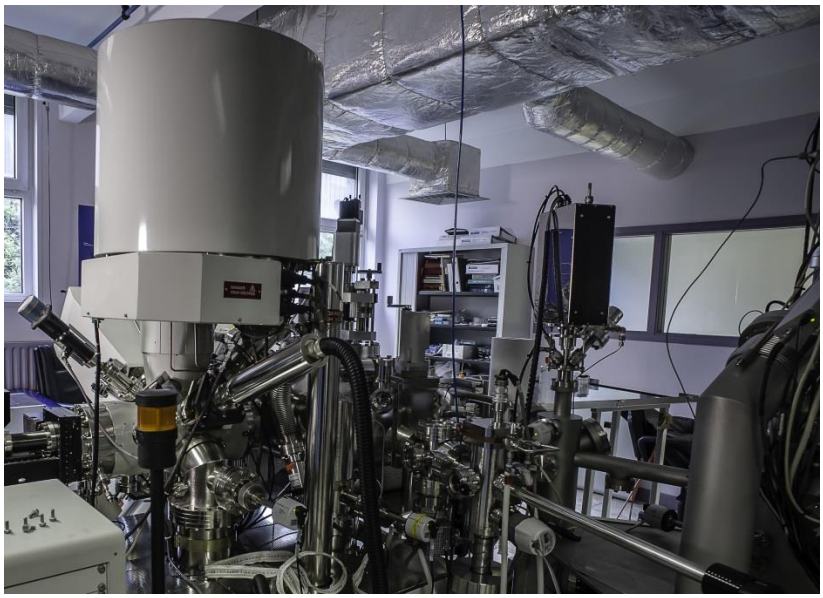

Figure 2.3. Kratos Axis spectrometer used for XPS analysis.

- *Catalyst surface analysis by quasi in situ XPS*, performed for calcined samples using the same set up as that described above. Before the measurement, the

catalysts are pretreated in a separate chamber at 320°C using the following procedure:

- Methanol/Ethanol mixture (ratio = 1) mixed with Helium during 2h,
- Methanol/Ethanol mixture (ratio = 1) with Oxygen and Helium during 2 h.

After each stage the spectra was taken.

- *Catalyst surface analysis by Near Ambient Pressure (NAP) XPS*, performed at SOLEIL Synchrotron (Saint-Aubin, France) in the near to reaction conditions. The calcined samples were using a SPEC Phoïbos 150 NAP hemispherical analyzer coupled with a DLD detector (Figure 2.4). The setup was equipped with mass spectrometer which controlled the products and the substrates in a gas phase. The powdered samples were deposited on a gold foil, in order to get rid of any annoying charge effect, and placed into a catalysis chamber. The analysis was performed for a catalytic system heated at 320 °C and consisted on two stages:
  - Reduction with methanol and ethanol mixture with a molar ratio of 1 - 0.5 mbar,
  - Oxygen addition into the system (ratio 1 relative to the sum of the alcohols) – 1 mbar,

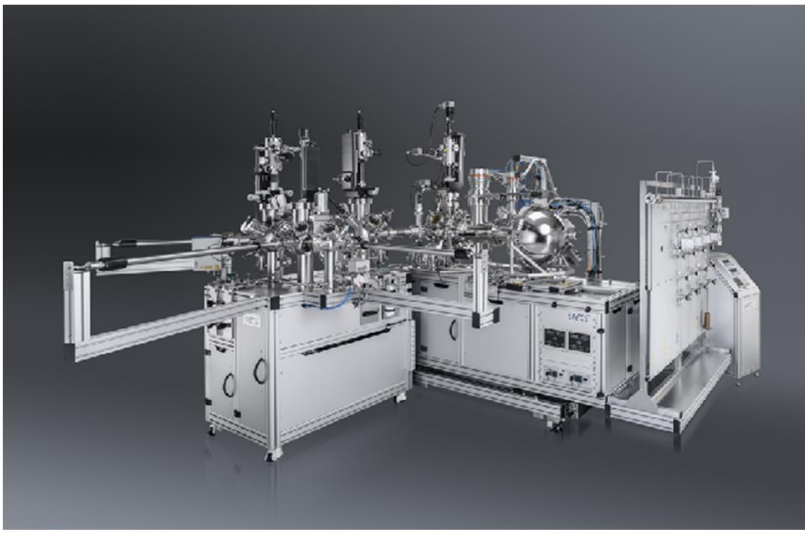

Figure 2.4. SPECS Phoïbos hemispherical analyzer used for this study.

2.2.5. X-ray fluorescence (XRF).

The calcined samples were analyzed in a S2Ranger Bruker apparatus in a tub through Mylar sheet 6 microns under He. Four measurement conditions were used to detect all the elements in the range from Na to U:

- 50 kV with copper filter of 250 microns,
- 40 kV with aluminum filter of 500 microns,
- 20 kV without filter,
- 10 kV without filter.

2.2.6. Low energy ion scattering (LEIS).

LEIS experiments were performed in a Qtac^{100} instrument (ION-TOF GmbH) at a base pressure of 10^{-8} mbar. The instrument is fitted with a double toroidal energy analyser (DTA) which collects the scattered ions at a scattering angle of 145 from all azimuth angles. The samples were analysed using a 3 keV He^+ primary ion beam directed perpendicularly to the target surface. The area of analysis is 1 mm x 1 mm and the experiments have been performed with a total dose per spectrum of $1{,}9x10^{14}$ ions/cm^2. Quantification and simulation of the peaks were carried out using SurfaceLab software.
As LEIS is highly sensitive to the outermost surface, before analysis, the pressed samples were cleaned from carbon contamination by using an atomic oxygen plasma ($1\text{-}2x10^{-5}$ mbar, 10 min).

2.2.7. CO_2-Temperature programmed desorption (TPD).

The calcined samples were analyzed with Micrometrics Autochem 2920 apparatus coupled with MS Pfeiffer. First, the catalysts were pretreated under He flow (50 mL/min) at 200 °C (temperature reached at a rate of 10 °C/min) during 1 h. Then, CO_2 adsorption was performed at room temperature during 30 min using a carbon dioxide flow (5% CO_2, 95% He). Finally, the desorption was performed until 700 °C (this temperature being reached at a rate of 10 °C/min) during 30 min in helium (30 mL/min).

2.2.8. Adsorption (CO_2, Pyridine) coupled infrared (IR) *in situ*.

These measurements were made for calcined samples with different chemicals (CO_2, Pyridine) in order to define the basic and acid properties of the solids. The scheme of the setup is presented in Figure 2.5.

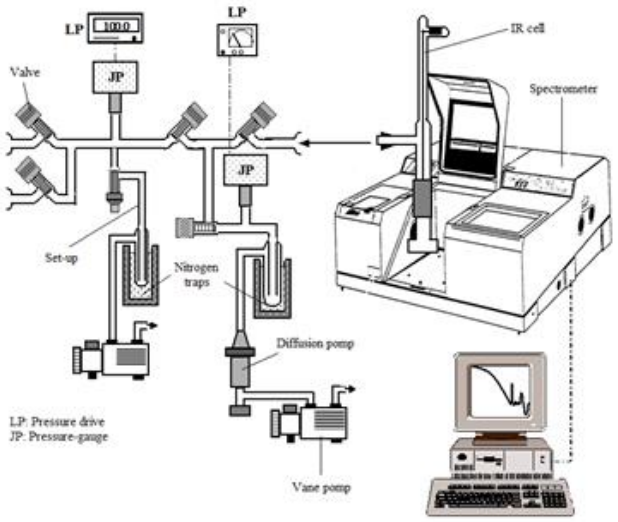

Figure 2.5 Schematics of the setup used for adsorption experiments.

Before analysis, weighed catalysts were ground in an agate mortar and pressed to get self-supporting wafers. Then, they were then placed in the experimental setup under vacuum for 30 min, before being heated to 450 °C under dynamic vacuum for 2 h. After cooling to room temperature, the desired probe molecule adsorption was performed by introducing a defined quantities in the cell each 5 min and taking IR spectra (Nicolet Protege System 460 equipped with a MCT detector). Further, the non-adsorbed molecules were evacuated under vacuum at ambient temperature during 10 min. After several repetitions, the desorption was performed by maintaining a dynamic vacuum and heating. IR spectra were taken at several temperatures: 50, 150, 250 and 350 °C. The numbers of Lewis and Brønsted sites were calculated based on the Beer-Lambert equation as follows (Eq. 2.3):

$$n = \frac{A \cdot S}{\varepsilon \cdot m} \qquad (2.3)$$

Where n is the number of sites, A is the integrated band area, S is the pellet surface, ε is the molar extinction coefficient and m is the sample mass.

2.3. Catalytic tests.

Acrolein production from mixtures of methanol and ethanol was tested in the gas phase. First, in order to find the optimal reaction conditions a method based on Design of Experiment (DoE) was used. This method allowed us to perform such optimization with a minimum number of experiments. Subsequently, the synthesized catalysts performances were examined with procedures described in the following subsections.

2.3.1. Catalytic test rig.

The setup dedicated to the methanol and ethanol oxidative coupling to form acrolein is presented in Figure 2.6.

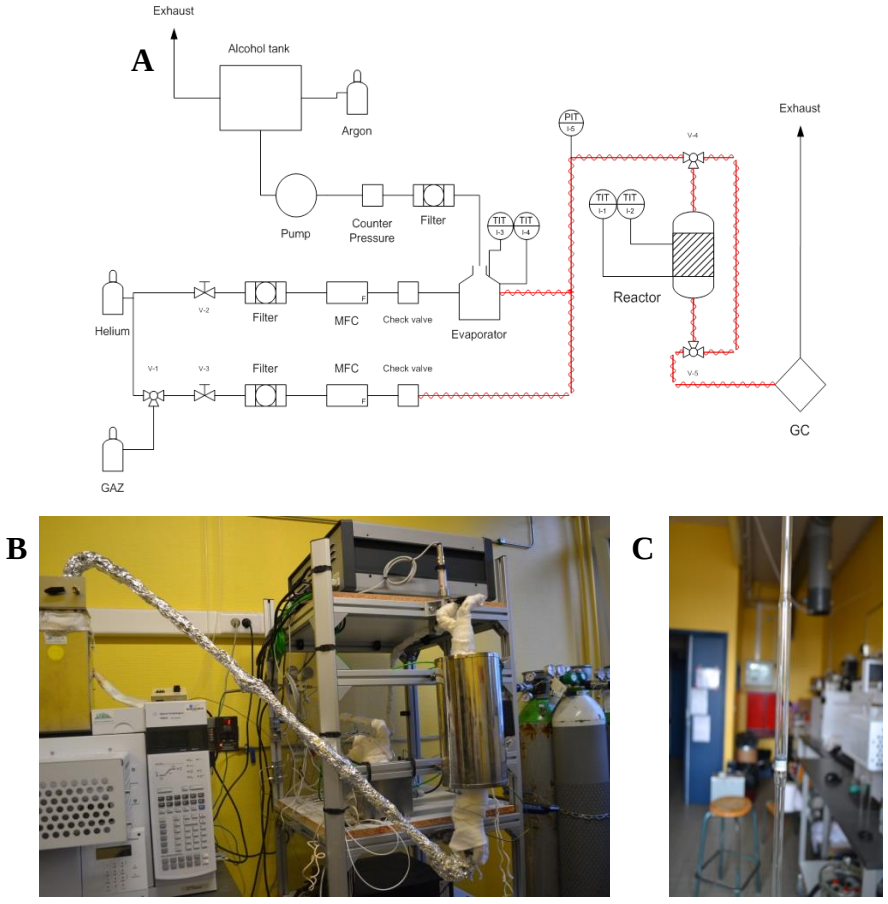

Figure 2.6. A: Schematics of the catalytic test rig, B: Photograph of the setup, C: Close up on the glass fixed-bed reactor.

First, the alcohols mixture was sent by a pump (HPLC pump GILSON) to the vaporizer heated at 120 °C. Simultaneously, helium (carrier gas) and oxygen were flown through the vaporizer. The gases flow rates were monitored using Mass flow Controlers (Brooks controllers). The as-prepared gaseous mixture was sent through heated lines to the glass fixed-bed reactor (Figure 2.6C), which was placed in the furnace (ERALY). The reactor temperature was controlled thanks to a thermocouple connected with the computer. The reaction products were analyzed online using a GC-MS apparatus (Agilent Technologies, 7890A GC System, 5975C VL MSD with Triple Axis Detector) equipped with a ZB-Bioethanol capillary column (Zebron, length 30 m, I.D. 0.25 mm, film thickness 1.0 μm). Due to the possible product condensation and polymerization, it was decided to fix the reactor exit (lines) temperature at 190 °C, based on the literature data collected in Table 2.3.

Table 2.3. Boiling points of the substrates and of the three main reaction products [6].

Product	Boiling point [°C]
Ethanol	78.3
Methanol	64.7
Acrolein	52.6
Formaldehyde	-19.5
Acetaldehyde	20.8

2.3.2. Acrolein production from methanol and ethanol mixtures using a single catalyst.

Two different acrolein synthesis strategies were used: the reaction over one catalyst and the reaction over a tandem of catalysts.

The first strategy was carried out over iron molybdates: 200 mg of catalyst were mixed with the same quantity of carborundum. Both materials were previously sieved to standardize the granulometry at a 125 μm diameter. 500 mg of SiC were then placed at the top of the as-prepared catalytic layer (Figure 2.7).

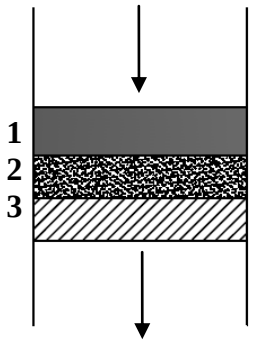

Figure 2.7. Catalytic bed (downflow): 1: 500 mg SiC, 2: 200 mg catalyst + 200 mg SiC, 3: frit.

Depending on their composition, mixtures of methanol, ethanol and oxygen can form flammable atmospheres. Therefore, the O_2 percentage was chosen with a particular attention based on experimental flammability triangles found in the literature (Figure 2.8). The inlet alcohols quantity was fixed at 13.2 vol% and the remainder of the reactional flow consisted of He as the carrier/dilutent gas.

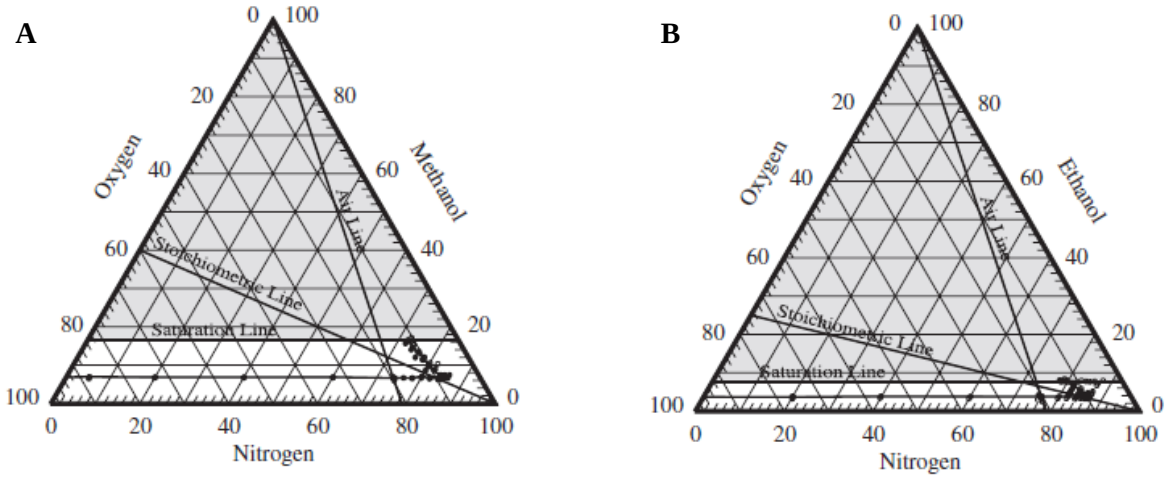

Figure 2.8. Flammability diagrams. A: Methanol, B: Ethanol (25 °C, 1 atm) [7].

2.3.3. Acrolein production from methanol and ethanol mixtures using a tandem of catalysts.

As aforementioned, the second strategy consisted on the utilization of two different catalysts: iron molybdate necessary for the process oxidation part and a basic catalyst, with the purpose of improving the aldol condensation of the as-formed aldehydes to acrolein. The total quantity of the two catalysts was fixed at 200 mg. Their quantity ratio was optimized as well as the way of filling the reactor (*e.g.*, 2 separate beds, mixing, etc…). Figure 2.9 accordingly presents two possible catalytic bed designs. In the A case, both catalysts are mixed together with 200 mg of SiC. In the B case, the catalysts (100 mg

each) are separated by an intermediate layer consisting of 200 mg of carborundum. Each catalyst layer is mixed with 100 mg of SiC.

The next steps are the same as those described above for the first strategy.

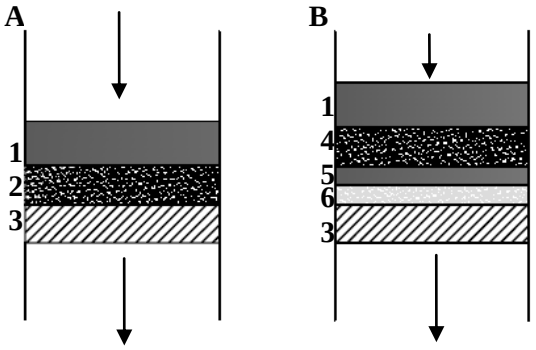

Figure 2.9. Examples of catalytic beds used in strategy 2. A: Mixed catalysts, B: Separated catalysts. 1: 500 mg SiC, 2: 200 mg of two catalysts + 200 mg SiC, 3: filter, 4: $FeMoO_x$ catalyst + SiC, 5: 200 mg SiC, 6: second catalyst + SiC.

2.3.4. Design of experiments (DoE).

In order to find the optimal conditions of methanol and ethanol oxidation process, the Design of Experiments was performed. This method allows to perform the optimization with the lowest possible number of experiments. It concentrates on parameters that influence the most on the reaction giving the information about their importance [8]. General principle of DoE method is presented on Figure 2.10.

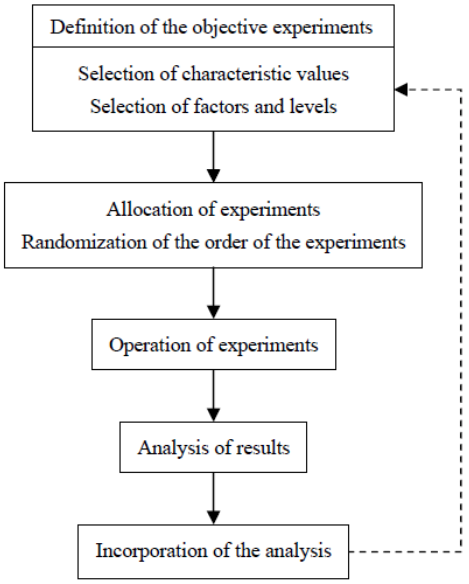

Figure 2.10. General design of experiment process [9].

In the case of the considered reaction herein, there are four independent main factors that can have an influence on the acrolein yield. All of them are presented below with their values range used during optimization:

- Temperature: 25 °- 350 °C,
- Oxygen quantity: 7 - 12%,
- Methanol/Ethanol molar ratio: 0.5 – 2
- GHSV: 3900 – 7700 h^{-1}

In the DoE experiments, the catalyst quantity was kept constant (200 mg). The influence of GHSV (calculated as Standard Gas Flow Rate/Catalyst Volume) was evaluated by changing the total flow rate. Based on the flammability diagrams for the alcohols, helium and oxygen mixture, the alcohols inlet volume was fixed at 13.2% [10]. DoE is based on mathematical matrix and we decided to set up a standard centred composite matrix built of three parts: full factorial matrix, star matrix and central matrix. This type of approach enables obtaining responses surfaces enabling rapid location of an optimum whether local or global. For the complete factorial design, the number of experiments is determined from the following equation (Eq. 2.4):

$$n = n_0 + 2k + 2^k \qquad (2.4)$$

Here, n_0 represents the number of experiments in the centre of the studied domain and k is the factors number. As a consequence, 27 experiments (see Table 2.4) were performed with different operational conditions obtaining acrolein yields as a response [11,12]. The results were treated with the Modde5.0 (UMETRI AB, Box 7960, S-90719 UMEA, Sweden, 2000) software which thanks to mathematical modelling defines correlation between every factor. It was then possible to determine the optimal reaction conditions.

Table 2.4. Experiments conditions used for DoE.

N°	GHSV [1/h]	Temperature [°C]	Quantity of oxygen [Vol.%]	Molar ratio MetOH/EtOH
1	4800	255	8.25	0.875
2	6700	255	8.25	0.875
3	4800	320	8.25	0.875
4	6700	320	825	0.875
5	4800	255	10.75	0.875
6	6700	255	10.75	0.875
7	4800	320	10.75	0.875
8	6700	320	10.75	0.875
9	4800	255	8.25	1.625
10	6700	255	8.25	1.625
11	4800	320	8.25	1.625
12	6700	320	8.25	1.625
13	4800	255	10.75	1.625
14	6700	255	10.75	1.625
15	4800	320	10.75	1.625
16	6700	320	10.75	1.625
17	3900	300	9.5	1
18	7700	300	9.5	1
19	5800	225	9.5	1
20	5800	350	9.5	1
21	5800	300	7	1
22	5800	300	12	1
23	5800	300	9.5	0.5
24	5800	300	9.5	2
25	5800	300	9.5	1
26	5800	300	9.5	1
27	5800	300	9.5	1

2.3.5. Products analysis.

The main reaction products were acrolein, acetaldehyde, formaldehyde, carbon dioxide, dimethyl ether (DME) and methoxyethane. They were quantified by FID except CO_2 (which was detected using a MS detector). An example of an obtained chromatogram is given in Figure 2.11.

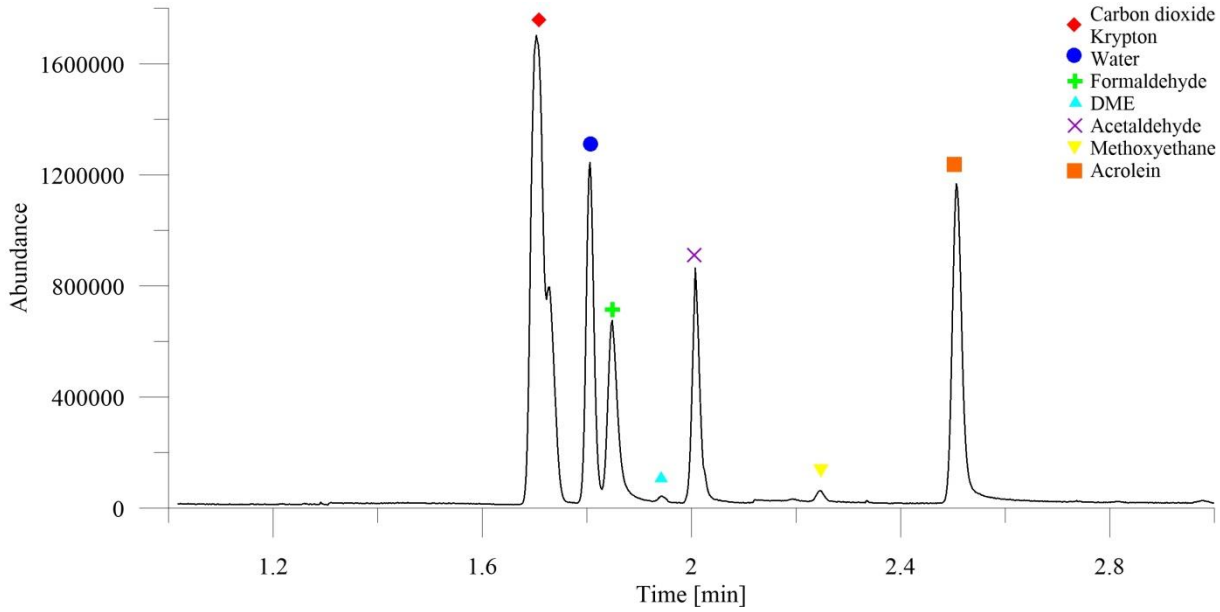

Figure 2.11. Example of an obtained chromatograph with the MS detector.

The obtained peaks were integrated and the surfaces were converted to mole numbers using calibration curves. The calibration was made by liquid injections of products solutions with defined concentrations and surface measurements. Each analysis was repeated three times in order to confirm obtained results. Then, these data were processed to get conversion, selectivity, yields and validated by calculating the carbon balance.

Conversions

The substrates conversions are defined as the proportion of reacted substrate. Equations (Eq. 2.5, 2.6) present the formulas used in this study.

$$X_{MetOH} = \frac{n_{MetOH,in} - n_{MetOH,out}}{n_{MetOH,in}} \cdot 100\% \quad (2.5)$$

$$X_{EtOH} = \frac{n_{EtOH,in} - n_{EtOH,out}}{n_{EtOH,in}} \cdot 100\% \quad (2.6)$$

Selectivities

Selectivity is defined here as the proportion of the obtained product's carbon moles number relative to the total reacted carbon number of moles. In this work, the products selectivity was then calculated as follows (Eq. 2.7-2.12):

$$S_{AC} = \frac{3 \cdot n_{AC}}{(n_{MetOH,in} - n_{MetOH,out}) + 2 \cdot (n_{EtOH,in} - n_{EtOH,out})} \cdot 100\% \quad (2.7)$$

$$S_{Formol} = \frac{n_{Formol}}{(n_{MetOH,in} - n_{MetOH,out}) + 2 \cdot (n_{EtOH,in} - n_{EtOH,out})} \cdot 100\% \quad (2.8)$$

$$S_{MetCHO} = \frac{2 \cdot n_{MetCHO}}{(n_{MetOH,in} - n_{MetOH,out}) + 2 \cdot (n_{EtOH,in} - n_{EtOH,out})} \cdot 100\% \quad (2.9)$$

$$S_{CO2} = \frac{n_{CO2}}{(n_{MetOH,in} - n_{MetOH,out}) + 2 \cdot (n_{EtOH,in} - n_{EtOH,out})} \cdot 100\% \quad (2.10)$$

$$S_{DME} = \frac{2 \cdot n_{DME}}{(n_{MetOH,in} - n_{MetOH,out}) + 2 \cdot (n_{EtOH,in} - n_{EtOH,out})} \cdot 100\% \quad (2.11)$$

$$S_{Methoxyethane} = \frac{3 \cdot n_{Methoxyethane}}{(n_{MetOH,in} - n_{MetOH,out}) + 2 \cdot (n_{EtOH,in} - n_{EtOH,out})} \cdot 100\% \quad (2.12)$$

Yields

The yields were calculated for the three main products: acrolein, acetaldehyde and formaldehyde. Yield can be defined as the ratio between product's carbon moles number and total initial carbon quantity (Eq. 2.13-2.15).

$$Y_{AC} = \frac{3 \cdot n_{AC}}{n_{MetOH,in} + 2 \cdot n_{EtOH,in}} \cdot 100\% \quad (2.13)$$

$$Y_{Formol} = \frac{n_{Formol}}{n_{MetOH,in} + 2 \cdot n_{EtOH,in}} \cdot 100\% \quad (2.14)$$

$$Y_{MetCHO} = \frac{2 \cdot n_{MetCHO}}{n_{MetOH,in} + 2 \cdot n_{EtOH,in}} \cdot 100\% \quad (2.15)$$

Carbon balance

Carbon balance can be described as the proportion between the sum of the total final (recovered/detected) carbon moles number and the total initial carbon number of moles. The experiment can be considered as reliable if the obtained value is close to 100%. During our study, the carbon balance was always comprised between 90-105%, which validated the performed catalytic tests.

$$CB = \frac{(n_{MetOH,unreact}+2\cdot n_{EtOH,unreact}+3\cdot n_{AC}+2\cdot n_{MetCHO}+n_{Formol}+2\cdot n_{DME}+n_{CO2}+3\cdot n_{Methoxyethane})}{n_{MetOH,in}+2\cdot n_{EtOH,in}}\cdot 100\% \quad (2.16)$$

2.4. References.

[1] PCT Patent WO2014068213, assigned to Arkema France, Priority date Oct 17, 2013

[2] *N. Pernicone* Journal of the Less-Common Metals 36 (1974) 289-297

[3] *N. Pernicone et al.* Journal of Catalysis 14 (1969) 293-302

[4] *A. Douy* Journal of European Ceramic Society 7 (1991) 397-403

[5] *S. Brunauer, P.H. Emmett, E. Teller,* Journal of the American Chemical Society 60 (1938) 309

[6] PubChem https://pubchem.ncbi.nlm.nih.gov/, verified 15 May 2016

[7] *M.R. Brooks, D.A. Crowl*, J. of Loss Prevention in the Process Industries, 20 (2007) 144

[8] *S. Bretsznajder et al.* Podstawy ogolne technologii chemicznej, WNT, Warszawa (Poland) 1973

[9]*Park, Gyung-Jin* Analytic Methods of Design Practice, Springer-Verlag London 2007

[10] *M.R. Brooks, D.A. Crowl*, J. of Loss Prevention in the Process Industries, 20 (2007) 144

[11] *G.E.P. Box, WG. Hunter, JS.Hunter*, Statistics for experimenters, John Wiley and Sons, New York 1978 p.653

[12] *J. Goupy*, Plans d'experiences pour surface de reponses, Dunod, 1999, Paris

Chapter 3. Acrolein production from methanol and ethanol mixtures over a single catalyst – results and discussion

In this chapter the methanol and ethanol oxidative coupling to acrolein is studied over FeMo-based catalyst. First, the reaction conditions optimization was performed applying a Design of Experiments (DoE) method. The theoretical results obtained through the mathematical modeling of the data were then experimentally validated. In order to optimize the aldolisation reaction (*i.e.*, the second step to obtain acrolein after oxidation of the respective alcohols to their corresponding aldehydes), the FeMo native formulation was modified by addition of basic elements (*i.e.*, La and Ce). During the preparation, different calcinations temperatures and Mo/Fe ratios were selected in order to determine their influence on the catalytic performances. The materials were characterized by: XPS (including near ambient pressure XPS), BET, XRD, TGA-DSC, XRF, LEIS, CO_2-TPD and pyridine adsorption with FTIR.

3.1. Thermodynamic calculations of methanol and ethanol oxidative coupling to acrolein[*].

As mentioned before, the considered acrolein production process consists of two sequential reactions, namely methanol and ethanol oxidation followed by the as-formed formaldehyde and acetaldehyde condensation. We first checked about thermodynamic limitations and equilibrium reactional mixture composition. For doing so, three hypotheses were formulated:

- Methanol and ethanol oxidation are considered as irreversible and occur at total conversion,

[*] This study was performed in the Laboratoire de Génie des Procédés Catalytiques (LGPC-CNRS/CPE Lyon, 43 bd du 11 Novembre 1918, 69616 Villeurbanne Cedex) with the precious helps of Dr. Yousef Swesi and Prof. Pascal Fongarland.

- Alcohols molar ratio is equal 1,
- There are no sides reactions.

At the equilibrium, in the case of isothermal and isobaric transformations, the Gibbs free energy change is equal to 0 (Eq. 3.1).

$$\Delta G = 0 \tag{3.1}$$

Which can be defined as well as:

$$\Delta G = \Delta G^0 - RTln(K) \tag{3.2}$$

Where *R* is the gas constant equal to 8.314 J/(mol·K) and *K* is the equilibrium constant. Matching these two equations together, we obtain (Eq. 3.3):

$$\Delta G^0 = -RTln(K) \tag{3.3}$$

The thermodynamic equilibrium constant *K* for the general reaction $\vartheta_a A + \vartheta_b B = \vartheta_c C + \vartheta_d$ can be defined as (Eq. 3.4):

$$K = \frac{[C]^{\vartheta_c}[D]^{\vartheta_d}}{[A]^{\vartheta_a}[B]^{\vartheta_b}} \tag{3.4}$$

Therefore, it is possible to determine products and substrates concentrations at the reaction equilibrium. This constant can be calculated from Eq. 3.3 connecting with following relations:

$$\Delta G = \Delta H_T - T\Delta S_T \tag{3.5}$$

$$\Delta H_T = \Delta H^0 + \int_{298}^{T} \Delta Cp dT \tag{3.6}$$

$$\Delta S_T = \Delta S^0 + \ln\left(\frac{T}{298}\right) \int_{298}^{T} \Delta Cp dT \tag{3.7}$$

Here, *H* is the enthalpy, *S* is the entropy and *Cp* is the specific heat. In order to find the equilibrium constant value, standard thermodynamic properties of the considered compounds are reported in Table 3.1.

Table 3.1. Standard thermodynamic properties at 25 °C under a 1 bar pressure for the aldol condensation substrates and their products in the gas phase (data obtained from HYSYS).

Compound	**Molecular formula**	**ΔH_f^0 [kJ/mol]**	**Cp [J· mol/K]**	**S^0 [J· K/mol]**
Acetaldehyde	CH_3CHO	-164.4	53.8	138.2
Formaldehyde	HCHO	-116.0	35.0	160.7
Acrolein	CH_2CHCHO	-70.9	65.8	191.1
Water	H_2O	-284.9	75.7	6.5

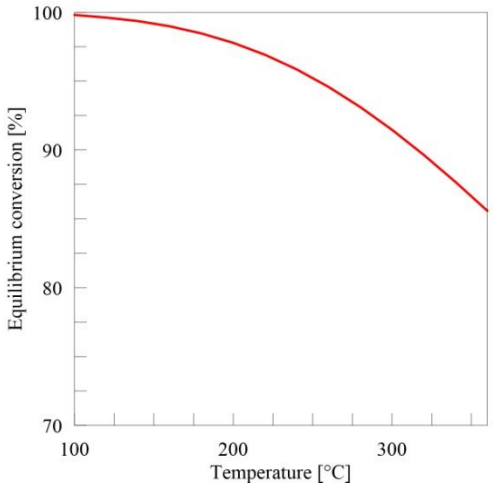

Figure 3.1. Equilibrium acetaldehyde and formaldehyde conversion as a function of temperature.

As mentioned before, the equilibrium constant directly depends on the temperature. For that reason, several approaches for different reaction conditions were screened (Table 3.2). Following that, based on *K* values, formaldehyde and acetaldehyde conversions were calculated and further plotted in Figure 3.1. It can be remarked that with increasing temperature, the considered system equilibrium moves to the reverse reaction to the initial considered reactants.

Table 3.2. Estimated values of ΔG, K and equilibrium compositions for different temperature.

Temperature [°C]	ΔG [kJ/mol]	Constant equilibrium K	Equilibrium composition [$\%_{molar}$]			
			Acetaldehyde	Formaldehyde	Acrolein	Water
100	-38.1	214599.6	0.095	0.095	49.905	49.905
120	-36.3	66998.7	0.191	0.191	49.809	49.809
140	-34.6	23782.7	0.319	0.319	49.681	49.681
160	-32.9	9422.7	0.508	0.508	49.492	49.492
180	-31.3	4104.1	0.768	0.768	49.232	49.232
200	-29.8	1940.5	1.109	1.109	48.891	48.891
220	-28.2	985.7	1.543	1.543	48.457	48.457
240	-26.8	533.2	2.075	2.075	47.925	47.925
260	-25.3	304.8	2.708	2.708	47.291	47.291
280	-23.9	183.0	3.441	3.441	46.558	46.558
300	-22.6	114.8	4.268	4.268	45.732	45.732
320	-21.3	74.9	5.179	5.180	44.820	44.820

Based on the presented results (Table 3.2), the possible maximum acrolein yield at 320 °C was estimated at 89% what indicates the thermodynamical limitation.

3.2. Iron molybdate catalysts characterization.

Based on previous results [1], it was decided to first consider the methanol and ethanol coupling process development using the "conventional" iron molybdate catalyst. The material was synthesized using the procedure presented by *Pernicone et al.* [2,3]. This catalyst is industrially used for the transformation of methanol to formaldehyde. The corresponding active phase has been determined as $Fe_2(MoO_4)_3$. Industrially, it has been demonstrated that, during the methanol oxidation reaction, reduced molybdenum species are progressively stripped out. For this reason, the quantity of molybdenum is usually increased so that to constitute a Mo reservoir, and, *in fine*, the catalyst consists of a mixture of $Fe_2(MoO_4)_3$ and MoO_3. This kind of catalyst is stable and robust, and can be used in industrial reactors during one year and even more, as required. It has been shown that the Mo/Fe ratio plays an important role during the alcohols oxidation reaction [4,5,6,7]. This process is the first stage of the reaction considered herein. For this reason,

catalysts with different theoretical Fe/Mo ratios were synthesized. We also checked the effect of the calcination temperature, which notably induces textural differences.

In order to follow the crystallization of the amorphous powder during the calcination and to choose the *ad-hoc* calcination temperature, we performed TGA and DSC measurements of the uncalcined samples. They were placed under air flow (100 mL/min) and heated them up to 600 °C (heat rate 10 °/min). Figure 3.2 presents the TGA analysis (*i.e.*, evolution of catalyst mass during the heating of the sample) for tree different Mo/Fe ratio (*i.e.*, 1.5, 2 and 2.5). Weight lost occured before 300 °C for all the samples starting from 100 °C. In that temperature an endothermic peak is observed at DSC curves (Figure 3.3). These phenomena are assigned to the decomposition of the precursors and a loss of H_2O and NH_3.

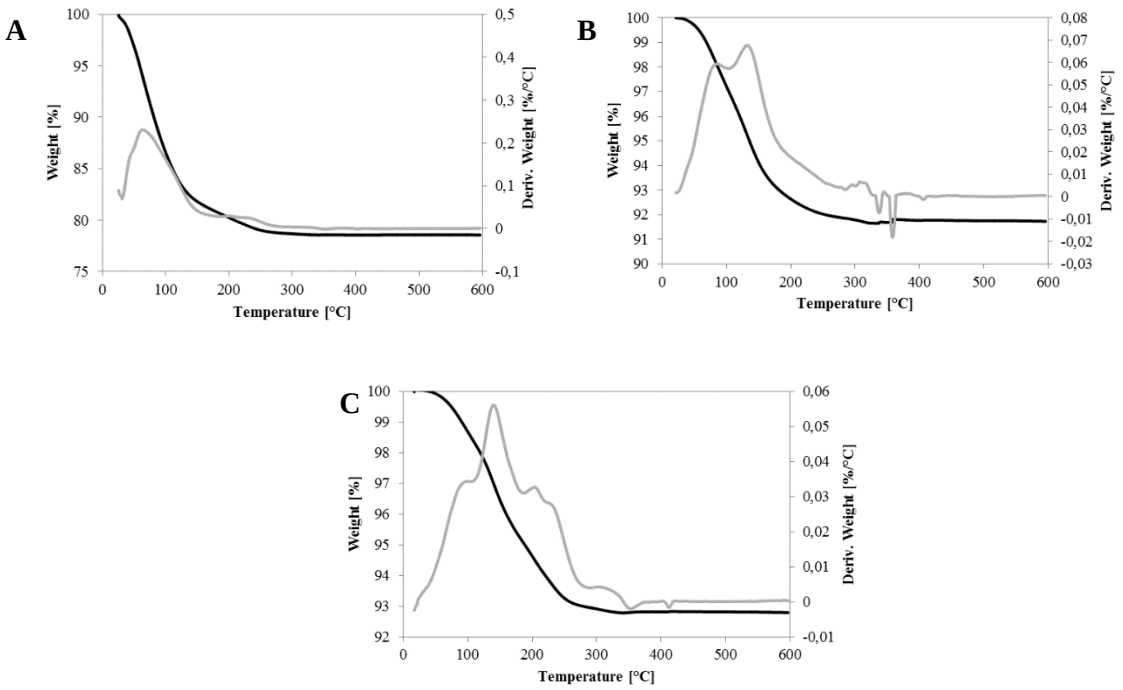

Figure 3.2. TG(black) and DTG(grey) curves for A: FeMo1.5, B: FeMo2.0, C: FeMo2.5. The analysis was performed in the temperature range 20-600 °C with heating rate of 10 °C/min under air flow.

After the endothermic peaks at 100°C, the DSC curves for synthetized FeMo catalysts exhibit two exothermic peaks around 400 °C (Figure 3.3). These phenomena correspond to the crystallization of the different phases present in the samples. In order to identify these formed phases, XRD analysis was performed.

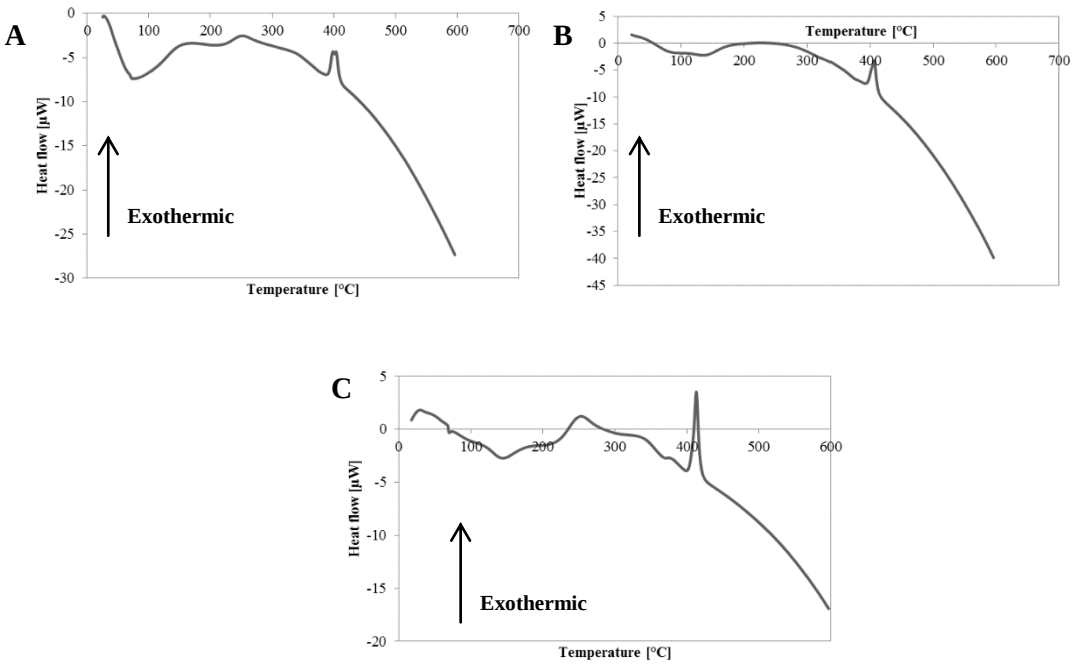

Figure 3.3. DSC curves for A: FeMo1.5, B: FeMo2.0, C: FeMo2.5. The analysis was performed in the temperature range 20-600 °C with a heating rate of 10 °C/min under air flow

XRD-HT analysis gave similar results over all the FeMo catalysts (Annex: Figure C.1-2). In Figure 3.4, the results for FeMo2.0 are presented as an example. The crystallization process starts at 400 °C. This temperature is in agreement with the aforementioned TGA-DSC data. Note that two peaks observed at 2θ 28 and 44° correspond to Ag of the sample holder. The phases identification was performed using the Eva software (Figure 3.4.B). As expected, we observed the formation of two phases for the reference Fe-Mo catalyst: $Fe_2(MoO_4)_3$ (#PDF 00-031-0642) and MoO_3 (#PDF 01-089-5108). In Table 3.3, the relative proportion for each phase determined by Eva software is presented. As expected, the $Fe_2(MoO_4)_3$ phase relative quantity increased when decreasing the Mo/Fe ratio. Note that we did not obtain the pure $Fe_2(MoO_4)_3$ phase with the ratio Mo/Fe = 1.5.

Table 3.3. Phases proportions obtained from XRD analysis.

Catalyst	$Fe_2(MoO_4)_3$ content [%]	MoO_3 content [%]
FeMo1.5	75	25
FeMo2.0	67	33
FeMo2.5	66	34

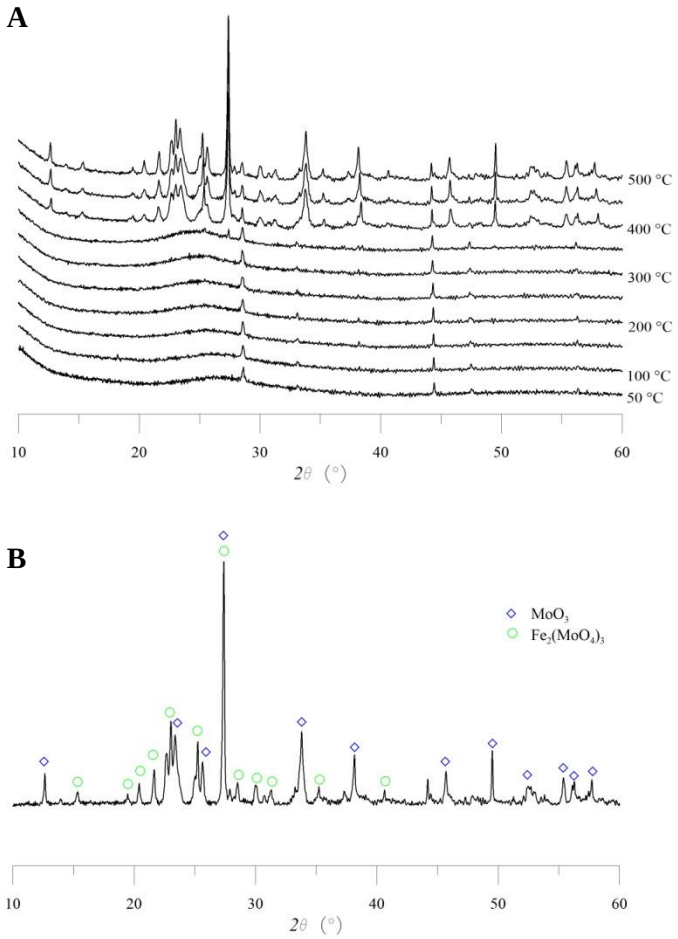

Figure 3.4. A: XRD-HT diffractograms for FeMo2.0; B: XRD patterns at room temperature with phases matching for FeMo2.0.

Then, in order to determine the FeMo catalysts surface compositions, XPS analysis was performed. Figure 3.5A and B present the decomposed spectra corresponding to the Fe2p and Mo3d respectively for the FeMo2.0 sample (450 °C). The Mo 3d doublet is present at binding energies of 232.8 and 235.9 eV. These values correspond to Mo^{+VI} [8]. This oxidation level is in agreement with the two crystalline phases detected by XRD. In the case of iron (Figure 3.5A), Fe $2p_{1/2}$ and Fe $2p_{3/2}$ components are located at 711.9 and 726.2 eV. These values correspond to the + III oxidation state of iron [9,10]. Indeed, the Fe $2p_{3/2}$ peak located at 711.9 eV presents an asymmetric character due to multiplet splitting of high spin Fe^{III} ions [11] and it has an associated satellite peak located at around 8 eV at higher energy. Similar XPS spectra were observed for all tested samples. For FeMo1.5, FeMo2.0 and FeMo2.5, the surface Mo/Fe ratio is higher than the theoretical one, indicating an enrichment of the surface in Mo.

Table 3.4. XPS results for synthetized FeMo1.5, FeMo2.0, FeMo2.5 calcined in different temperatures.

Catalyst	Energy level		FWHM		Atom concentration [%]			Mo/Fe ratio
	Mo3d	Fe2p	Mo3d	Fe2p	Mo3d	Fe2p	C1s	
FeMo1.5(450°C)	233.2	712.1	1.12	2.49	18.1	4.0	24.8	4.5
FeMo2.0(450°C)	232.8	711.9	1.10	2.83	16.8	6.4	26.1	2.6
FeMo2.5(450°C)	233.0	711.9	1.13	2.32	10.3	1.9	50.1	5.4

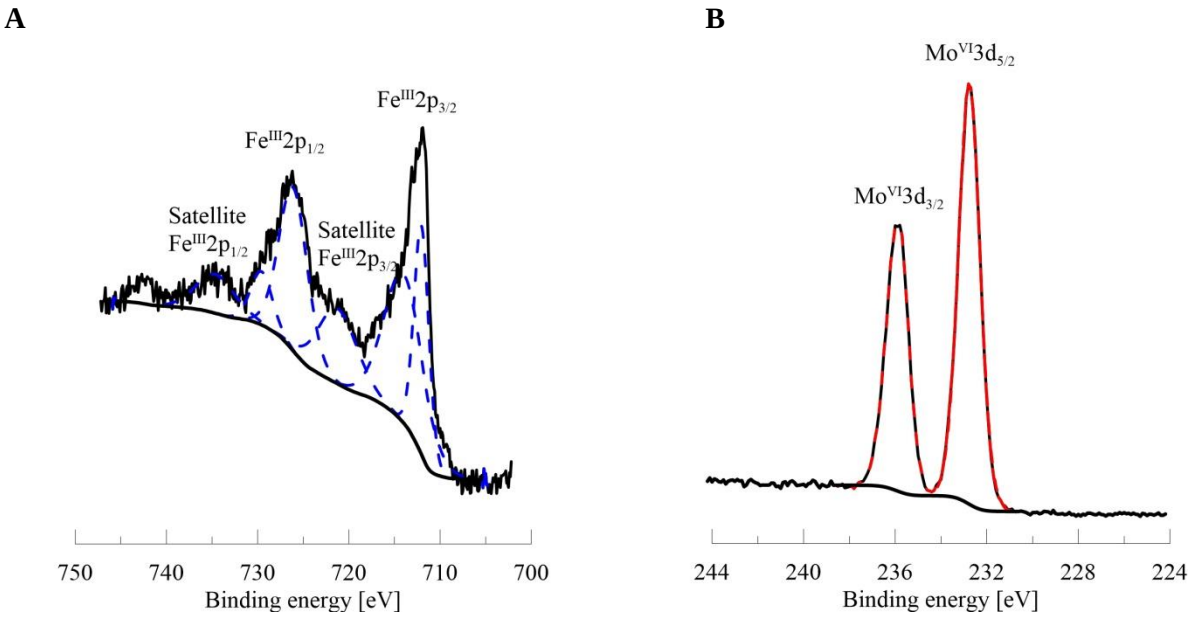

Figure 3.5. XPS analysis results for FeMo2.0 catalyst. A: Fe 2p; B: Mo 3d.

The specific surface area (SSA) was measured using the single point BET method (Table 3.5**)**. The samples developed low SSAs and the highest value was measured for FeMo2.0 and 2.5 with values at around 5 m^2/g. These values are very low, but consistent with this kind of bulk catalysts. Regarding the evolution of the SSA, it seems that the slight increase is linked with the proportion of the MoO_3 phase determined by XRD analysis.

Table 3.5. Catalysts specific surface areas measured by the BET method.

Catalyst	Specific surface area [m^2/g]
FeMo1.5(450°C)	1.8
FeMo2.0(450°C)	5.1
FeMo2.5(450°C)	5.1

3.3.Design of experiments.

The DoE was performed for the industrial FeMo catalyst provided by Arkema, so that to use a homogeneous material from a unique batch. Figure 3.6 shows the results obtained for a characteristic catalytic test - alcohols conversion and products selectivities (*e.g.* acrolein, formaldehyde, acetaldehyde, etc…) in a function of time. After 3 or 4 hours, depending of the conditions/catalysts, the system reached an equilibrium. The results used for the DoE are taken at the equilibrium. For all the runs, the carbon balance was between 90 and 105%.

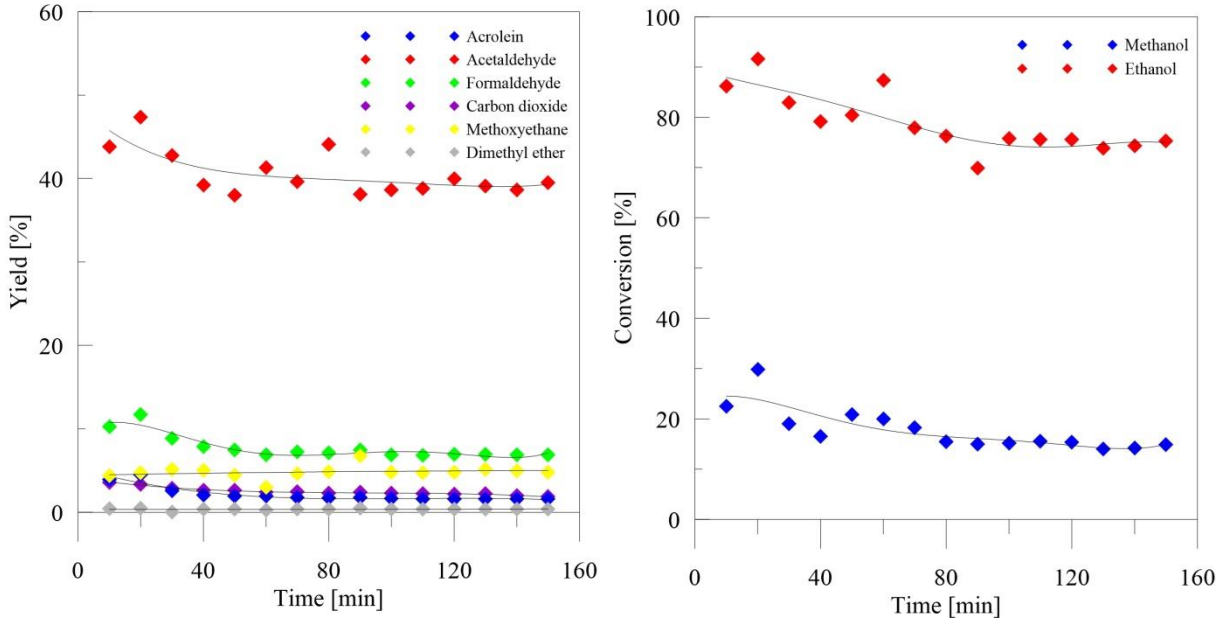

Figure 3.6. Experimental results for the following conditions: GHSV = 6700 h^{-1}, O_2 = 8.3%, Temperature = 320 °C, MetOH/EtOH = 0.875.

27 experiments were performed in the experimental domain summarized for the four factors in Table 3.7. The levels "0" were chosen based on technical constraints (*e.g.*,

maximum temperature acceptable by the setup, explosive limit, …) and on literature data (*e.g.*, GHSV, etc…). The calculated output parameters were acrolein, formaldehyde and acetaldehyde yields.

Based on the experimental results (Figure 3.6), it was possible to mathematically build relationships between the chosen factors and to model their influence on the acrolein yield: 3D figures were obtained as results visualization (Figure 3.7) based on the mathematical model represented in equation (Eq.3.8):

$$y = b_0 + \sum_i b_i x_i + \sum_i b_i x_i^2 + \sum_{ij} b_{ij} x_i x_j \quad (3.8)$$

With:

y – response (*i.e.*, acrolein yield)

b_0 – constant

b – coefficient of the model calculated from the relation $b = (x^t \cdot x) \cdot x^t \cdot y$ (x is the matrix in coded variables, x^t is transposed matrix and y is the matrix of answers).

The Analysis of Variance (ANOVA) results of the model indicated a good performance with R^2 and Q^2 of 0.95 and 0.646, respectively. These values mean that over 95 percent of the data could be explained by the model [12,13].

Table 3.6. Experimental domain and coding of variables for experimental design on acrolein production

Factor	**-α**	**-1**	**0**	**+1**	**+α**	**Standard Coefficient**
Temperature[°C]	225	255	300	320	350	14.16
Oxygen quantity[%]	7	8.25	9.5	10.75	12	2.86
Gas space velocity[h^{-1}]	3900	4800	5800	6700	7700	-0.13
Ratio MetOH/EtOH	0.5	0.875	1	1.625	2	1.56

Table 3.7. Results of the 27 runs of the DoE strategy.

N°	GHSV [1/h]	Temperature [°C]	Quantity of oxygen [%]	Ratio MetOH/EtOH	Acrolein Yield [%]	Acetaldehyde Yield [%]	Formaldehyde Yield [%]	Potential Acrolein Yield [%]
1	4800	255	8.25	0.875	0.3	22	2.9	7.3
2	6700	255	8.25	0.875	1.6	39	6.9	18.1
3	4800	320	8.25	0.875	15.2	46	23	70
4	6700	320	8.25	0.875	35	26	36	66
5	4800	255	10.75	0.875	1.5	34	5.8	15.4
6	6700	255	10.75	0.875	1	32	5.2	13.4
7	4800	320	10.75	0.875	35	31	33	73
8	6700	320	10.75	0.875	34	31	36	71
9	4800	255	8.25	1.625	3.1	7.8	10.4	12.5
10	6700	255	8.25	1.625	3.9	32	13.6	37
11	4800	320	8.25	1.625	31	30	48	67
12	6700	320	8.25	1.625	32	33	49	71
13	4800	255	10.75	1.625	4.2	29	11.8	32
14	6700	255	10.75	1.625	1	26	7.1	18.1
15	4800	320	10.75	1.625	19.5	57	34	88
16	6700	320	10.75	1.625	28	34	45	69
17	3900	300	9.5	1	26	38	28	72
18	7700	300	9.5	1	27	36	34	70
19	5800	225	9.5	1	3.4	41	9.6	26
20	5800	350	9.5	1	34	28	33	68
21	5800	300	7	1	7.7	44	16	46
22	5800	300	12	1	38	23	36	66
23	5800	300	9.5	0.5	19.7	55	19	65
24	5800	300	9.5	2	29	23	49	57
25	5800	300	9.5	1	24	33	34	64
26	5800	300	9.5	1	25	35	35	67
27	5800	300	9.5	1	25	35	35	67

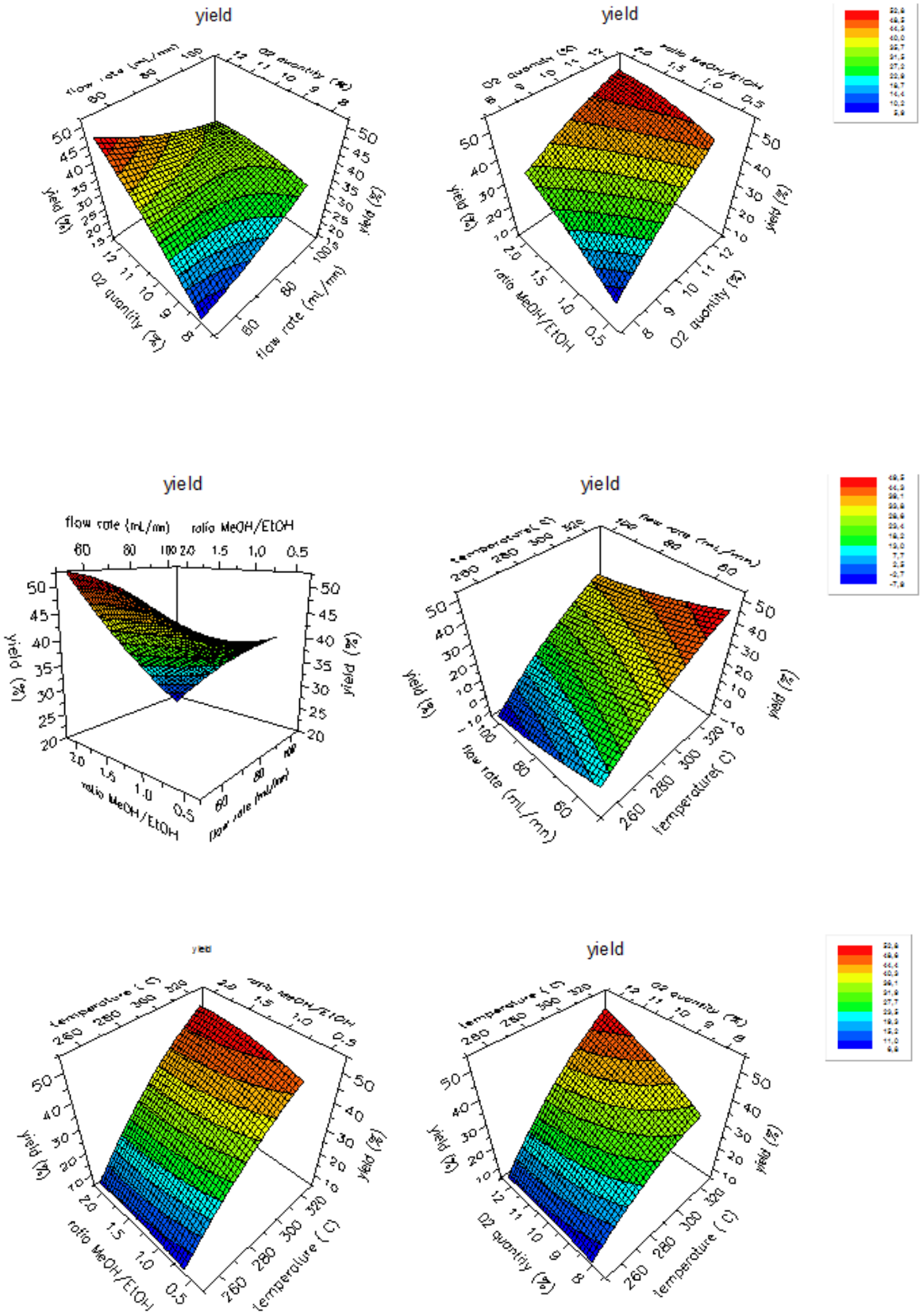

Figure 3.7. 3D figures obtained with DoE.

In Figure 3.7, each graph represents the combined influences of two different factors on the acrolein yield. The red colour indicates the highest acrolein yield and the blue one the lowest one. The factors influence is expressed with Standard Coefficient (Table 3.6) determined using the least squares method, and we thus found that the temperature was the parameter the most sensitive towards the acrolein yield while the total flow rate was the lowest one.

According to the aforementioned results, the following conditions were determined as optimal to obtain the acrolein yield as high as possible: temperature 320 °C, GHSV 3900h^{-1}, oxygen quantity 12% and alcohol ratio (methanol/ethanol) 1. However, we can remark that the curves maxima are placed nearby the fixed factors limits. In our case, we could not explore further these limits, because of the flammability triangle limitation (O_2 quantity) and the set up limitations (temperature). The prediction of the model is an acrolein yield equal to 50% for the optimal factors theoretical values mentioned before.

Afterwards, the optimal point mathematically found for the industrial FeMo catalyst was experimentally verified. Figure 3.8 presents the evolution of acrolein, formaldehyde and acetaldehyde yields during the reaction performed using the optimal conditions for strategy 1 (*i.e.*, GHSV = 3900 h^{-1}, O_2 = 12%, Temperature = 320 °C and MetOH/EtOH = 1). In this case, the stability of the system was reached after only 40 minutes. The acrolein yield reached 44% with alcohols conversion of 100%.

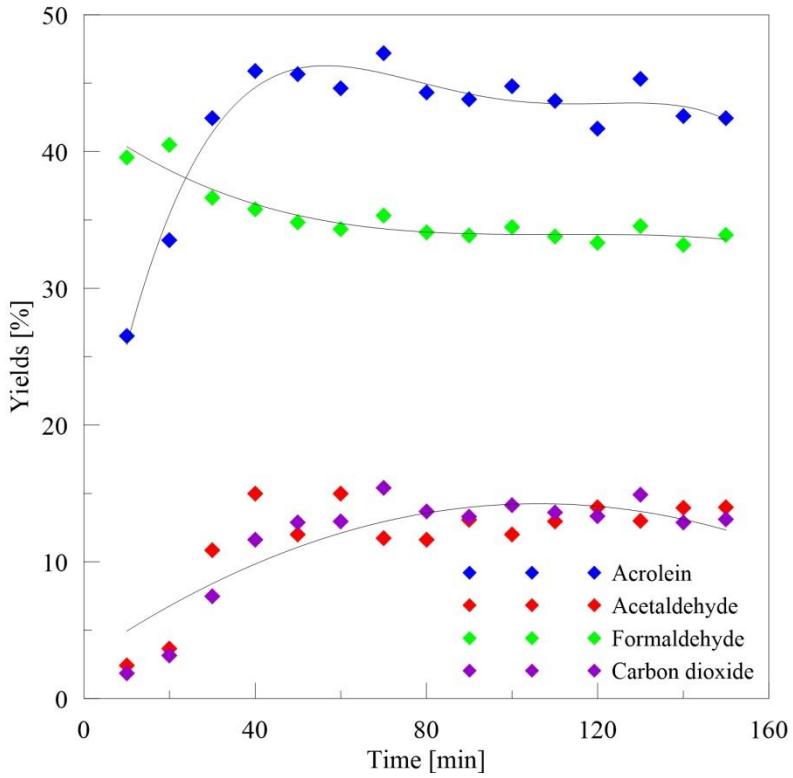

Figure 3.8. Catalytic test in the optimal conditions over the commercial FeMo catalyst (GHSV = 3900 h^{-1}, O_2 = 12%, Temperature = 320 °C and MetOH/EtOH = 1

Using the same set of data (Table 3.7), the optimal reaction conditions were calculated for the tandem strategy (*i.e.*, use of two catalysts, with the second one to further promote the aldolisation reaction). In order to determine the highest potential acrolein yield with a second catalyst addition using following equation (Eq. 3.9):

$$Y_{ACpot} = Y_{AC} + 80\%\min(1.5Y_{MetCHO}, 3Y_{Formol}) \qquad (3.9)$$

In this relation, the obtained acrolein yield (Y_{AC}) during DoE is summed with the lower value between acetaldehyde yield (Y_{MetCHO}) and formaldehyde yield (Y_{Formol}). Values 1.5 and 3 comes from carbon number in the acrolein molecule (*i.e.*, 3) divided by aldehydes carbons atoms content (*i.e.*, 2 and 1 for acetaldehyde and formaldehyde, respectively). It was found that its highest value (*i.e.*, 88%) can be obtained with the following conditions: temperature 320 °C, GHSV 4800 h^{-1}, oxygen quantity 10.75% and alcohol ratio (methanol/ethanol) 1.625. This optimal point was used therefore for second strategy (*i.e.*, tandem of catalysts).

3.4.Catalytic performance measurement – iron molybdate catalysts.

Catalytic activity of the synthesized materials was explored in the optimal conditions found owing to the DoE strategy (*i.e.*, GHSV = 3900 h^{-1}, O_2 = 12%, Temperature = 320 °C, MetOH/EtOH = 1).

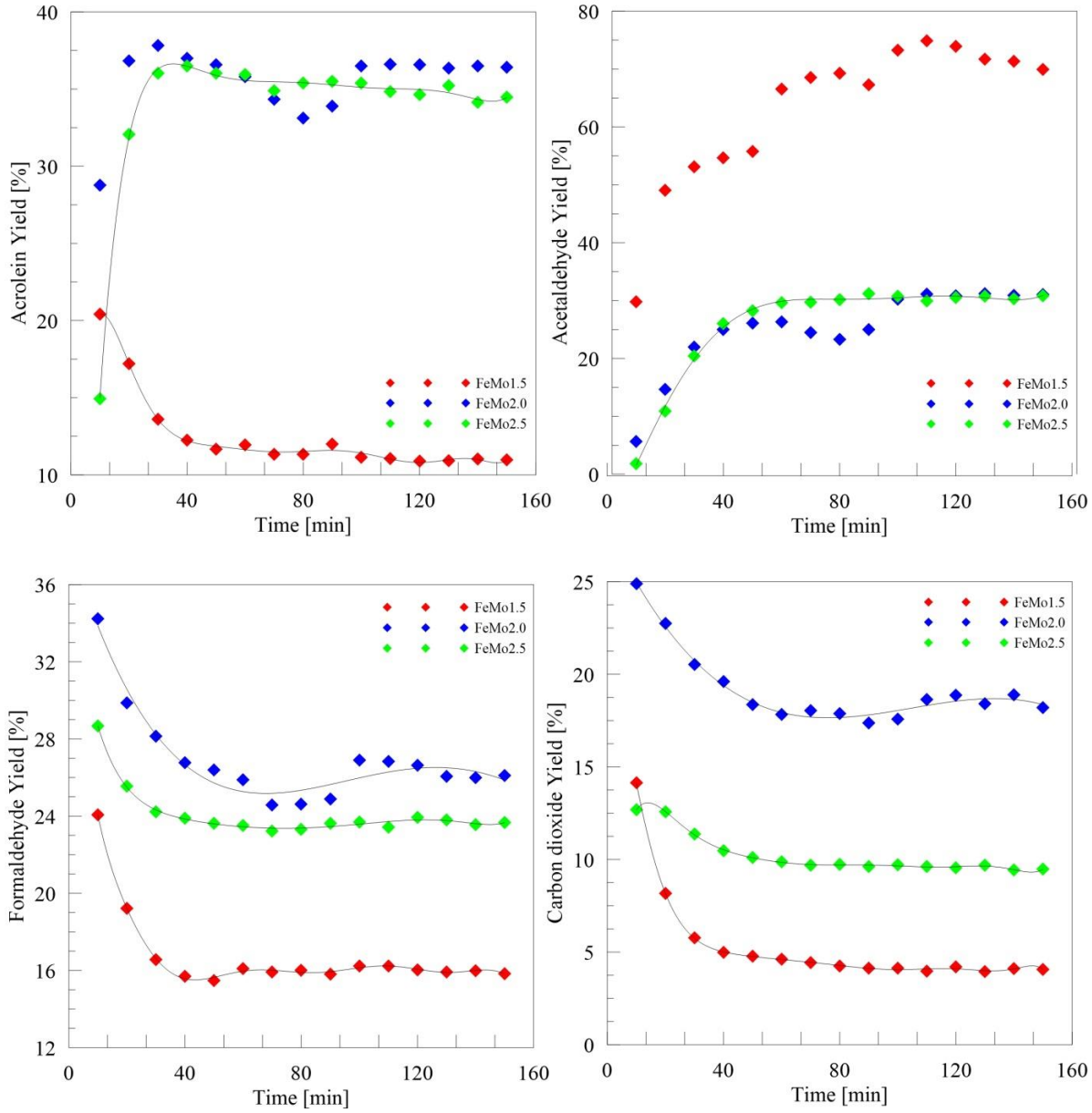

Figure 3.9. Acrolein, acetaldehyde, formaldehyde and carbon dioxide yields evolution as a function of time on f stream for FeMo1.5, FeMo2.0 and FeMo2.5 calcined at 450 °C (GHSV = 3900 h^{-1}, O_2 = 12%, Temperature = 320 °C, MetOH/EtOH = 1).

The main detected products were acrolein, acetaldehyde, formaldehyde and carbon dioxide. In Figure 3.9, the evolution of the products yields for the FeMo catalysts

calcined at 450 °C is presented as a function of time on stream. As expected, the Mo/Fe ratio had a critical influence on the catalytic performances. The behavior of FeMo1.5 was very different from that of FeMo2.0 and FeMo2.5. FeMo1.5 exhibited the lowest acrolein yield (*i.e.*, 11%), which was obtained after a progressive decrease, while, for FeMo2.0 and FeMo2.5 the acrolein yield increased during an induction phase to *ca.* 36.5 %. FeMo1.5 produced more acetaldehyde, which did not react to further form acrolein.

Table 3.8 shows catalytic tests results after 2.5 h for the FeMo catalysts calcined at different temperatures. This parameter had a strong influence on the products yields, particularly for the Mo/Fe ratio of 2.0. In this case, decreasing the temperature caused a decrease in acrolein yield (*i.e.* up to 11.5%). The same behavior was less pronounced for FeMo1.5, while for FeMo2.5, the calcination temperature had not influence (*i.e.*, the best result was obtained for a calcination temperature of 400 °C).

Table 3.8. Catalytic tests results for the FeMo catalysts calcined at different temperatures, after 2.5 h on stream (GHSV = 3900 h^{-1}, O_2 = 12%, Temperature = 320 °C, MetOH/EtOH = 1).

Catalyst	Conversion [%]		Yield [%]			
	Ethanol	**Methanol**	**Acrolein**	**Acetaldehyde**	**Formaldehyde**	**CO_2**
FeMo1.5(450°C)	99	100	11	71	16	4
FeMo1.5(400°C)	97.5	100	9	73	14	3.5
FeMo1.5(350°C)	98	100	7.5	75	13.5	3
FeMo2.0(450°C)	100	100	36.5	31	26	18.5
FeMo2.0(400°C)	100	100	27.5	50	21	7
FeMo2.0(350°C)	100	100	15	54	20.5	15
FeMo2.5(450°C)	100	100	35	30	24	9.5
FeMo2.5(400°C)	100	100	39	27	23	11
FeMo2.5(350°C)	100	100	31	3	26	16.5

3.5.Modified iron molybdate catalysts – characterization.

The ultimate purpose of our work was to obtain the highest possible acrolein yield. To this respect, the efficiency of the second process stage, namely formaldehyde and acetaldehyde aldolization, is also an important parameter. The literature review presented in the Chapter 1 shows that this reaction is mostly catalyzed by basic catalysts. Thus, it was decided to add basic elements in the native FeMo formulation. During the synthesis

of these samples, several factors were varied: the additive (*e.g.*, lanthanum or cerium), the Mo/Fe ratio (*e.g.*, 1.5, 2.0 and 2.5) and the calcination temperature (350 °C, 400 °C and 450 °C). Afterwards, the as-obtained catalysts were characterized by differential thermal analysis-thermogravimetric analysis (TGA-DSC), X-ray diffraction (XRD), X-ray photoelectron spectroscopy (XPS), nitrogen single-point adsorption (BET), X-ray fluorescence (XRF) and temperature-programmed reduction (TPR) before catalytic tests.

Differential thermal analysis and thermogravimetric analysis and X-ray diffraction gave results were similar to those of the conventional FeMo catalysts presented previously (Annex: Figure B.1-4, Figure C.3-4). This is due to the fact that only very small quantities of lanthanum and cerium were added (*i.e.*, 1% $_{molar}$).

The XPS results are presented in Table 3.9. Like for the non-doped FeMo samples, the surface Mo/Fe ratio obviously deviated from the theoretical composition (for all the samples, the experimental ratio was higher than the bulk one), but with a clear influence of the addition of basic elements.

Table 3.9. XPS results for FeMoCe1.5, FeMoLa1.5, FeMoCe2.0, FeMoLa2.0, FeMoCe2.5, FeMoLa2.5 after calcination at 450 °C.

Catalyst	Position		FWHM		Atom concentration [%]			Mo/Fe
	Mo3d	Fe2p	Mo3d	Fe2p	Mo3d	Fe2p	C1s	ratio
FeMoCe1.5(450°C)	232.9	711.9	1.16	2.74	17.5	4.8	25.0	3.6
FeMoLa1.5(450°C)	233.0	711.9	1.20	2.85	10.6	3.8	49.5	2.8
FeMoCe2.0(450°C)	232.9	711.9	1.14	2.66	11.9	2.6	48.4	4.6
FeMoLa2.0(450°C)	232.8	711.8	1.09	2.85	16.7	4.5	29.5	3.7
FeMoCe2.5(450°C)	232.9	711.8	1.18	2.61	15.1	4.0	33.8	3.8
FeMoLa2.5(450°C)	232.9	712.3	1.24	3.12	12.6	3.2	43.9	3.9

La and Ce were not detected at the surface of the catalysts, which can be due to their low quantities and also to the way they have been introduce in the solids (*i.e.*, coprecipitation method and not impregnation). One doubt still exists due to the fact that La 3d and Ce 3d signals can be hidden by the Auger signal of Iron. In order to clarify this point, we performed LEIS analysis for FeMo2.0, FeMoCe2.0 and FeMoLa2.0. This technique enables probing the first atomic layer of the samples (Figure 3.10).

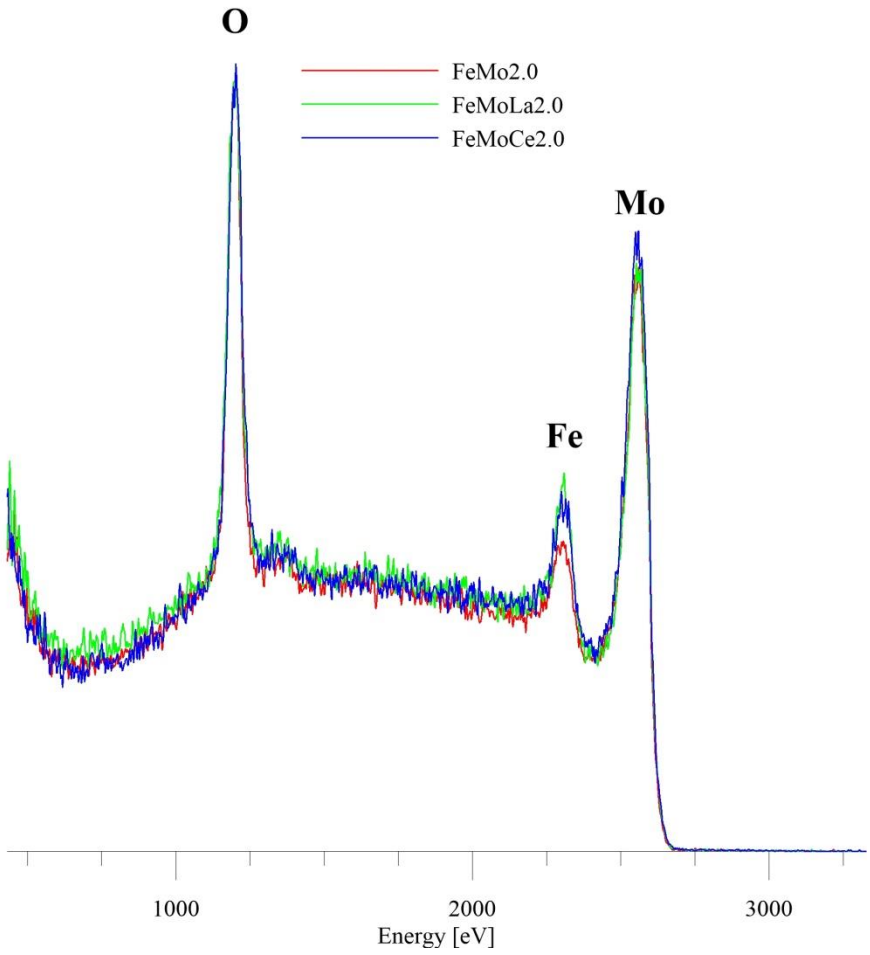

Figure 3.10. LEIS spectra of FeMoLa, FeMoCe and FeMo. (The LEIS spectra are normalised regarding the O peak).

Only three peaks assigned to O, Fe and Mo were detected. The absence of Ce and La signals on these spectra is a direct proof that such species where actually not present at the surface of the materials. Further, this suggests that any modification of the basic character of the catalyst would be an indirect phenomenon. Probably, lanthanum and cerium could have not been measured because of the LEIS detection limit is in 500 – 10 ppm of a monolayer range for higher masses elements. Moreover, these two LEIS spectra (*i.e.*, FeMoCe2.0 and FeMoLa2.0) are similar to that of the FeMo reference catalyst, but with different relative intensities. The LEIS surface Mo/Fe ratio was calculated (Table 3.10), which showed that the introduction of basic elements caused the iron atoms migration to the surface.

Table 3.10. Mo/Fe ratios of FeMo2.0, FeMoCe2.0 and FeMoLa2.0 calcined at 450 °C obtained with LEIS.

Mo/Fe ratio		
FeMo2.0	**FeMoCe2.0**	**FeMoLa2.0**
6.7 (±0.9)	5.5 (±0.2)	4.5 (±0.2)

In order to confirm the actual incorporation of the basic elements which were not detected neither by XPS nor by LEIS, X-ray fluorescence experiments were performed. The catalysts calcined at 450°C were analysed (Table 3.11). La and Ce were detected in very low concentrations (limit of detection of the apparatus) and their quantification was not possible. These additives are then mostly located in the catalyst bulk. The Mo/Fe ratios in the catalysts bulk was determined as well by this method (Table 3.11). The obtained values are lower than those determined by XPS. These results suggest a migration of molybdenum species at the surface of the solids.

Table 3.11. XRF results for FeMo and modified FeMo catalysts calcined in 450 °C.

Catalyst	**Molar concentration [%]**				**Mo/Fe Ratio**
	Mo	**Fe**	**La**	**Ce**	
FeMo1.5	20.2	7.6	-	-	2.6
FeMoCe1.5	18.9	9.7	-	Trace	1.9
FeMoLa1.5	19.4	8.9	Trace	-	2.2
FeMo2.0	20.1	7.8	-	-	2.6
FeMoCe2.0	20.4	7.3	-	0.001	2.8
FeMoLa2.0	20.1	7.9	Trace	-	2.5
FeMo2.5	20.8	6.7	-	-	3.1
FeMoCe2.5	20.4	7.3	-	0.001	2.8
FeMoLa2.5	20.1	7.9	Trace	-	2.6

Table 4.9 presents the SSAs of the catalysts with the different Mo/Fe ratios. The observed values are low and no clear trend could be observed.

Table 3.12. Catalysts specific surface areas measured by the BET method.

Catalyst	Specific surface area [m^2/g]
FeMoCe1.5(450°C)	5.8
FeMoLa1.5(450°C)	5.6
FeMoCe2.0(450°C)	7.5
FeMoLa2.0(450°C)	12.2
FeMoCe2.5(450°C)	4.5
FeMoLa2.5(450°C)	6.3

The La and Ce addition was expected to bring more basic sites to the FeMo catalyst, which would theoretically improve the second process stage – formaldehyde and acetaldehyde condensation. These elements were not present at the surface of the solids (XPS, LEIS), but we decided to check the potential influence of their introduction on the acid-base properties of the synthesized materials. CO_2-TPD analysis was performed for the FeMo2.0, FeMoCe2.0 and FeMoLa2.0 samples calcined at 450 °C (Figure 3.11).

First of all, the CO_2 desorbed quantities were very low due to the very low SSAs (at max 10.24 m^2/g). The CO_2 desorption occurred at different temperatures, according different strengths of the basic sites. All the samples exhibited 3 peaks at 300, 450 and 700 °C, characteristics of weak, medium basic sites (for the two first) and strong basic sites (for the last one), respectively. The total desorbed carbon dioxide quantities were calculated and are presented in Figure 3.11. Introduction of La and Ce in the FeMo based catalysts actually induced an increase in the number of basic sites, which is an indirect phenomenon, as these elements are not present at the surface (*i.e.*, absence of signal in XPS and LEIS). However, thanks to LEIS analysis (Table 3.10) we suppose that the acidity increase comes from the iron atoms migration on the surface (*i.e.*, decreasing Mo/Fe ratio) observed for doped catalysts.

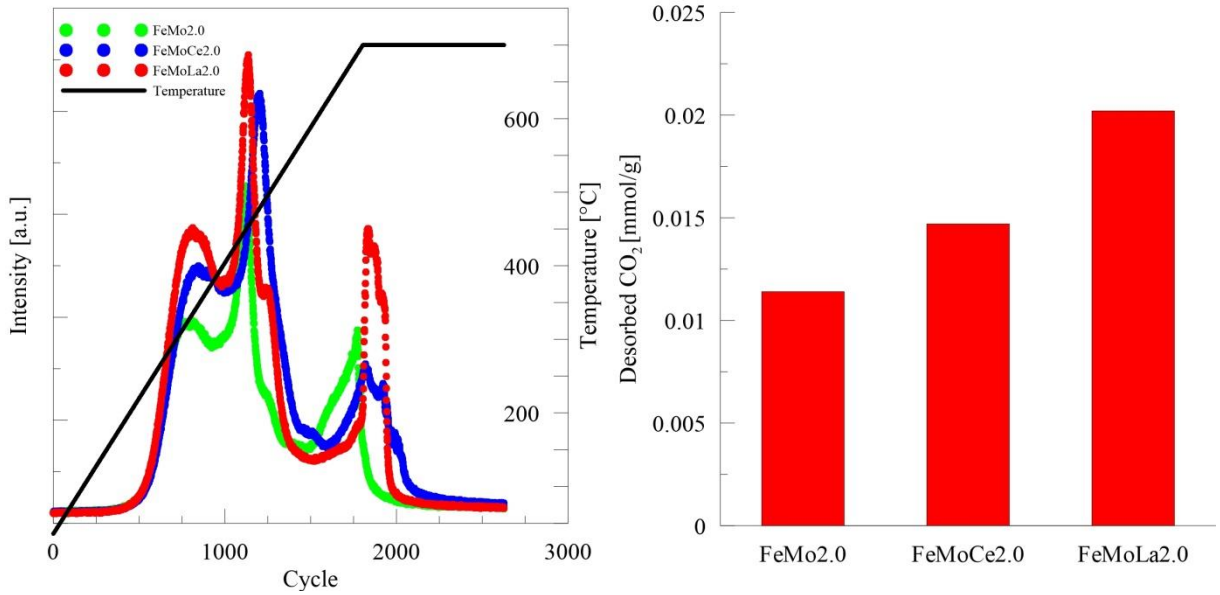

Figure 3.11. CO_2-TPD results for FeMo2.0, FeMoCe2.0 and FeMoLa2.0 calcined at 450 °C.

As previously shown [7], the FeMo-based catalysts also present acid sites. In order to characterize them, we have performed pyridine adsorption followed by FTIR. This technique allows identifying the type of sites (*i.e.*, Brønsted or Lewis) as well as quantifying their number (Figure 3.12). Like for the basic sites, the number of acid sites is quite low due to the low SSA of the materials. The FTIR spectra were recorded after pyridine adsorption and thermal treatment at different temperatures. After heating at 350 °C, no signal was observed, indicating that the catalysts do not behave very strong acid sites. The Lewis acid sites are characterized by a band located at 1450 cm^{-1} and the Brønsted acid sites are characterized by a band located at 1525 cm^{-1}. All the samples have a higher number of Lewis acid sites compared to the Brønsted ones (Figure 3.13). The sample presenting the highest acid site number is also that presenting the higher basic sites numbers: FeMoLa2.0 (12 mmol/g). Comparing with the obtained results with CO_2-TPD shown previously (Figure 3.11), we can conclude that the addition of La generates not only basic but also acid sites. However, the acid sites are more numerous over all the analyzed catalysts. For example, in the case of FeMoLa2.0, it was found that there is 0.02 mmol/g of basic sites while the quantity of acid ones reaches 12 mmol/g (Figure 3.13).

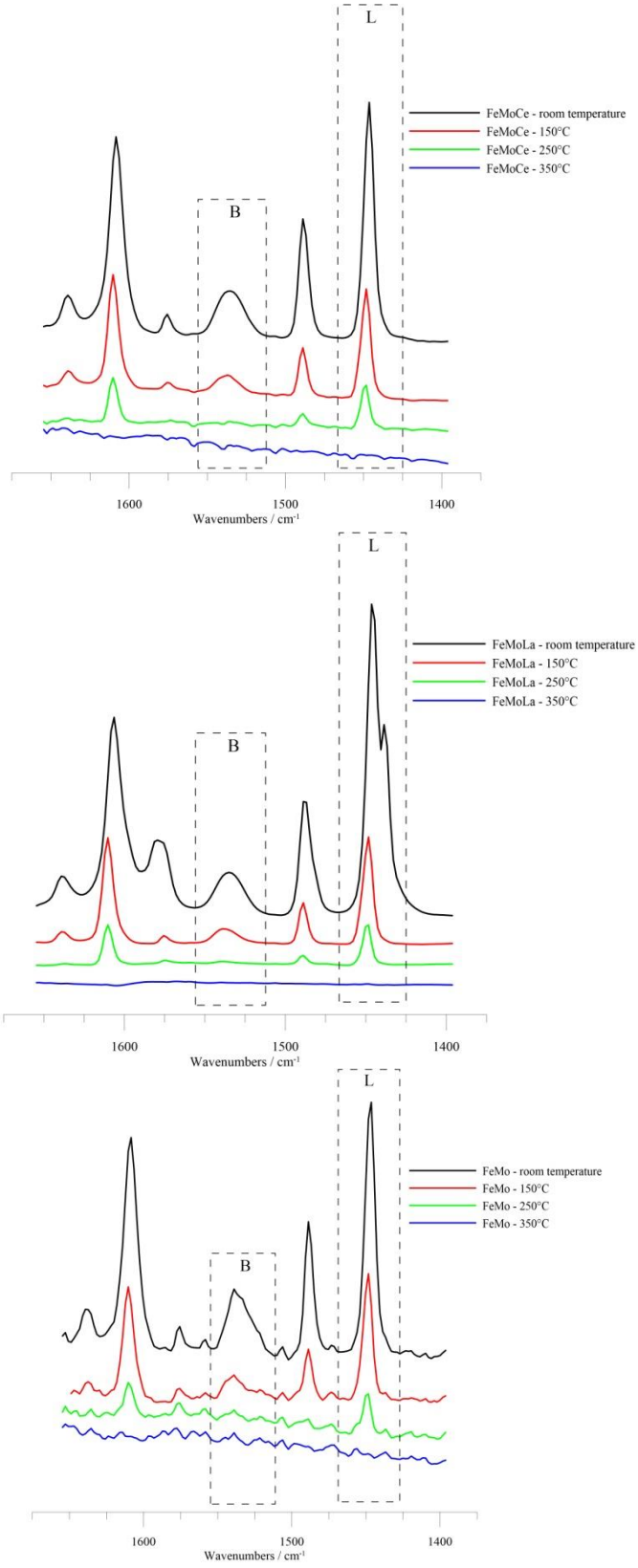

Figure 3.12. Pyridine desorption in different temperature. A: FeMo2.0, B : FeMoCe, C: FeMoLa calcined at 450 °C (B- Brønsted sites, L- Lewis sites).

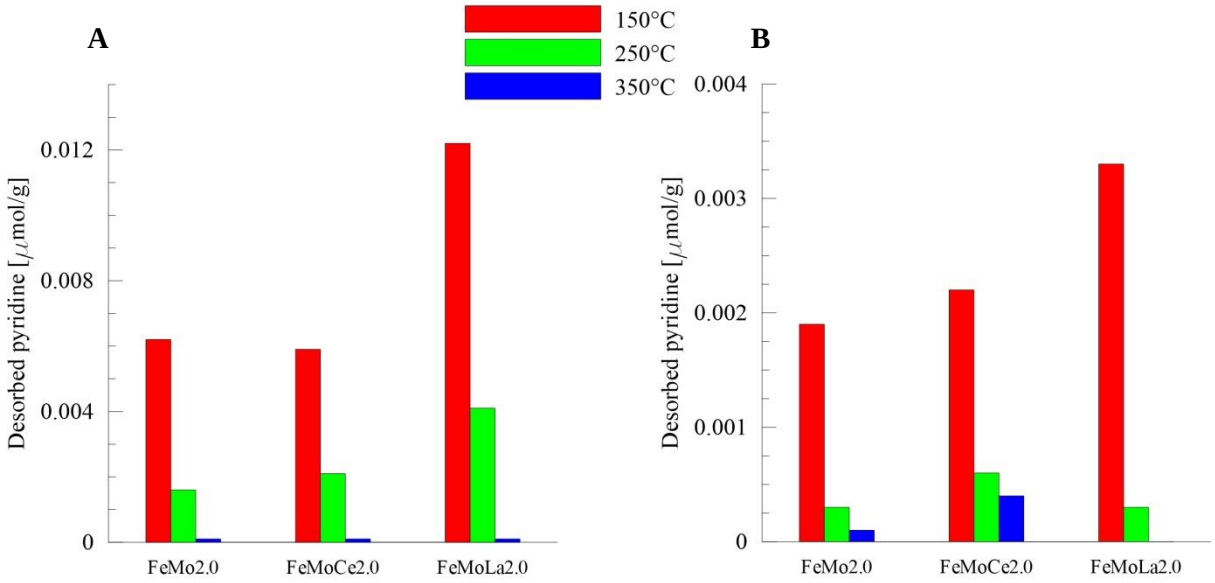

Figure 3.13. Adsorbed pyridine on FeMo2.0 and FeMoCe2.0 at 50°C. A: Lewis sites; B: Brønsted sites.

3.6.Catalytic performances– modified iron molybdate catalysts.

The catalytic activity of the modified FeMo catalysts was evaluated in the same conditions as previously (*i.e.*, GHSV = 3900 h^{-1}, O_2 = 12%, Temperature = 320 °C, MeOH/EtOH = 1). The following compounds were detected: acrolein, acetaldehyde, formaldehyde, carbon dioxide, dimethyl ether (trace) and methoxyethane (trace) (Figure 3.14), similarly to what was observed over conventional FeMo. In order to define the influence of the additives on the acrolein yield, the FeMo2.0 sample calcined at 450 °C (*i.e.*, 36.5% of acrolein yield) was chosen as the reference catalyst. As a result, basic elements addition showed that it is possible to improve slightly the selectivity to acrolein (up to 42% of acrolein yield). It can be noticed that the La-modified catalyst was that which formed the lowest quantity of acetaldehyde and the highest quantity of CO_2. The aforementioned product formation is certainly due to over oxidation of acetaldehyde, as an undesired side reaction.

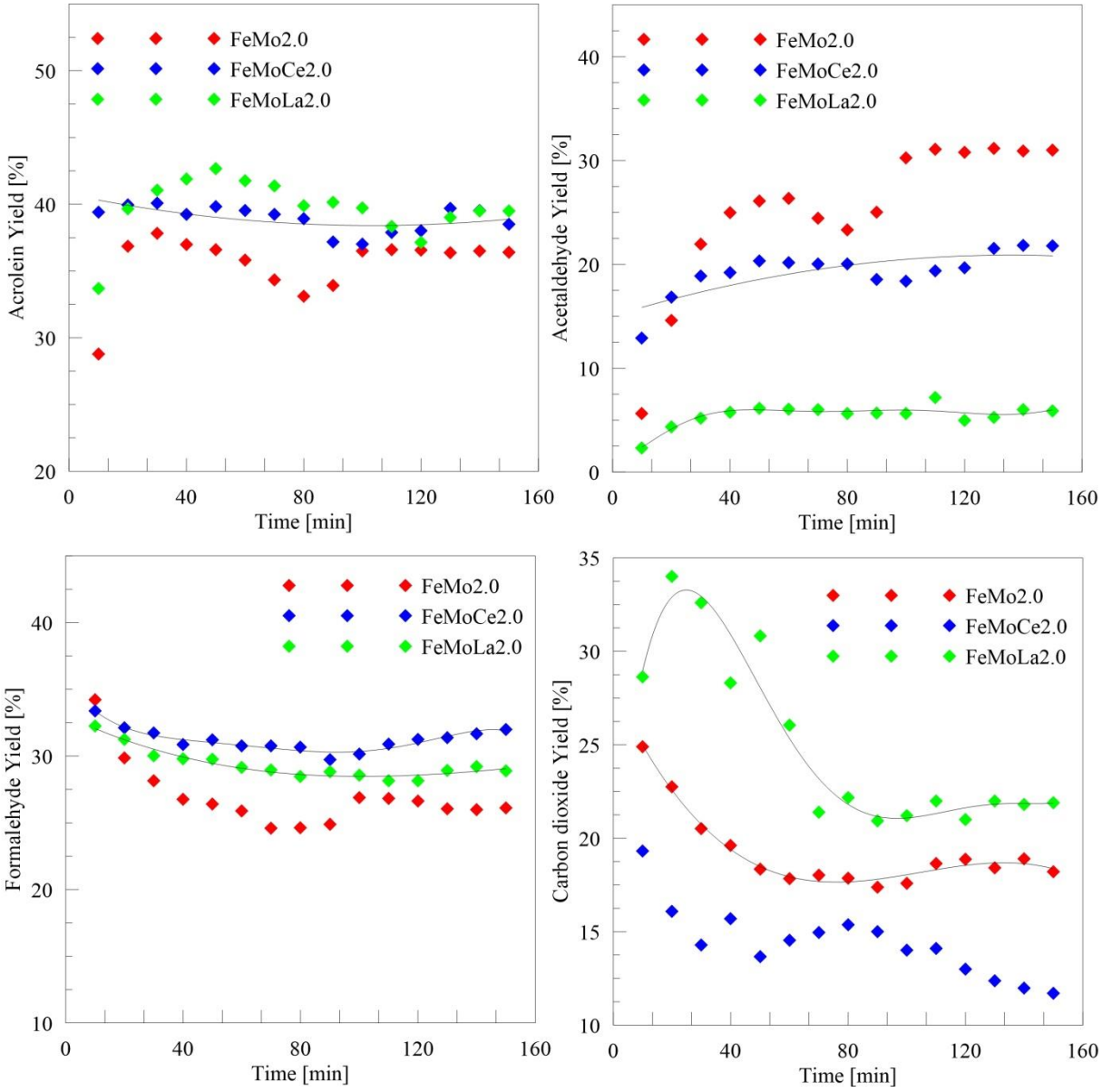

Figure 3.14. Acrolein, acetaldehyde, formaldehyde and carbon dioxide yields evolution as a function of time on stream for FeMo2.0, FeMoCe2.0 and FeMoLa2.0 calcined at 450 °C (GHSV = 3900 h-1, O2 = 12%, Temperature = 320 °C, MetOH/EtOH = 1).

We have then tested the different synthesized catalysts with various Mo/Fe ratios, different calcination temperatures and with doping elements (Table 3.13). The highest yield of acrolein was observed for FeMoCe2.0(400°C) - 42%, which is a + 5 points improvement compared to pure FeMo. Similarly a 4 points of improvement was obtained for FeMoLa2.0, which confirms the positive influence of lanthanum addition. Matching these observations with catalysts characterization, it can be concluded that the catalytic performance improvement comes probably from the acido-basic properties modification upon dopant introdcution. A small increase in acid sites content (*i.e.*, + 6 mmol/g (100%)

compared to FeMo2.0) has a positive influence on the acrolein yield. Concerning the influence of the calcination temperature, similarly like for conventional FeMo, the lowest acrolein yield was observed for a calcination performed at 350 °C while the differences between temperatures 400 and 450 °C were not that significant. The last studied point was the impact of the Mo/Fe ratio impact. Similarly to the pure FeMo series, the lowest acrolein quantity was produced over the catalyst with a Mo/Fe ratio equal 1.5 while the highest values are obtained for the ratio 2.0. This suggests, that the minimal value favouring our target molecule production should not be lower than 2.0.

Table 3.13. Catalytic tests results over the synthetized FeMo catalysts (GHSV = 3900 h^{-1}, O_2 = 12%, Temperature = 320 °C, MetOH/EtOH = 1).

Catalyst	**Conversion [%]**		**Yield [%]**			
	Methanol	**Ethanol**	**Acrolein**	**Acetaldehyde**	**Formaldehyde**	**CO_2**
FeMo1.5(450°C)	99	100	11	71	16	4
FeMoCe1.5(450°C)	100	100	33.5	28	21	18
FeMoCe1.5(400°C)	100	100	34	20.5	22	22
FeMoCe1.5(350°C)	100	100	32	12	23	17
FeMoLa1.5(450°C)	100	100	20	65	18	4
FeMoLa1.5(400°C)	100	100	36.5	30.5	25	10
FeMoLa1.5(350°C)	100	100	36.5	7	28	14
FeMo2.0(450°C)	100	100	36.5	31	26	18.5
FeMoCe2.0(450°C)	100	100	38	20	31	28
FeMoCe2.0(400°C)	100	100	42	14	36	34
FeMoCe2.0(350°C)	100	100	38	18	29	22
FeMoLa2.0(450°C)	100	100	39	6	29	30
FeMoLa2.0(400°C)	100	100	35	2	35	30
FeMoLa2.0(350°C)	100	100	21	Trace	41	36
FeMo2.5(450°C)	100	100	35	30	24	9.5
FeMoCe2.5(450°C)	100	100	32	30	20	9
FeMoCe2.5(400°C)	100	100	34	34.5	22	10
FeMoCe2.5(350°C)	100	100	32	9	25	14
FeMoLa2.5(450°C)	100	100	35.5	26.5	20	10
FeMoLa2.5(400°C)	100	100	40.5	22	20	13.5
FeMoLa2.5(350°C)	100	100	30	11	20	10

3.7. Advanced X-ray photoelectron spectroscopy.

In order to understand the FeMo catalysts surface behaviour during the reaction, quasi *in situ* and Near Ambient Pressure (NAP) XPS were performed. In this latter characterization method, the reduction with methanol and ethanol mixture was followed in the presence or the absence of oxygen. For *in situ* method, the sample the procedure was similar, but each treatment occurred in the separated chamber. The evolution of XPS spectra is presented herein for both of these methods.

3.7.1. Quasi *in situ* XPS.

In order to understand the catalysts surfaces behaviour during the reaction, we performed Quasi *in situ* XPS. Three materials were: FeMo2.0(450 °C) as the reference, FeMoCe2.0(400 °C) with the best catalytic performances and FeMo1.5(350 °C) with the worst catalytic performances. The samples were pre-treated at the optimal reaction temperature (*i.e.*, 320 °C) in a separate chamber under two different atmospheres:

(1) Under He + Methanol/Ethanol mixture (ratio = 1) for 2 h,
(2) Under He + Methanol/Ethanol mixture (ratio = 1) + Oxygen (12 Vol.%) for 2 h.

After pre-treatment, the samples were analysed without intermediate re-exposure to the air. All the three fresh catalysts are composed of Mo^{+VI} and Fe^{+III}, as described previously (XPS). Under reductive atmosphere (*i.e.*, He + Methanol/Ethanol mixture (ratio = 1)), all the catalysts behave in a similar. Surprisingly, iron atoms got reduced and stayed at the +II oxidation state during the treatments while drastic changes were noted for molybdenum. The obtained Mo3d spectrum for the reference FeMo2.0 catalyst is presented below in Figure 3.15 (the similar graphs obtained for FeMoCe2.0 and FeMo1.5 are given in Annex (Figure D.1 and Figure D.2, respectively). We observed, that after the treatment under methanol and ethanol mixture molybdenum in majority reduced to Mo^{+V}3d (blue colour photopeaks at 231.26 eV and 234.4 eV) and Mo^{+IV}3d (red colour peaks at 230.01 eV and 233.15 eV. Then, after oxygen introduction, molybdenum was almost totally re-oxidized to +VI (green colour peaks at 232.8 eV and 235.98 eV) similarly on the fresh catalyst surface.

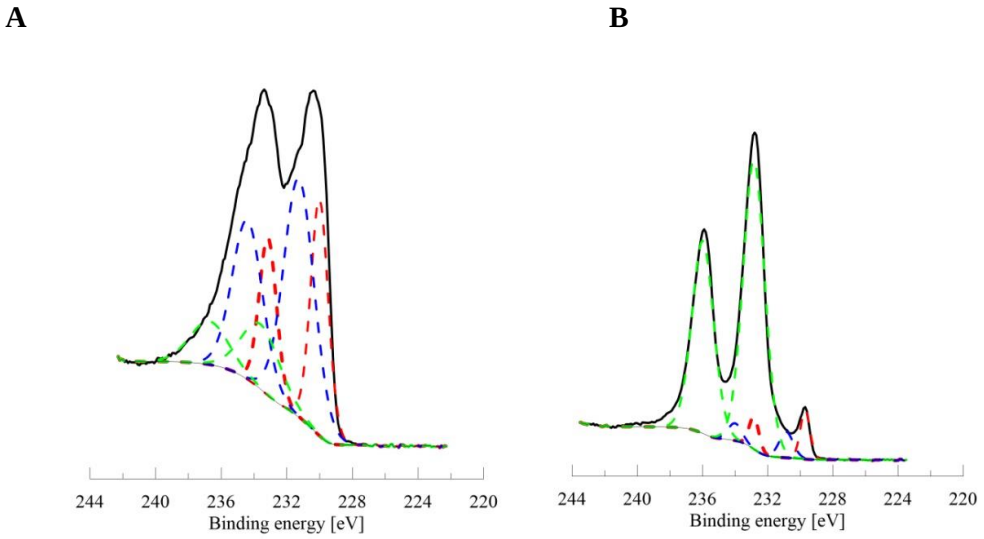

Figure 3.15. FeMo2.0 calcined at 450 °C quasi in situ XPS results (320°C, MetOH/EtOH = 1, Alcohols = 13.2%, O_2 = 12%). A: under He + MetOH/EtOH flow; B: under He + MetOH/EtOH + O_2 flow.

The quantification of the molybdenum species (*i.e.*, different oxidation states) is presented in Table 3.14 in Figure 3.16. Comparing results obtained during the reduction, we remark that the most reduced catalyst is FeMoCe2.0 which presents the lowest Mo $^{+VI}$ content (*i.e.*, 15.8%) and the highest Mo $^{+IV}$ content (*i.e.*, 30.5%). On the other hand, for FeMo1.5 we observe the lowest quantity of +IV species (i.e., 28.4%) and the highest non-reduced Mo $^{+VI}$ presence (*i.e.*, 22.9%). In terms of oxidation, similarity, the highest Mo^{+VI} quantity was noted for FeMoCe2.0 (*i.e.*, 91.1%) while the lowest one was found for FeMo1.5 (*i.e.*, 68%). These observations are in agreement with catalytic tests results where the most performant was FeMoCe2.0 and the least FeMo1.5. It suggests, that the molybdenum capacity of reduction is an important factor influencing on acrolein yield.

Methanol and ethanol oxidation thus induced molybdenum reduction, which is conflictual with a previous study performed in the laboratory in which it was found that under methanol, the Fe species get reduced while the Mo species stays at a +VI oxidation state through the analysis over FeMo catalysts [7]. These differences can be explained by a selective adsorption of ethanol at the surface which interact more with molybdenum than with iron. The influence of methanol and ethanol reduction might yield different, and similar experiments with ethanol are planned.

Table 3.14. Mo content evolution during quasi *in situ* XPS.

Catalyst	Content [%]		
	Mo $^{+IV}$	**Mo $^{+V}$**	**Mo $^{+VI}$**
FeMo2.0 reduced	29.9	52.2	17.9
FeMo2.0 oxidized	6.7	5.1	88.2
FeMoCe2.0 reduced	30.5	53.8	15.8
FeMoCe2.0 oxidized	3.9	5.0	91.1
FeMo1.5 reduced	28.4	48.6	22.9
FeMo1.5 oxidized	18.8	12.9	68.2

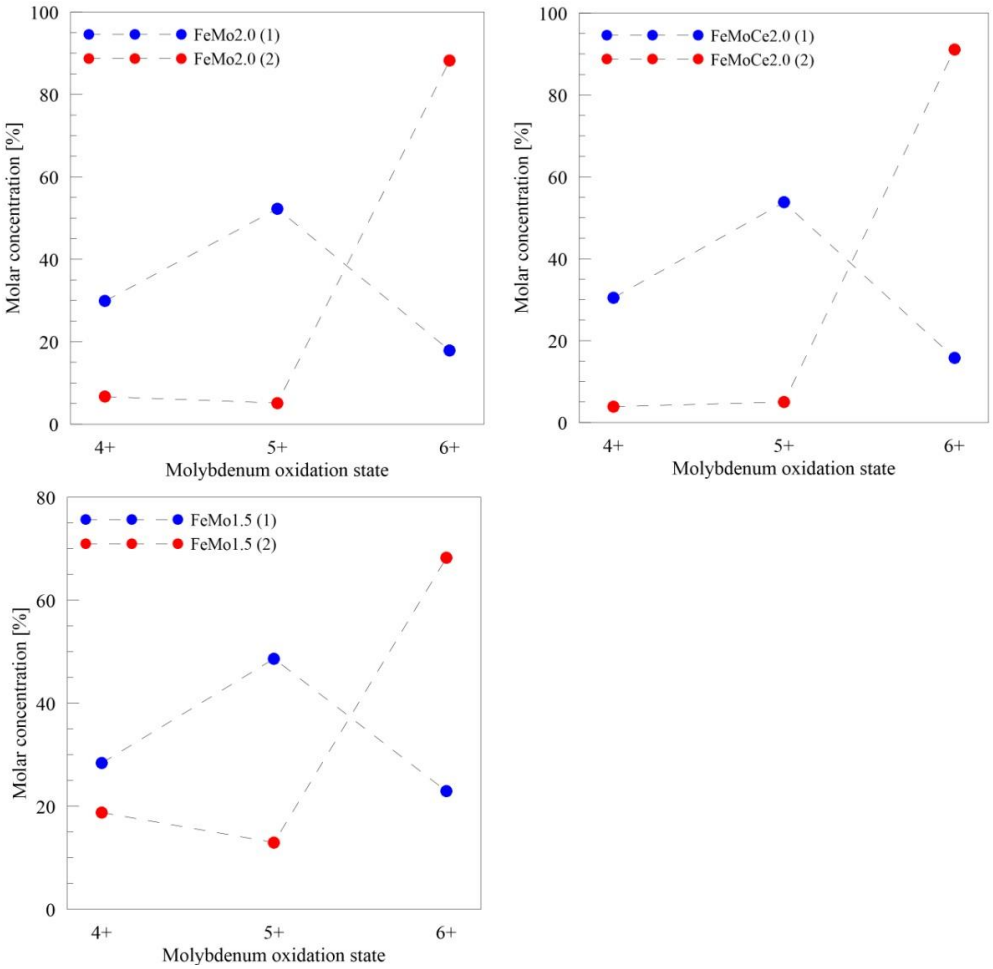

Figure 3.16. Mo molar concentration obtained by quasi in situ XPS for FeMo catalysts. (1) He + MetOH/EtOH; (2) He + MetOH/EtOH + O_2.

3.7.2. Near Ambient Pressure (NAP) XPS.

In order to approach closer to the reactional conditions, NAP XPS was performed focusing on molybdenum behaviour under alcohols mixture flow, using successive conditions:

(1) Reduction under Methanol/Ethanol mixture (ratio = 1),
(2) Re-oxidation under Methanol/Ethanol mixture (ratio = 1) + Oxygen (1:1).

In both conditions, the temperature was raised gradually until 320 °C and spectra were taken every 25 s. Figure 3.17 presents the Mo3d spectra evolution function of the temperature (*i.e.*, from 250 to 350 °C) and time, under alcohols flow. The increase in temperature caused the gradual reduction of molybdenum from a +VI oxidation state to a +IV oxidation state.

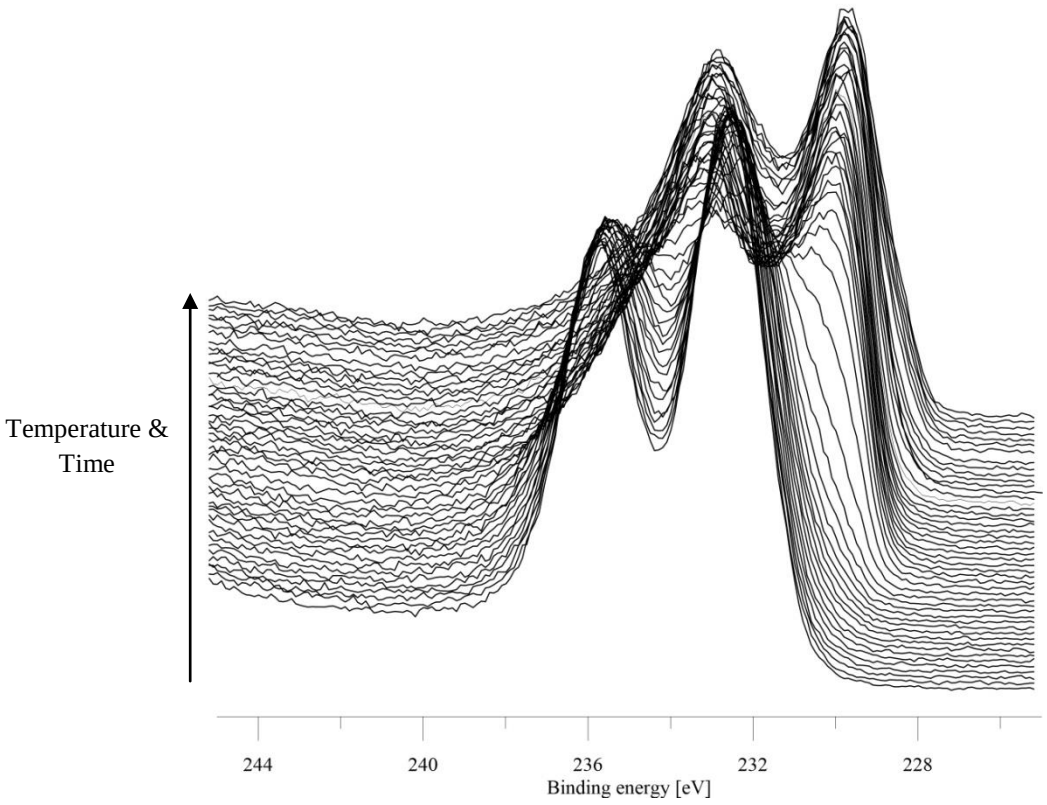

Figure 3.17. The Mo 3d spectra evolution as a function of time and temperature (250 – 320 °C) during reaction under methanol and ethanol flow.

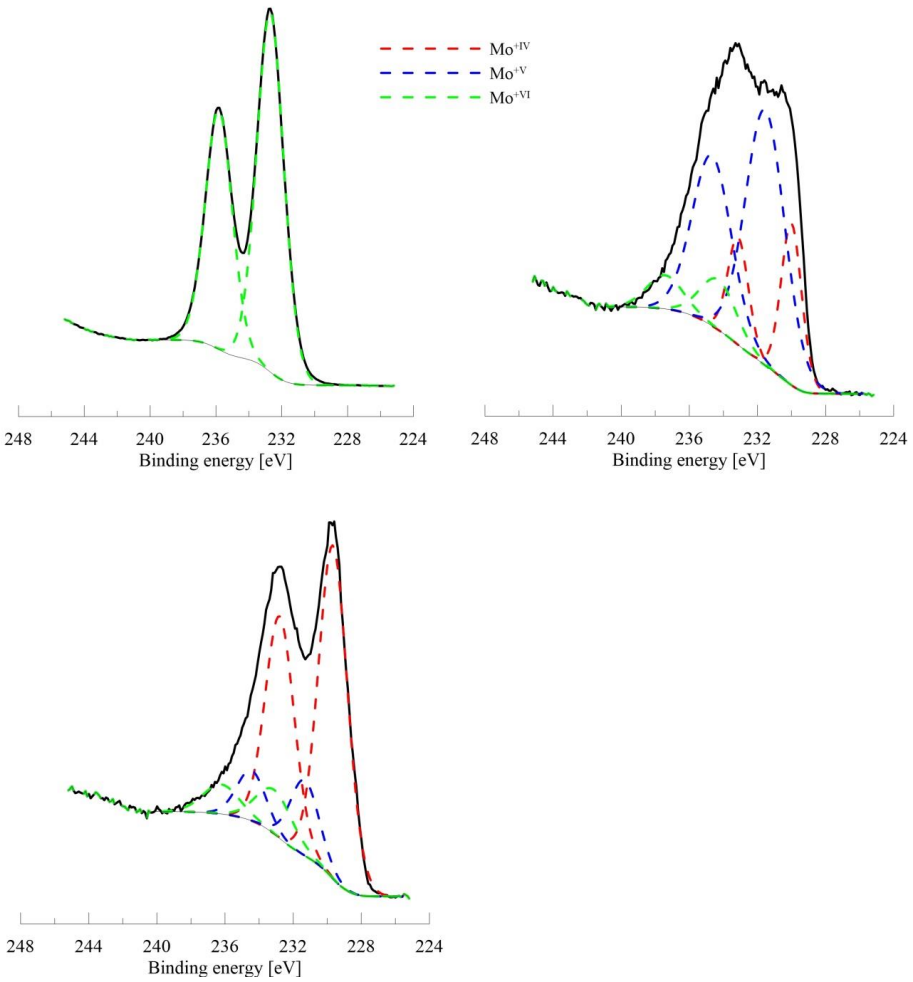

Figure 3.18. Mo3d spectra evolution during reaction under methanol and ethanol flow (250 – 320 °C).

Figure 3.18 shows the spectra taken at three different points of analysis under alcohols flow (oxygen-free atmosphere): at the beginning (*i.e.*, 250 °C), at mid stage (~ 290 °C) and at the end (*i.e.*, 320 °C). At the beginning, FeMo2.0 contained only Mo^{+VI} species (Mo 3d at 232.7 eV and 235.8 eV), with a Mo 3d signature identical to that recorded at room temperature meaning that the reduction did not occur below 250 °C. Then, increasing the temperature actually caused the reduction of Mo species mostly into Mo^{+V}, as can be seen in Figure 3.19. In the final stage of analysis, molybdenum +VI proportion was only 10%. In the same time, the Mo^{+IV} quantity increased (to 49.9%) and Mo^{+V} content decreased to 43.9%. So the reduction of molybdenum seems to occurs in two steps, first Mo^{VI} is reduced to Mo^{V} and this formed Mo^{V} is then reduced to Mo^{IV}. The observed evolution is represented in Figure 3.19. In this graph, we can see that the first reduction step occurs between 280 and 290 °C while the second step occurs at 300 °C. The observed results are in agreement with the *in situ* measurement which showed that

molybdenum is mostly reduced to the +V oxidation state (*i.e.*, 52.2% for FeMo2.0). However, we remark that with the NAP analysis method we are able to perform the complete reduction due to the analysis conditions close to these used during catalytic tests.

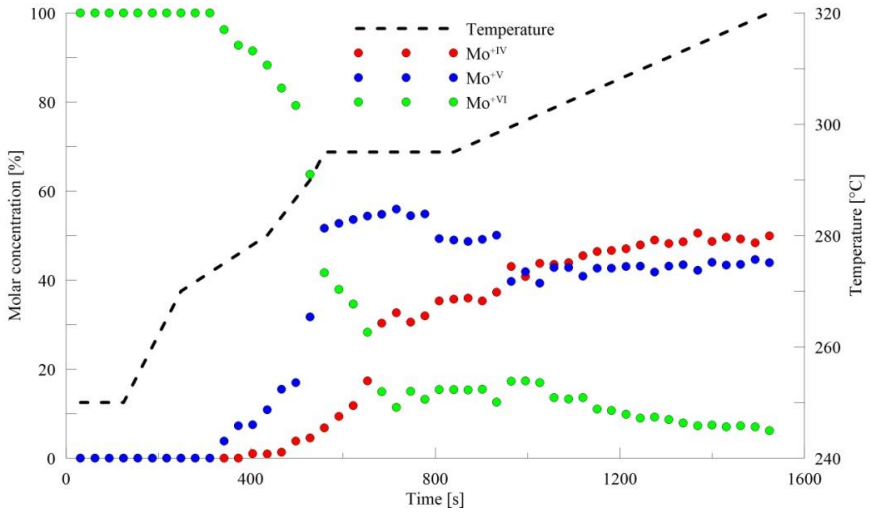

Figure 3.19. Evolution of Mo species concentration as a function of time under temperature increase (Error Δ = 10-15%).

In order to follow the re-oxidation of the FeMo2.0 catalyst, the system was first "quenched" by naturally decreasing the temperature to room temperature before then introducing 1 mbar of oxygen in the feed. Then, we increased the temperature linearly with time (20 – 320 °C). Figure 4.20 shows three spectra taken at the beginning (room temperature), at mead stage (~220 °C) and at the end (320 °C) of analysis. At room temperature, we start almost at the same point compared to the end of the previous stage of reduction experiment. When the temperature reached 150-175 °C, the oxidation process took place, which is characterized by a photopeaks intensities decrease of the Mo^{+IV} and Mo^{+V} and an increase of the Mo^{+VI}. At the end of the experiment, almost 100% of the molybdenum species returned to the +VI oxidation number (Figure 3.21). At this stage, we applied a new reduction step, by removing again oxygen from the feed (not shown) and the same phenomena than those presented in the Figure 3.17 occured, showing a nice reversibility of the system.

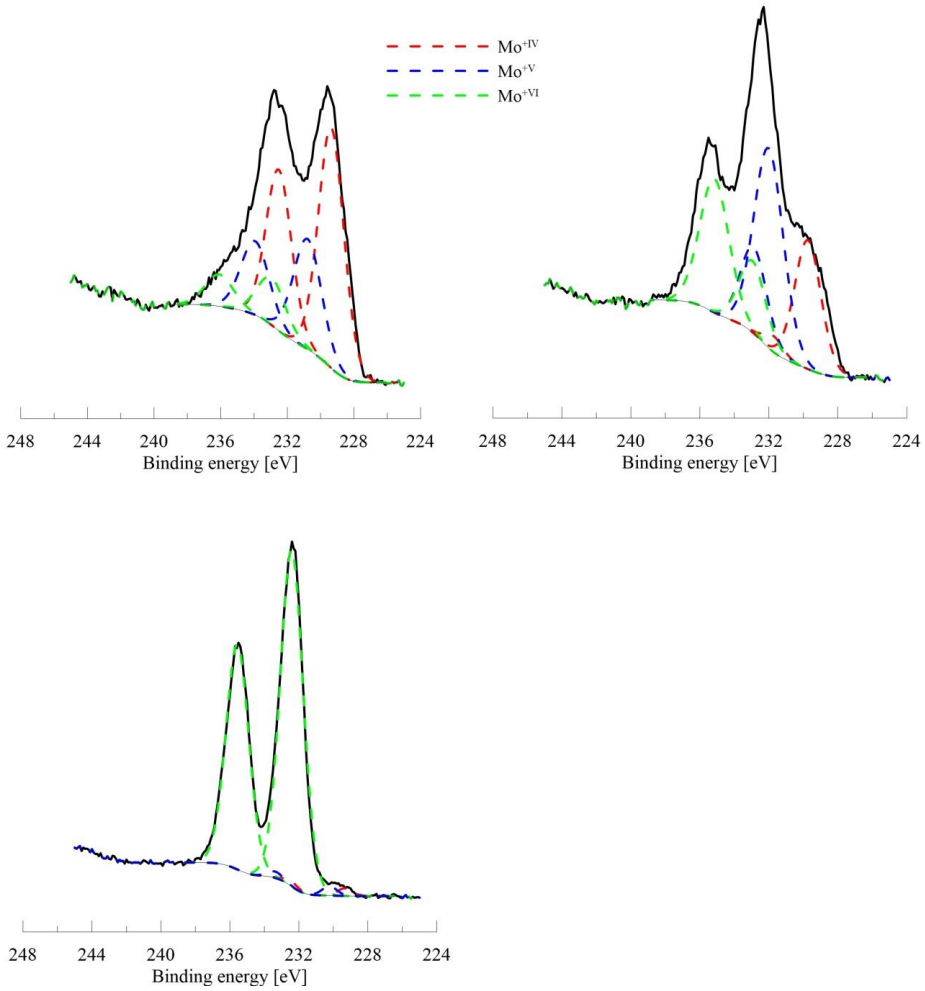

Figure 4.20. Mo3d spectra evolution during catalyst re-oxidation under alcohols and oxygen flow with temperature increase (20 – 320 °C).

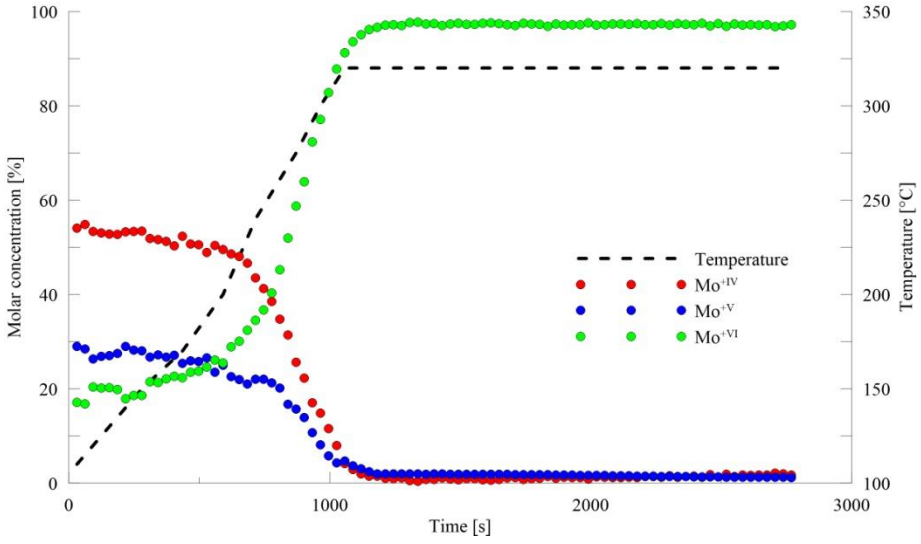

Figure 3.21. Evolution of Mo species concentration as a function of time under temperature increase (Error Δ = 10-15%).

3.8. Discussion and conclusions.

In this chapter, studies on methanol and ethanol oxidative coupling over FeMo-based catalysts are presented. First, the reaction conditions were optimized using a Design of Experiments method in order to obtain the acrolein yield as high as possible. It was found that the most sensitive factor is the temperature while the total flow rate influence is negligible. Afterwards, the theoretically determined optimal point over the industrial $FeMoO_x$ catalyst was verified and the measured acrolein yield amounted 44% (for a theoretical value of 50%). Therefore, these conditions were chosen to perform the following catalytic tests. FeMo-based catalysts were then synthetized using a co-precipitation method and varying two parameters: the Mo/Fe ratio (*i.e.,* 1.5, 2.0 and 2.5) and the calcination temperature (*i.e.,* 350°, 400° and 450 °C). FeMo2.5 (400 °C) exhibited the highest performance (39% of acrolein yield) while FeMo1.5 (350 °C) gave the worst one (7.5% of acrolein yield). Subsequently, analysing the calcination temperature influence, we remarked that the lowest acrolein yield was obtained always for catalysts treated at 350 °C. This phenomenon can be explained looking at XRD-HT results, which showed that the total FeMo crystallization occurs from 400 °C. Thus, the crystalline structure develops the active sites.

Acetaldehyde and formaldehyde condensation to form acrolein is usually performed over basic catalysts. We then decided to modify the FeMo formulation by introduction of $1\%_{molar}$ of lanthanum and cerium. The choice of these basic elements was motivated by their +III oxidation state, which is the same as iron in $Fe_2(MoO_4)_3$ catalysts. It was assumed that La and Ce can partially replace Fe in the $Fe_2(MoO_4)_3$ structure and create the basic sites needed for the second stage of the process (acetalization). Materials were synthetized with different Mo/Fe ratio (*i.e.,* 1.5, 2.0 and 2.5) and calcination temperatures (*i.e.,* 350°, 400° and 450 °C). Their catalytic activity was measured in the optimal conditions previously found and compared with those of FeMo2.0 calcined at 450 °C. The highest acrolein yield was obtained for FeMoCe2.0 calcined at 400°C (*i.e.,* 42%) with thus an improvement of 5.5 points compared to the Ce-free sample. The catalyst modified with La brought the expected improvement as well giving an acrolein yield of 40.5% (FeMoLa2.5 calcined at 400 °C). In order to understand the influence of basic elements addition several characterization methods were performed. First, thanks to XPS and LEIS analysis, it was found that La and Ce are not present on the surface, but their

addition increases the surface Mo/Fe ratio. XRF measurements proved that La and Ce are actually present in the catalyst structure (bulk). The La and Ce addition influence on the catalyst basicity was checked using CO_2-TPD. The number of basic sites of the modified FeMo catalysts was increased (medium and strong sites were formed), which suggests and indirect effect of La and Ce incorporation are these elements are not present on the surface In order to better understand all phenomena accompanying FeMo modification upon La and Ce introduction, it would be valuable to synthesize and characterize materials with different contents.

The last part of this chapter presents the quasi *in situ* and NAP XPS studies under reactional mixture. It was presented previously [7] that upon methanol reduction, the iron species in the FeMo catalyst gets reduced from +III to +II. On the other hand, molybdenum species were only +VI. Here, over the FeMo2.0 treated with methanol and ethanol mixture (ratio = 1), surprisingly, the iron atoms stayed at an oxidation number of +III while molybdenum species were reduced to +V and +IV oxidation states. This suggests that methanol mixed with ethanol has a different reductive capacity on the FeMo catalyst surface. On the other hand, it was remarked that a higher temperature facilitates the Mo species reduction. Thanks to NAP XPS, we found that the reduction/oxidation process are almost 100% reversible in our conditions which is a property very useful thinking about industrialisation of the process.

3.9.References.

[1] PCT Patent WO2014068213, assigned to Arkema France, Priority date Oct 17, 2013

[2] *N. Pernicone* Journal of the Less-Common Metals 36 (1974) 289-297

[3] *N. Pernicone et al.* Journal of Catalysis 14 (1969) 293-302

[4] *J. Gornay et al.* Green Chemistry 12 (2010) 1722–1725

[5] *J. Gornay et al.* Oil & Gas Science and Technology, 65, 5 (2010) 751 – 762

[6] *K. Thavornprasert et al.* Biofuels 3 - 1 (2012) 25-34

[7] *K. Thavornprasert et al.* Applied Catal. B 145 (2014) 126-135

[8] *Y.V. Plyuto, I.V. Babich, I.V. Plyuto, A.D. Van Langeveld, J.A. Moulijn*, Applied Surface Science 119 (1997) 11

[9] *T. Yamashita, P. Hayes*, Applied Surface Science 254 (2008) 2441-2449

[10] *M.C. Biesinger, B.P. Payne, A.P. Grosvenor, L.W.M. Lau, A.R. Gerson, R. St. C. Smart*, Applied Surface Science 257 (2011) 2717

[11] A.P. Grosvenor, B.A. Kobe, M.C. Biesinger, N.S. McIntyre, Surface and Interface Analysis 36 (2004) 1564

[12] *G.E.P. Box, WG. Hunter, JS.Hunter*, Statistics for experimenters, John Wiley and Sons, New York 1978 p.653

[13] *J. Goupy*, Plans d'experiences pour surface de reponses, Dunod, 1999, Paris.

Chapter 4. Acrolein production from methanol and ethanol mixtures using a tandem of catalysts – results and discussion

As it was shown before, the main products obtained through methanol and ethanol coupling reaction using $FeMoO_x$ were acrolein, acetaldehyde and formaldehyde. Keeping in mind that the ultimate goal of the present study is to obtain the acrolein yield as high as possible, we looked for a method for condensing *in situ* the unreacted intermediate aldehydes to acrolein. In the literature, numerous authors pointed out that optimal aldol condensation needs a defined balance between acid and basic sites. The $FeMoO_x$ catalyst we used clearly develops acidity [1] so that we decided to add a second catalyst of the basic type (chosen among single oxides: MgO, CaO, BaO and silica-based: Mg-Si, Ca-Si, Ba-Si) in the catalytic bed, in a tandem strategy (Figure 4.1).

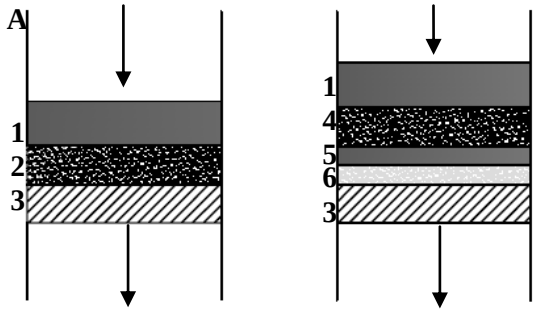

Figure 4.1. Catalytic beds schemes for the tandem of catalysts. A: Mixed catalysts, B: Separated catalysts. 1: 500 mg SiC, 2: 200 mg of both catalysts mixed with 200 mg of SiC, 3: fixed bed profile, 4: FeMo catalyst + SiC, 5: 200 mg SiC, 6: basic catalyst + SiC.

The catalytic tests were performed using the optimal conditions, as found using the DoE approach presented in Chapter 3. The relative catalyst's quantity (for a total of catalytic solid of 200 mg) and the catalytic bed volume were optimized. All the synthetized

materials were characterized by XPS, BET, XRD, TGA-DSC and CO_2 adsorption followed by FTIR.

4.1. Silica-based solids as the second catalyst.

In this study, the silica-based materials (*i.e.*, Mg-Si, Ca-Si, Ba-Si) behavior as the second catalyst was examined. They were synthetized by a sol-gel method, characterized and their catalytic performance was measured. The results are presented hereafter.

Differential thermal analysis and thermogravimetric analysis were performed in the 20-800 °C temperature range under air. Figure 4.2 presents TG and DTG curves for all the freshly synthesized catalysts before calcination. All the samples presented the same behavior. At the beginning, we observe a first mass loss (up to 10%) between 100°-200°C assigned to physisorbed water desorption. Then, at about 500°C a second mass loss is observed (up to 70% of mass loss), which is attributed to TEOS and nitrates (used as a precursors) decomposition. Then, the solid mass remains stable at least up to 800 °C. These observations led to the selection of a proper calcination temperature (*i.e.*, 750°C) in order to ensure elimination of all the undesired compounds (residual organics).

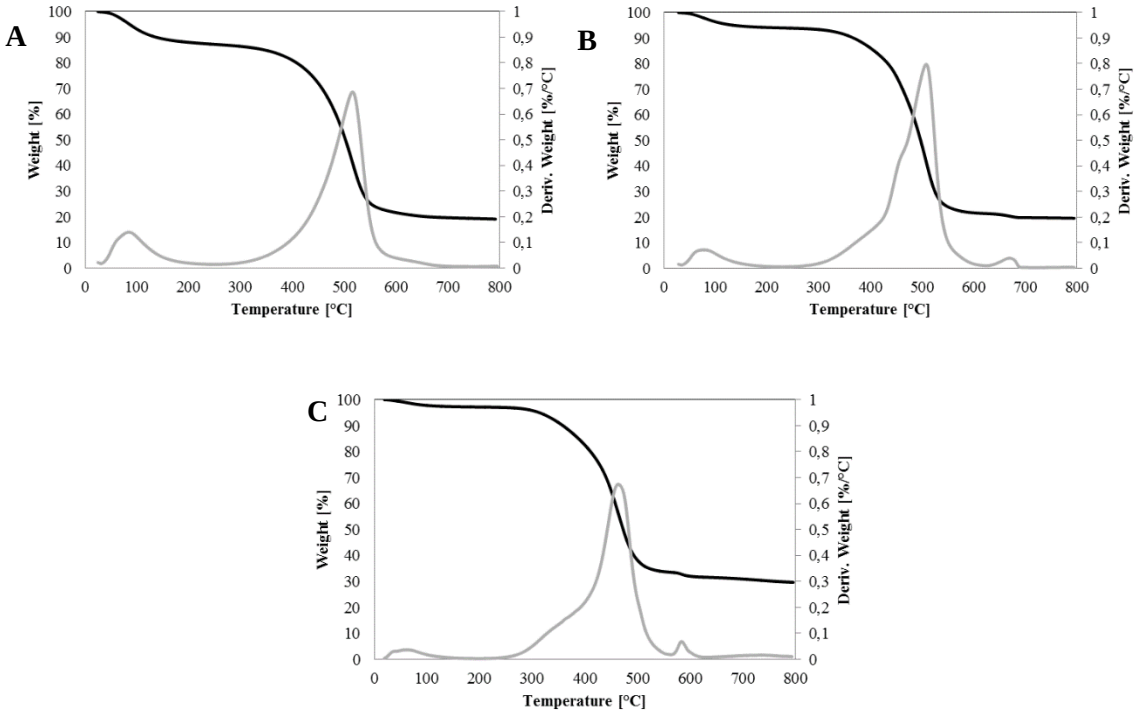

Figure 4.2. TG(black) and DTG(grey) curves for A: Mg-Si, B: Ca-Si, C: Ba-Si. The analysis was performed in the temperature range 20-800 °C at a heating rate of 10 °C/min under air flow.

Figure 4.3 shows the heat flow evolution as a function of the temperature for the Mg-Si, Ca-Si and Ba-Si samples. For all the catalysts, we observed two peaks: one small endothermic peak centered on 100 °C and a second intense exothermic peak centered on 500°C, respectively assigned to the elimination of water and the decomposition of the precursors (*i.e.*, TEOS and nitrates). In order to identify the crystallized phases potentially formed upon heat treatment of the solids, XRD analysis was then performed.

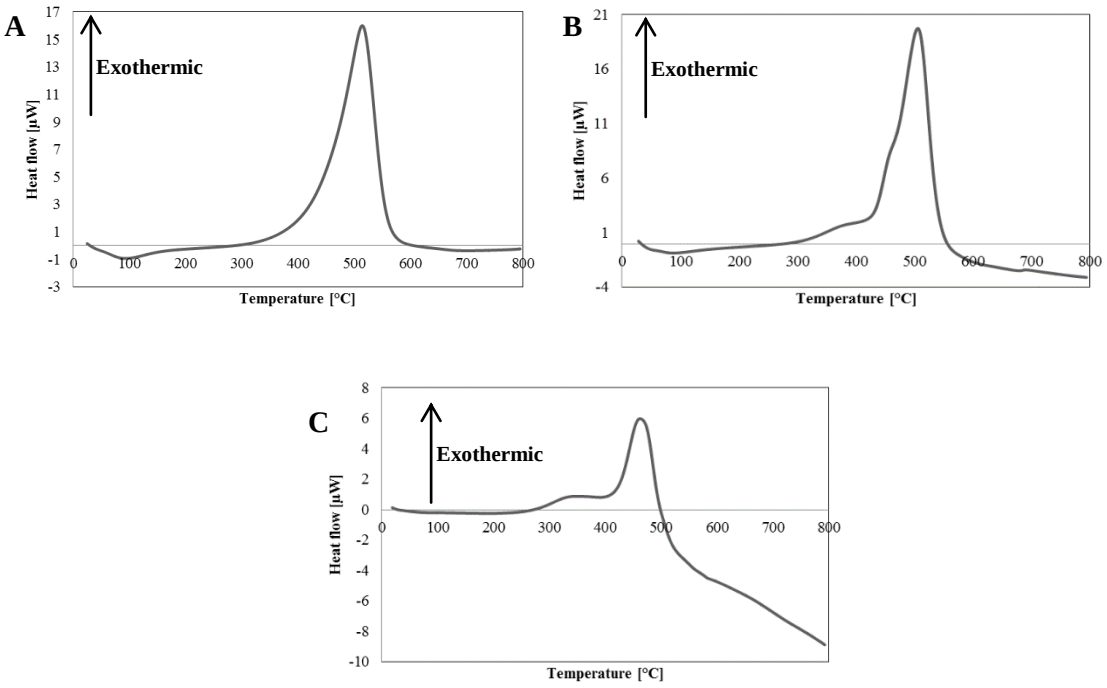

Figure 4.3. DSC curves for A: Mg-Si, B:Ca-Si, C:Ba-Si. The analysis was performed in the temperature range 20-800°C with a heating rate of 10°C/min under air flow.

Figure 4.4 presents the XRD diffractograms of the calcined Mg-Si catalyst. After calcination at 750 °C, the X-Ray diffractogram is characteristic of an amorphous material with however two small peaks at 45 and 65° corresponding to Mg_2SiO_4 (PDF# 00-004-0769). After calcination at 850 °C during 1 h, the $MgSiO_3$ phase (PDF# 00-019-0768) phase crystalline was detected in addition to the Mg_2SiO_4 phase (Figure 4.4B).

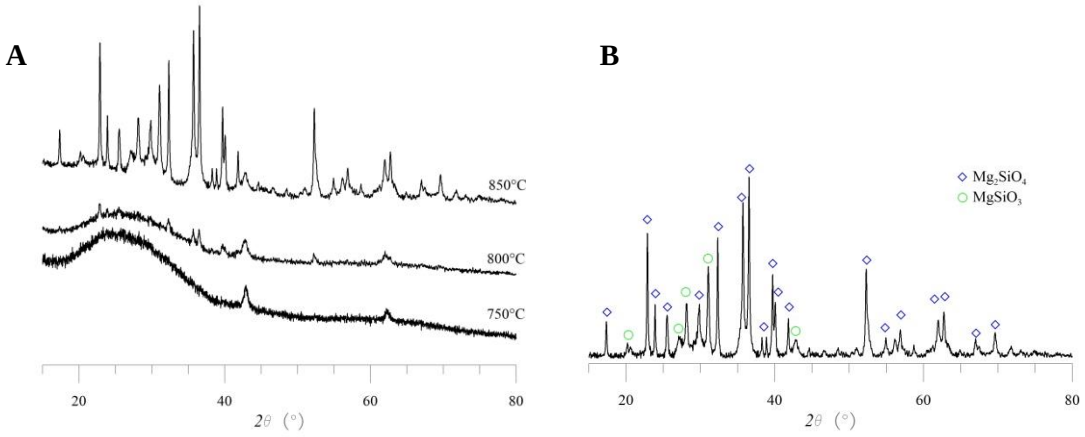

Figure 4.4. A: XRD patterns of the Mg-Si catalyst calcined at 750°, 800° and 850 °C. B: XRD patterns of the Mg-Si catalyst calcined at 850 °C with phases matching.

In the case of the Ca-Si catalyst calcined at 750 °C (Figure 5.5A), $CaCO_3$ (PDF# 01-083-1762) and Ca_2SiO_4 (PDF# 00-033-0303) were detected. However, similarly to Mg-Si, it seems that the crystalline phase formation is not finished with peaks only relatively sharp and well defined compared to the signal/noise ratio. For Ba-Si, $BaCO_3$ was identified (PDF# 00-045-1471) as well as barium silicate $BaSiO_3$ (PDF# 00-004-0504). Analyzing these data, it can be concluded that carbonates phases are major in these two latter cases, which can have a negative influence on the catalytic performances (*vide supra*).

The catalysts surfaces compositions were determined by XPS analysis, and the results are summarized in Table 4.1 The silica concentration is similar for all the examined samples (13~14%). In the contrary, the surface alkaline earth metal concentrations are very different from one sample to another. The highest alkaline metal content was found for magnesium (*i.e.*, 30.2%), while calcium and barium quantities were similar, at 11.4% and 9.1%, respectively. Concerning the surface carbon quantity, the lowest value is observed for Mg-Si (*i.e.*, 11.3%) and the highest one for Ba-Si (*i.e.*, 27.9%).

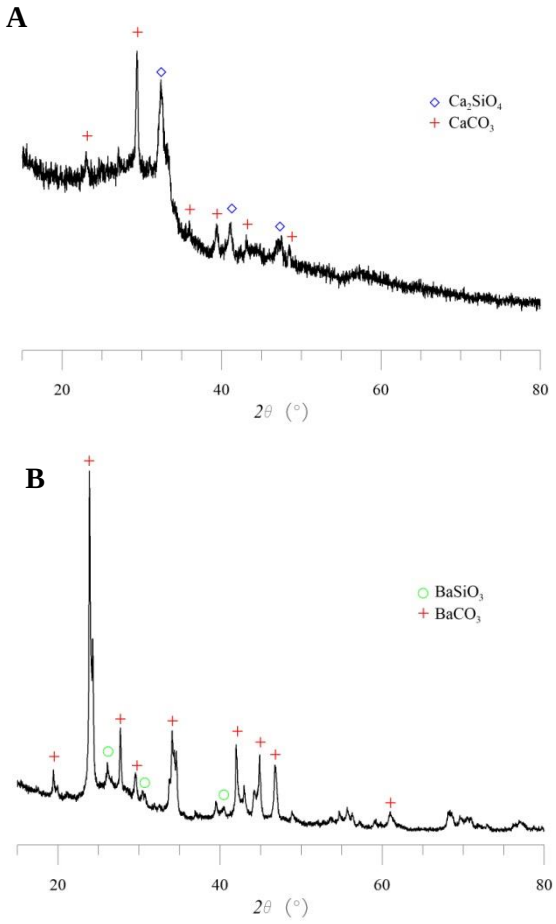

Figure 5.5. XRD patterns of catalysts calcined at 750 °C; A: Ca-Si, B: Ba-Si.

Table 4.1. XPS analysis results for silica based catalysts calcined at 750 °C, theoretical X/Si ratio = 1

Catalyst	Binding energy (eV)		Atom concentration [%]			
	Si 2p	Mg 2s, Ca 2p, Ba 3d	Si 2p	Mg 2s, Ca 2p, Ba 3d	C 1s	O 1s
Mg-Si	102.3	304.6	13.0	30.2	11.3	45.5
Ca-Si	103.9	349.0	14.3	11.4	21.7	52.7
Ba-Si	153.5*	780.2	14.3	9.1	27.9	48.7

* 2s because of recovery between Ba 2p and Si 2p

The C 1s photopeaks (Figure 4.6) results from the contribution of three components at 284.8 eV, 286 eV, and 289.5 eV, respectively. The first one marked with a green color is attributed to C=O bonds characteristic for carbonates, which is in agreement with the

presence of carbonate metal phases observed for each sample by XRD [2]. The second peak plotted in red color corresponds to C-OH bonds, while the third one (blue one) can be attributed to C-C and C-H bonds, which is due to the contaminating carbon usually used for calibration of the XPS spectra. The intensity of the carbonates peak increases going down along the alkaline earth metals column in the periodic table of the elements (see Table 4.1). This is a way to provide a ranking for basicity. Indeed, the atmospheric CO_2, as we will show after, is a good molecule to probe the basic sites. So the fact that the quantity of carbonates adsorbed at the surface of the Ba-containing catalyst is higher than for the others means that this catalyst exhibit a larger number of – occupied – basic sites. But at this stage, we have no information on the strength of basic sites.

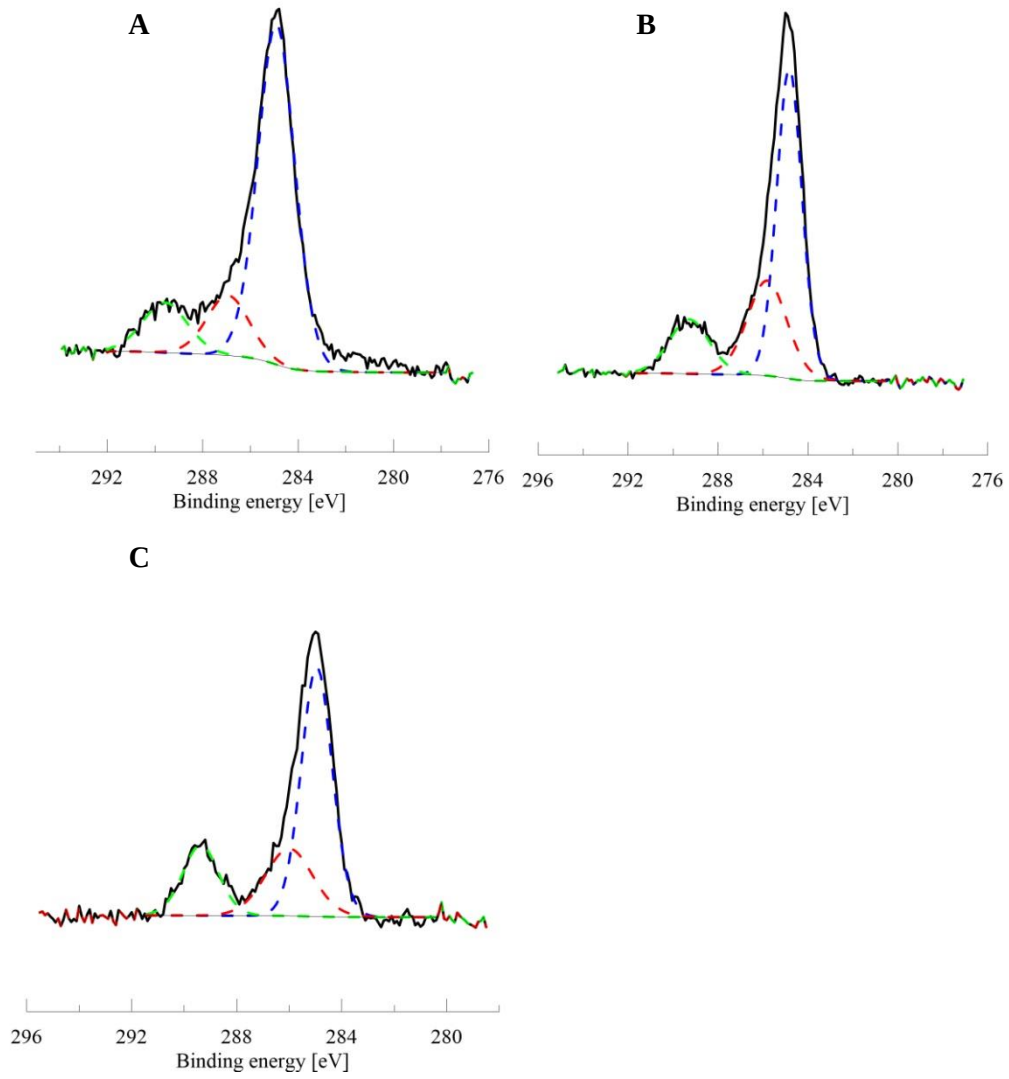

Figure 4.6. XPS analyses of the C 1s level for A: Mg-Si, B: Ca-Si, C: Ba-Si calcined at 750 °C.

Figure 4.7 shows the O 1s peaks for each catalyst. For the Ca-Si and Ba-Si catalysts, the photopeak envelop is strongly unsymmetrical. Two different oxygen environments can be identified: Si-O-Si and C=O. In the literature, we can find that, for silicates, the O 1s peak is detected usually between 532 and 533 eV [3]. This corresponds to the blue component in Figure 4.7 and its content varies from 11%$_{molar}$ for Ba-Si to 21.3%$_{molar}$ found for Mg-Si. Following that, the C=O bonds are suggested to appear at a BE from 531.5 to 532 eV [4,5], which corresponds to the red component. These types of connection are found in carbonates, which is in agreement with the C 1s part of the XPS spectra.

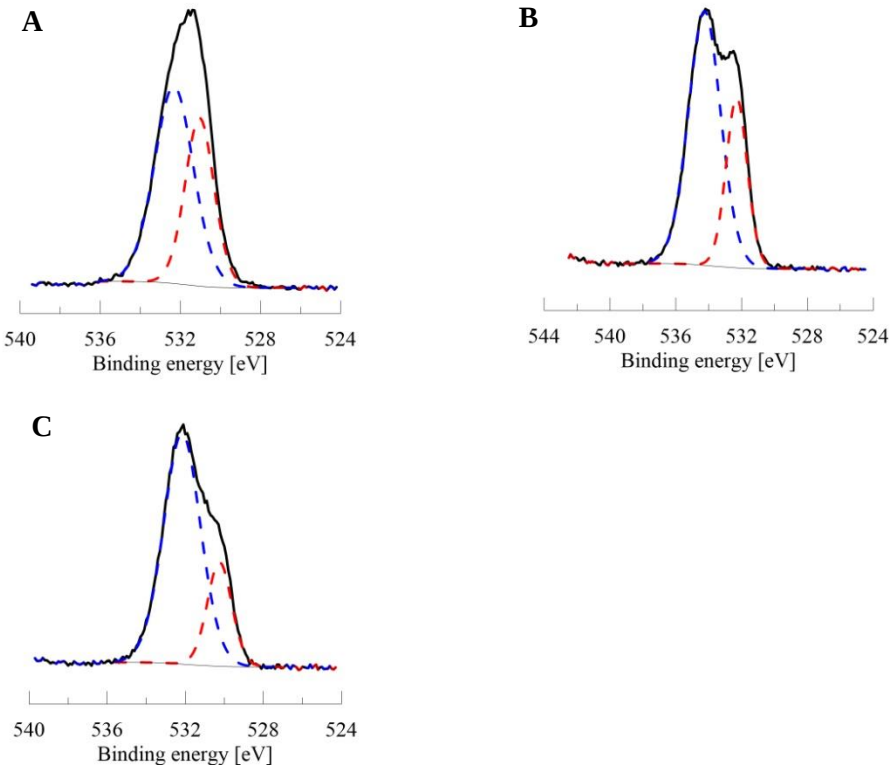

Figure 4.7. XPS analyses of the O 1s level for A: Mg-Si, B: Ca-Si, C: Ba-Si.

For all the synthetized materials, a symmetric Si 2p photopeak was detected. For Mg-Si and Ca-Si its location was 102.3 eV and 103.9 eV respectively what corresponds to silicates [6]. Surprisingly, in the case of Ba-Si, the Si 2s is observed at 153.5 eV (Figure 4.8). This difference is caused by recovery of Si 2p peak with Ba 2p which required to present silicon with 2s. Notwithstanding, the Si BEs correspond in all cases to silicates [7]. The surface silicon quantities were similar for Mg-Si, Ca-Si and Ba-Si, with 13, 14 and 14.3%$_{molar}$ respectively (Table 4.1).

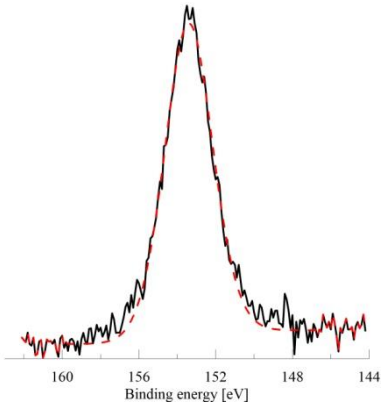

Figure 4.8. XPS analyse of the Si 2s level for Ba-Si.

Table 4.2 gives the specific surface areas of the samples. The highest values were found for Mg-Si calcined at 750 °C and 800 °C (121.3 and 126.1 m^2/g, respectively). However, the specific surface area decreased drastically when the sample was calcined at 850 °C, which is linked with the formation of crystalline phases. Ba-Si showed the less developed surface (*e.g.*, 14.8 m^2/g) due to a pronounced crystalline character, as observed on the XRD diffractograms (Figure 5.5).

Table 4.2. Specific surface area or the silica-based catalysts.

Catalyst (calcin. temp.)	**Specific surface area [m^2/g]**
Mg-Si (750 °C)	121.3
Mg-Si (800 °C)	126.1
Mg-Si (850 °C)	21.3
Ca-Si (750 °C)	84.7
Ba-Si (750 °C)	14.8

IR-followed carbon dioxide adsorption (FTIR) experiments were performed to assess the basicity of the samples. Broad bonds between 1200 and 1800 cm^{-1} were detected for the Mg-Si and Ca-Si samples pre-treated at 800 °C under oxygen during 1 h. These bands are assigned to carbonates [8]. It means, that it exists very strong basic sites on these samples, which are not free for the reaction as they strongly "trap" CO_2 from the atmosphere. Then, in Figure 4.8B, the spectra of Mg-Si after carbon dioxide exposure is shown, which confirms that no more molecules are adsorbed on the surface. Due to strong adsorption of atmospheric CO_2 on the surfaces, we were not able to propose a basicity ranking for the synthesised samples. Their very strong basic sites which are saturated with carbonates even after high temperature treatment under O_2.

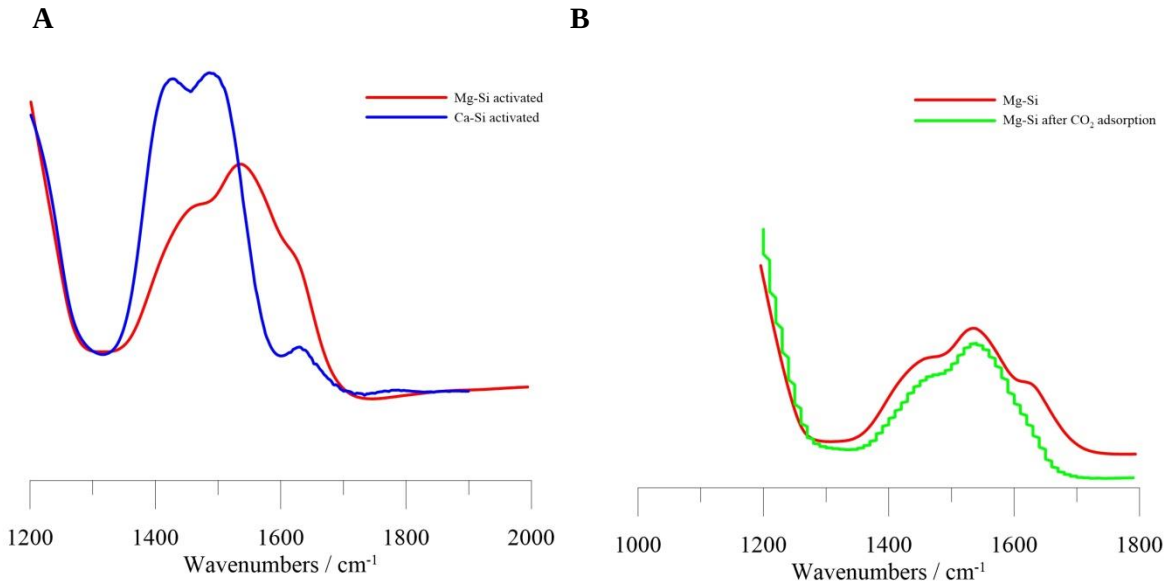

Figure 4.9. A: Infrared spectra of activated catalysts Mg-Si and Ca-Si calcined at 750 °C; B: Infrared spectra of CO_2 adsorbed on Mg-Si catalyst.

4.2. Catalytic performances.

In this part, acrolein production from a mixture of methanol and ethanol was performed in a single reactor packed with two catalysts. The catalytic performance was measured under the optimal conditions determined through the previous 'DoE' approach (O_2 = 10.8%, GHSV = 4800 h^{-1}, Temperature = 320 °C, MetOH/EtOH ratio = 1.63). The results were benchmarked against the acrolein yield obtained for the commercial $FeMoO_x$ and MgO catalyst working as a single phase (*i.e.*, 38% and 0% respectively). In this study, it was

necessary to make the optimization of the catalytic system (*e.g.*, second catalyst quantity, second catalyst location in the catalytic bed…).

4.2.1. Catalytic system optimization.

In order to find the optimal catalysts relative quantities, several experiments were performed by varying the percentage of each catalyst (*i.e.*, from 5 to 50% of mass of the second catalyst) using the commercial $FeMoO_x$ and magnesium oxide. Afterwards, the catalytic bed volume influence was explored by keeping a constant catalysts mass and changing the carborundum (diluent) amount (*i.e.*, 200 mg, 400 mg and 600 mg) using MgO as well. Ultimately, the way the second catalyst is introduced in the reactor was studied with magnesium and calcium oxides. Two different possibilities were considered: materials placed as layers or mixed altogether. The obtained optimal conditions were then used for further tests.

First, the catalysts quantities relative ratio optimization was performed. Commercial magnesium oxide (Aldrich, 99.99%) was chosen as a second catalyst. The iron molybdate was provided by Arkema. These two materials, for a total mass of 200 mg, were mixed with 200 mg of SiC. Figure 4.10 presents the evolution of the products yields when increasing the MgO proportion. In any case, introduction of MgO was beneficial to the acrolein yield. The increase in acrolein yield was quite low when the addition of MgO was between 10 and 40 mg (*i.e.*, acrolein yield between 43.5 and 46%). However, in the case of the catalytic bed composed with the same masses of both catalysts, it was observed a productivity decrease comparing to lower magnesium oxide quantity. The formaldehyde yield was rather stable, but the acetaldehyde yield significantly varied, with its lowest value for 20 mg of MgO (9%) and its highest one for 100 mg of MgO (39%). Its decrease is accompanied with increases of the acrolein and carbon dioxide yields. In brief, the best results were obtained with 10 and 20 mg of MgO mixed with 190 and 180 mg of $FeMoO_x$, respectively, which is beneficial for the acrolein production. Thus, for the following catalytic tests, it was decided to use $10\%_{mass}$ (20 mg) of the second catalyst.

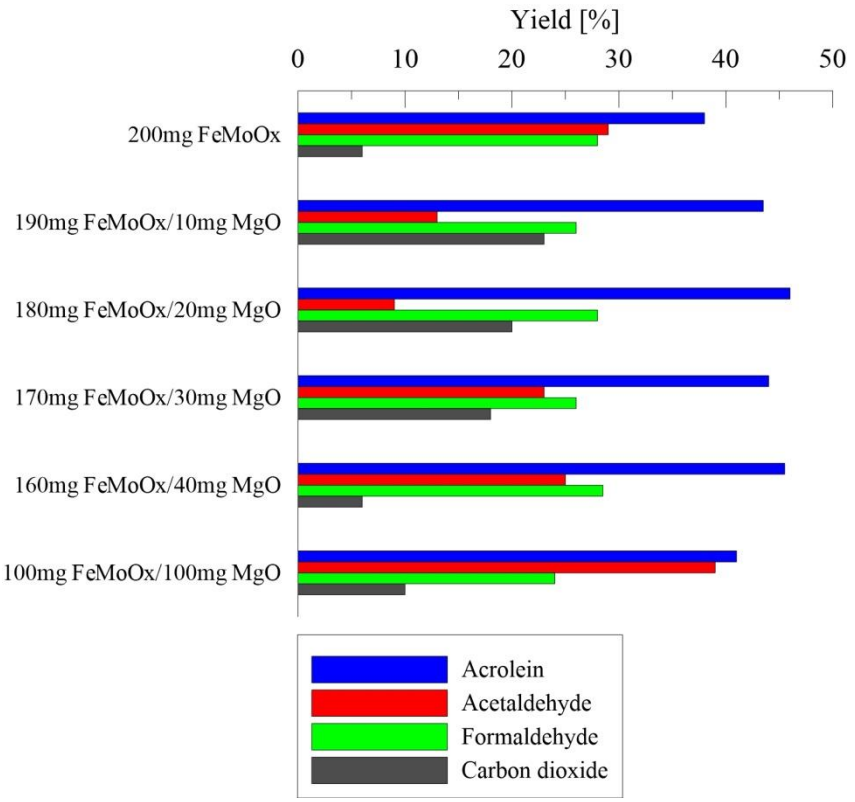

Figure 4.10. Influence on catalytic performance of the relative quantity of catalysts for the example of the $FeMoO_x$/MgO tandem (mixed catalysts, O_2 = 10.8%, GHSV = 4800 h^{-1}, Temperature = 320 °C, MetOH/EtOH ratio = 1.63).

Subsequently, the influence of the catalytic bed volume was studied. Indeed, the oxidation and condensation processes are exothermic and can lead to local hot spots. In order to get a better control of the heat dispersion and to avoid overoxidation on such hot spots (*i.e.*, CO_2 production), a proper dilution of the active phase can be desired. We thus decided to vary the carborundum mass. For these experiments, both catalysts (*i.e.*, 20 mg and 180 mg of MgO and $FeMoO_x$ respectively) were mixed with different masses of SiC (*i.e.*, 200 mg, 400 mg and 600 mg, which gave catalytic bed volumes of 0.06 mL, 0.12 mL and 0.19 ML, respectively). The products formation evolution is presented in Figure 4.11, with not any noticeable difference, which suggests that heat dispersion was correct in any case. For the following catalytic tests, it was however decided to use two different SiC quantities: 200 mg and 400 mg in order to get rid of any doubt with all the tested configurations.

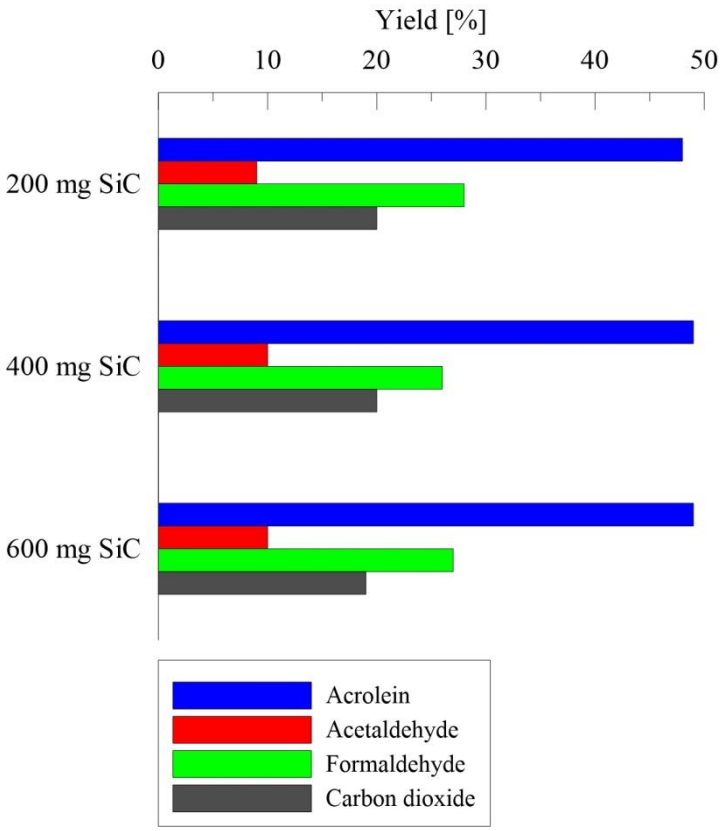

Figure 4.11. Catalytic bed volume influence for the example of 90%$FeMoO_x$/10%MgO tandem (O_2 = 10.8%, GHSV = 4800 h^{-1}, Temperature = 320 °C, MetOH/EtOH ratio = 1.63).

The multilayer strategy was also used (Figure 4.1). Figure 4.12 shows the products yields evolution when using MgO or CaO as the second catalysts, for both "mixed" and "layer" strategies. For the magnesium oxide-containing system, we can observe that in the layer case, the acrolein yield was lower than for the mixed case with a difference equal to 4 points. In the same time, acetaldehyde and formaldehyde yields decreased significantly in the mixed case, which suggests a higher aldol condensation efficiency. In the case of CaO, similar results were obtained for both configurations. Therefore, the answer for the catalysts configuration is not unequivocal and it was decided to use both "layers" and "mixed" strategies during catalytic performance studies.

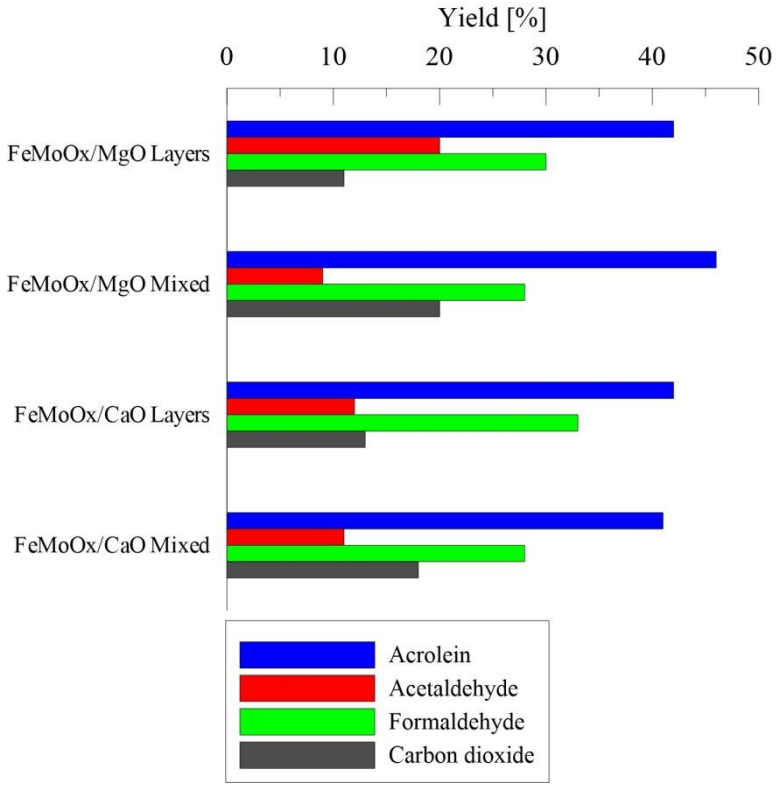

Figure 4.12. Influence of the second catalyst position in the example of 90%$FeMoO_x$/10%MgO and 90%$FeMoO_x$/10%CaO tandems (O_2 = 10.8%, GHSV = 4800 h^{-1}, Temperature = 320°C, MetOH/EtOH ratio = 1.63).

4.1.2. Single oxides.

In this study, four different commercial oxides were tested in the methanol and ethanol oxidation reaction to acrolein, as the second catalyst (*i.e.*, MgO, CaO, BaO). Based on the catalytic system optimization presented previously, the following configuration variations were studied:

- Catalysts placed as layers (180 mg FeMo + 180 mg SiC, 200 mg SiC, 20 mg 2nd material + 20 mg SiC),
- Catalysts mixed together (180 mg FeMo + 20 mg 2nd material + 200 mg SiC),
- Catalysts mixed together with doubled carborundum (180 mg FeMo + 20 mg 2nd material + 400 mg SiC).

First, the results for the second possibility are presented in Figure 4.13, showing the evolution of the acrolein yield as a function of time for the $FeMoO_x$ mixed with 20 mg of oxides and 200 mg of SiC. No significant activation period was needed and the yield of

acrolein was quite stable as a function of time. The highest values were observed for MgO and BaO (up to 6 points larger than CaO). It can be remarked as well that for any run the reported results are improved compared to the single $FeMoO_x$ (*i.e.*, acrolein yield of 38%). Therefore, it is clear that the second catalyst addition improves the produced quantity of desired acrolein.

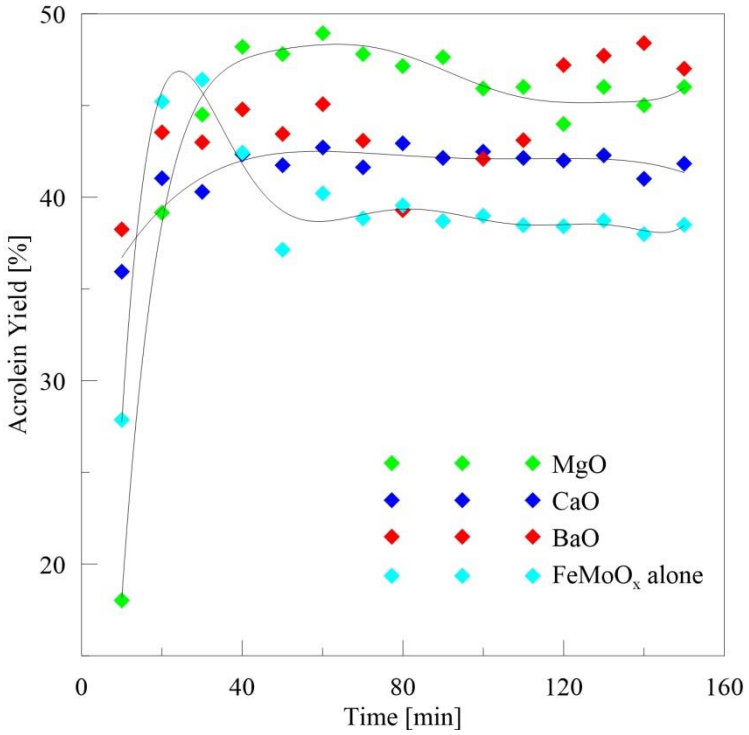

Figure 4.13. Acrolein yield as a function of time for single oxides (mixed catalysts, 200 mg SiC, O_2 = 10.8%, GHSV = 4800 h^{-1},

The detailed catalytic tests' results for commercial oxides are summarized in Table 5.1. It can be noticed that for all examined oxides the expected acrolein yield improvement was reached. Particularly good results were observed for the mixed configuration. In our studies, the highest selectivity to acrolein was observed here for 20 mg MgO mixed with 180 mg FeMoO*x* and 400 mg of SiC (*i.e.*, 49%).

Table 4.3. Catalytic test results for single oxides (O_2 = 10.8%, GHSV = 4800 h^{-1}, Temperature = 320 °C, MetOH/EtOH ratio = 1.63)

Catalyst	SiC [mg]	Layers/Mixed	Yield [%]			
			Acrolein	Acetaldehyde	Formaldehyde	Carbon dioxide
MgO	200	Layers	42	20	30	11
	200	Mixed	46	9	28	20
	400		49	10	26	20
CaO	200	Layers	42	33	12	13
	200	Mixed	42	28	11.5	18
	400		47	29	18	18
BaO	200	Layers	44	9	38	16.5
	200	Mixed	47	42	18	10
	400		44.5	35	12	12
$FeMoO_x$	200	-	38	29	28	6
MgO	200	-	0	8	0	9

4.2.3. Silica-based catalysts.

The synthetized silica based catalysts were tested under the same conditions as those used for the commercial single oxides (O_2 = 10.8%, GHSV = 4800 h^{-1}, Temperature = 320 °C, MetOH/EtOH ratio = 1.63, 180 mg $FeMoO_x$ and 20 mg silica-based catalyst) with the three different configurations mentioned before. Figure 4.14shows the products yields evolution as a function of the time on stream for Mg-Si, Ca-Si and Ba-Si, which gave similar acrolein yields (*ca.* 42%). However, the evolution of the other products selectivities significantly differs. The acetaldehyde yield was larger when using Ba-Si, while, for the same catalyst, carbon oxide yield was the lowest. It can then be concluded that the BaSi presence does not favor the acetaldehyde oxidation to CO_2 contrary to the other materials.

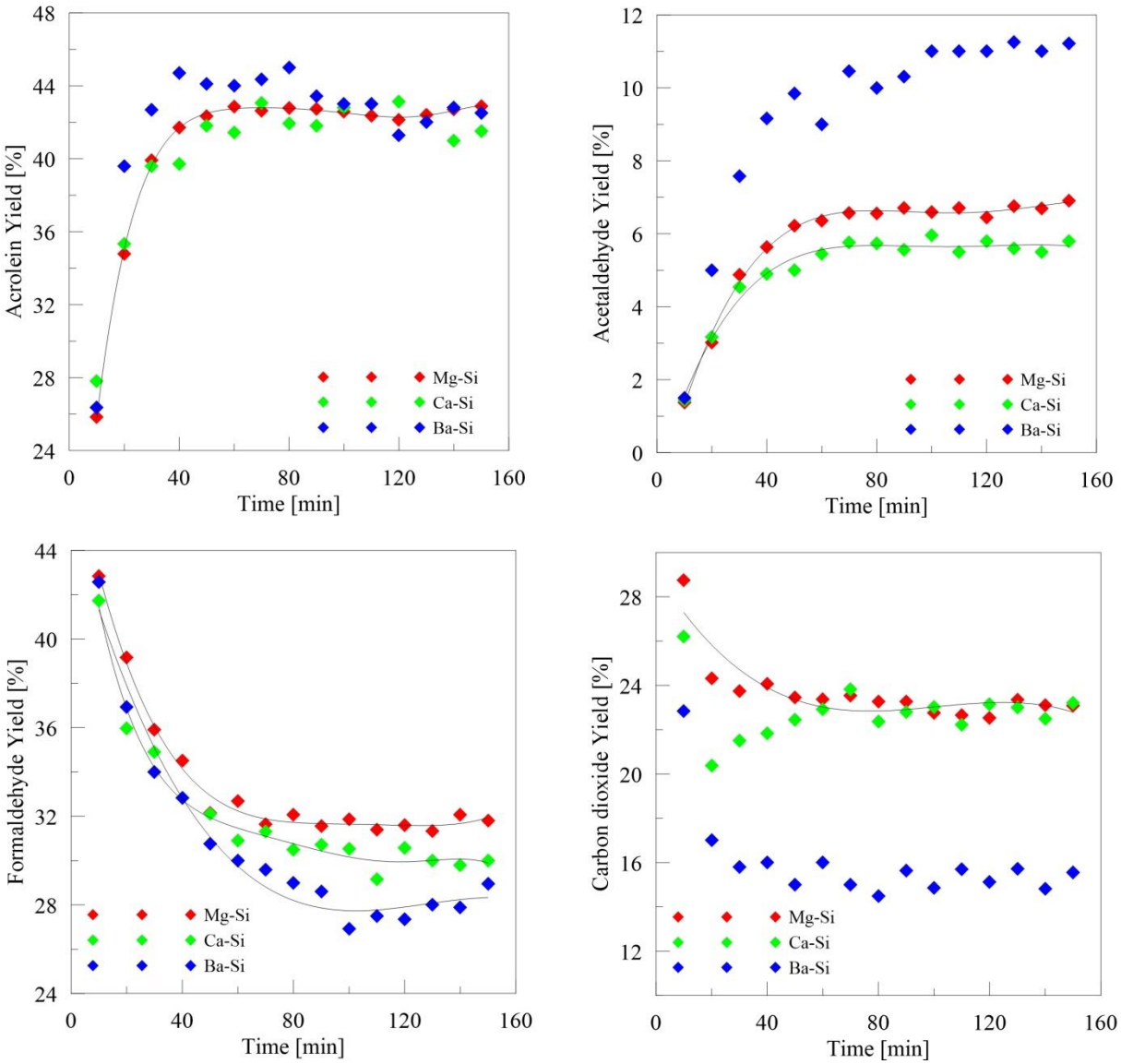

Figure 4.14. Products yields evolution functions of time for silica catalysts (mixed with 180mg FeMoOx, 200mg SiC, O_2=10.8%, GHSV=4800h^{-1}, Temperature=320°C, MetOH/EtOH ratio=1.63).

Table 4.4 presents the detailed comparison of the Mg-Si, Ca-Si and Ba-Si performance. For all the materials, the layer's case gives the lowest performances. Compared to single $FeMoO_x$ no improvement in acrolein yield was observed. Afterwards, by mixing catalysts together, the results changed significantly (up to 9 points of increase in acrolein yield). Moreover, the catalytic performance can be improved by doubling the SiC quantity which improves the heat dispersion. The best results were observed for the Ca-Si catalyst mixed with $FeMoO_x$ and 400 mg of carborundum (i.*e.*, 45.5%), with 7.5 points of improvement of the acrolein yield. Analyzing the other products yields, it can be remarked that Mg-Si, Ca-Si and Ba-Si have the same behavior. In all cases, the second major product was formaldehyde contrary to acetaldehyde of which the yield was not higher than 11.5%.

Table 4.4. Catalytic test results for silica-based catalysts (O_2 = 10.8%, GHSV = 4800 h^{-1}, Temperature = 320 °C, MetOH/EtOH ratio = 1.63).

Catalyst	SiC [mg]	Layers/Mixed	Yield [%]			
			Acrolein	Acetaldehyde	Formaldehyde	Carbon dioxide
Mg-Si	200	Layers	35	11	35	13
	200	Mixed	42.5	7	32	23
	400		44.5	8	38.5	17
Ca-Si	200	Layers	36	6	35	14
	200	Mixed	42	6	30	23
	400		45.5	10	33	15.5
Ba-Si	200	Layers	33	5	35	14
	200	Mixed	42	10	28	15
	400		45	11,5	28	16
$FeMoO_x$	200	-	38	29	28	6

4.3. Discussion and conclusions.

In this part, methanol and ethanol partial oxidation to acrolein was performed using two combined catalysts (*e.g.*, $FeMoO_x$ and basic/acid) placed in one reactor. First, the catalytic system optimization was made using different materials quantities, SiC quantities and layers or mixed in a 2nd catalyst configuration. An optimal MgO quantity was first determined, which most probably corresponds to an optimal acid-base balance in the catalytic system. Indeed, such a balance is needed to perform an efficient formaldehyde and acetaldehyde aldol condensation [9]. It is noteworthy that magnesium oxide alone does not enable acrolein production. The dual catalysts study was then extended to 2 other groups of catalysts combined with the $FeMoO_x$. The first studied group of catalysts were silica-based materials (*i.e.*, Mg-Si, Ca-Si and Ba-Si) synthesized by a sol-gel method. Over those, the presence of carbonates was detected, which was expected to have a negative influence on the catalytic performances. Nevertheless, it could be observed that the silica-based materials brought an improvement of the acrolein yield (up to 7.5 points). The second tested group of catalysts was constituted of commercial oxides. The highest acrolein yield (*e.g.*, 49%) was observed for the $FeMoO_x$/MgO couple mixed with 400 mg of carborundum. This value is 11 points higher than that observed over the single

$FeMoO_x$ catalyst and 5 points higher than the results obtained with the single catalyst strategy, which is thus a quite significant improvement.

We then found that higher acrolein yields are obtained by mixing two catalysts together with doubled carborundum quantity. Such a configuration allows to avoid the negative influence of the hot spots formed because of the exothermic character of process, by homogenizing the heat distribution in the catalytic bed ("dilution" of the hot spots). These improvements are still not completely understood even if it seems that the basic character of the second catalysts have a role on them. Our trials to characterise the number and the strength of the basic sites are not completely successful, but microcalorimetry analysis is planned and perhaps could help even if some carbonates are stuck at the surface, which does not facilitate the work.

4.4.References.

[1] N. *Pernicone et al.* Journal of Catalysis 14 (1969) 293-302

[2] http://xpssimplified.com/elements/carbon.php, verified 11 July 2016

[3] *M. E. Simonsen, C. Sønderby, Z. Li et al.* Journal of Materials Science 44 (2009) 2079

[4] http://xpssimplified.com/elements/oxygen.php , verified 11 July 2016

[5] *K.N. Dalby et al.* Geochimica et Cosmochimica Acta 71 (2007) 4297-4313

[6] http://xpssimplified.com/elements/silicon.php, verified 12 July 2016

[7] *Y. Song et al.* Langumir 28(49), 2012, 16890-16899

[8] *L.H. Little*, Infrared spectra of adsorbed species, Academic Press, 1966

[9] *M. Ai*, Bulletin of the Chemical Society of Japan 64 (1991) 1346-1350

Chapter 5. Conclusions and perspectives

This work was a part of the BioMA+ project realized with the financial support of ADEME within the framework of the French governmental program of Investments for the Future. There were two main goals of the BioMA+: the production of bio-isobutene through fermentation process and its subsequent conversion to methacrolein (and methacrylic acid) and new acrolein production route starting from methanol and ethanol. This thesis concerned the second part performed using FeMo-based catalysts. The mentioned direct reaction involves two steps, namely conversion of the alcohols to their corresponding aldehydes followed by the condensation of the as-obtained aldehyde through acetalization.

To do so, two strategies were investigated. The first one was based on the direct conversion using one single FeMo catalyst and the second one was based on the use of two catalysts (*i.e.,* $FeMoO_x$ with basic materials) packed in the same reactor, the second catalyst having the purpose of boosting the acetalization reaction. The reaction conditions optimization was first performed using DoE based on experiments performed over the native FeMo catalyst. As the results, an optimal conditions set was found for each strategy (Table 5.1), which was used for further tests over catalytic systems variants.

Table 5.1. Optimal conditions according to DoE.

Factor	**Strategy 1** **One catalyst – one reactor**	**Strategy 2** **Two catalysts – one reactor**
GHSV [h^{-1}]	3900	4800
Oxygen quantity [%]	12	10.75
Temperature [°C]	320	320
MetOH/EtOH ratio	1	1.63

Temperature was the most sensitive factor while GHSV was the less sensitive one. The mathematically determined model was experimentally verified. We obtained an acrolein yield of 44% over the commercial $FeMoO_x$ catalyst when actually using the as-determined optimal set of experimental conditions, which thus confirmed the accuracy of the model (predicted yield of 50%).

The next step was the synthesis of homemade FeMo catalysts varying the Mo/Fe ratio from 1.5 to 2.5 and the calcination temperature from 350 °C to 450 °C. The highest acrolein yield (39%) was obtained for FeMo2.5 calcined at 400 °C, while the lowest one (7.5%) was observed over FeMo1.5 calcined at 350 °C. A calcination temperature lower than 400 °C is not desired as it does not enable the crystallisation of the MoO_3 and $Fe_2(MoO_4)_3$ phases, which are needed to develop a proper catalytic activity.

In the above experiments, while oxidation of the alcohols to the corresponding aldehydes was very efficient over the FeMo catalysts, the aldolization was far for being complete, with substantial residual amounts of formaldehyde and acetaldehyde in the reactor outlet streams. In order to promote acetalization of the unreacted aldehydes, we decided to modify the FeMo formulation by La and Ce addition ($1\%_{molar}$). A series of catalysts with various Fe/Mo ratios calcined at various temperatures (same variations as those described above for the basic elements-free formulations) were prepared, tested and characterized. As a results, a significant improvement in acrolein yield was actually observed. The best results were obtained for FeMoCe2.0 (42%) and FeMoLa2.5 (40.5%) both calcined at 400 °C, which are, respectively 5.5 points and 4 points higher, compared to the reference catalyst. Regarding the non-reacted acetaldehyde (i.e., 14% in the FeMoCe2.0 case) and formaldehyde (i.e., 36% in the FeMoCe2.0 case), we suppose that the higher acrolein yield is still possible (up to 14% more). Over these catalysts, La and Ce were surprisingly not detected on their surface neither by XPS nor by LEIS, but while XRF analysis confirmed their bulk incorporation. The basicity of the catalysts was subsequently checked by CO_2-TPD. While not being present at the surface of the solids, La and Ce addition led to an increase in the number of medium and strong basic sites. Further, pyridine-FTIR showed that the addition of lanthanum also induces the formation of Lewis acid sites. These results confirm that La and Ce presence increase the catalysts basicity in an indirect way, which led to improvement of the FeMo catalytic performance in the considered reaction.

Then, we performed *in situ* (catalyst pre-treatment in a separate chamber) and NAP XPS (under reactional conditions) of selected FeMo formulations. We found that the reduction of our catalysts occurs through the reduction of molybdenum species initially with an oxidation degree of +VI, through oxidation state +V and further down to +IV. It was also found that the oxidation/reduction process is almost fully reversible, which suggests a good stability of our catalysts when applied under – industrial – working conditions.

Then, after having directly modified the native FeMo formulation, we applied the second strategy consisting on adding a co-catalyst to the native FeMo catalyst selected among two groups: commercial basic oxides (MgO, CaO and BaO) and basic elements-doped silica (Mg-Si, Ca-Si and Ba-Si synthesized by a sol-gel method). Different configurations were tested (*i.e.,* mixing with $FeMoO_x$ or use of sequential layers) and the effect of SiC dilution was assessed. The best result (acrolein yield of 49%) was obtained for 20 mg of commercial MgO mixed with 180 mg of $FeMoO_x$ and 400 mg of SiC, with a 11 points improvement in the acrolein yield compared to that observed over single $FeMoO_x$. It confirms, that by adding the second, basic material, in the catalytic bed it is possible to improves the formaldehyde and acetaldehyde condensation and in consequence increase the acrolein yield.

The dual catalysts strategy showed that the chosen catalyst packing configuration has a significant influence on the acrolein yield. Generally, it was preferable to mix both catalysts with a sufficient amount of SiC. Indeed, aldol condensation is exothermic, and proper calories diffusion is needed to avoid the promotion of undesired reactions, by diluting the hot spots.

The work presented herein opens many new perspectives for further improvement of the methanol and ethanol coupling to acrolein. Concerning strategy 1 (doping of the native catalyst), FeMo catalysts are quite promising. It was found that the Mo/Fe ratio has an influence on the acrolein yield with a value preferably equal or higher than 2.0. Further, NAP XPS analysis showed that it is molybdenum which is responsible for the redox during the reaction. Therefore, in the future, solids with higher Mo/Fe ratios (*i.e.,* 3.0 – 5) should be prepared and fully characterized. In the case of modified FeMo formulations, various lanthanum and cerium quantities (notably larger quantities as low quantities already enabled substantial improvement of the performances) should be used and other elements may be considered (*e.g.,* Mg, Ca, Na...). Further, DoE could be specifically

performed on the best performing catalysts found in the present study, namely FeMoCe2.0 and FeMoLa2.5, as the experimental parameters used to test these catalysts were those found for the native formulation. Regarding the second strategy with a co-catalyst, several ways of improvements can be envisioned. First of all, the catalytic tests rig may be developed by placing the second reactor. This solution allows to use two different optimal temperatures for each of materials what could improve the second catalyst performance. Further, in the case of the silica-based catalysts, they were saturated with carbonates what prevented to measure the acido-base properities. Thus, it is planned to try another analysis method (*i.e.,* microcalormetry). Then, the synthesis procedure modification (*i.e.,* the calcinations temperatures) or other preparation methods should be used in the future (*i.e.,* impregnation). Moreover, different material should be considered (*e.g.,* aluminates).

Finally, the main perspective is the process industrialization. In Figure 5.1, a tentative flow diagram is proposed. The acrolein production process consists of three main units: reactor, adsorption and distillation. In order to improve the condensation reaction, it may be envisaged that the unreacted formaldehyde and acetaldehyde are recycled using a dedicated loop.

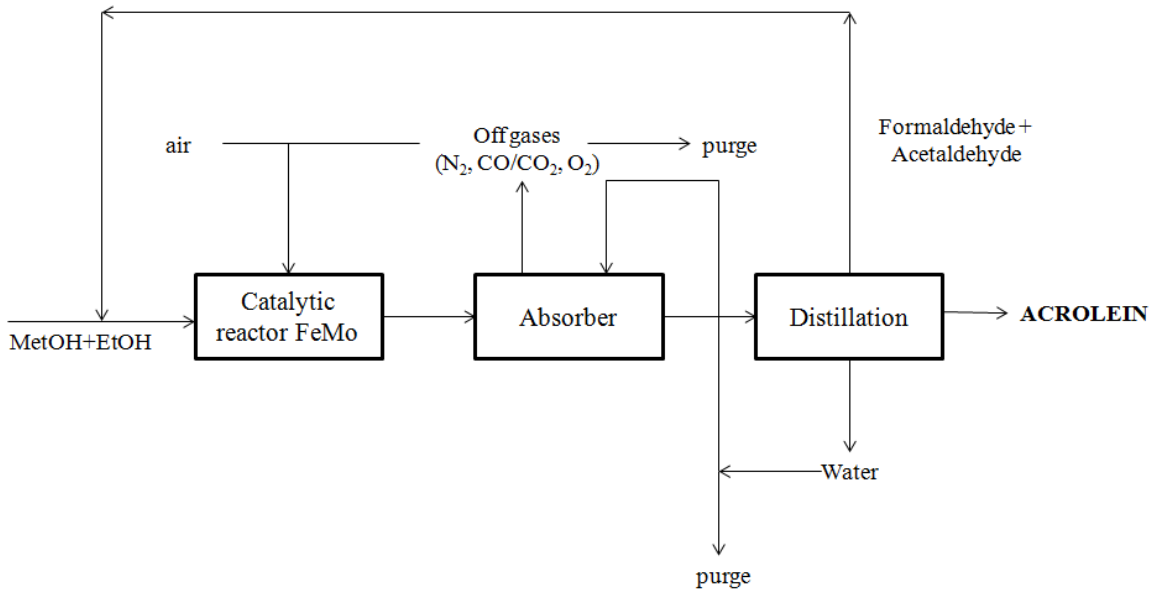

Figure 5.1. Tentative flow diagram for industrial implementation of a process of methanol and ethanol conversion to acrolein.

Annex

A. Isobutene hydration to tert-butanol.

Within the BioMA+ project, one of the main goals was to obtain methacrylic acid (MAA) from isobutene (IBN) produced by an innovative bio-process. This type of raw material contains several impurities, which are not found in the petrochemical streams: CO_2, acetone and ammonia. One of the purification method proposed is to transform IBN into t-butanol by hydration, which is a well-known process in the industry. This method brings the other advantage of facilitating the transport of the synthesized product (Figure A.1). Indeed, the liquid phase chemicals are easier to move between cooperating factories. In this section, the influence of bio-isobutene impurities on the hydration reaction is presented.

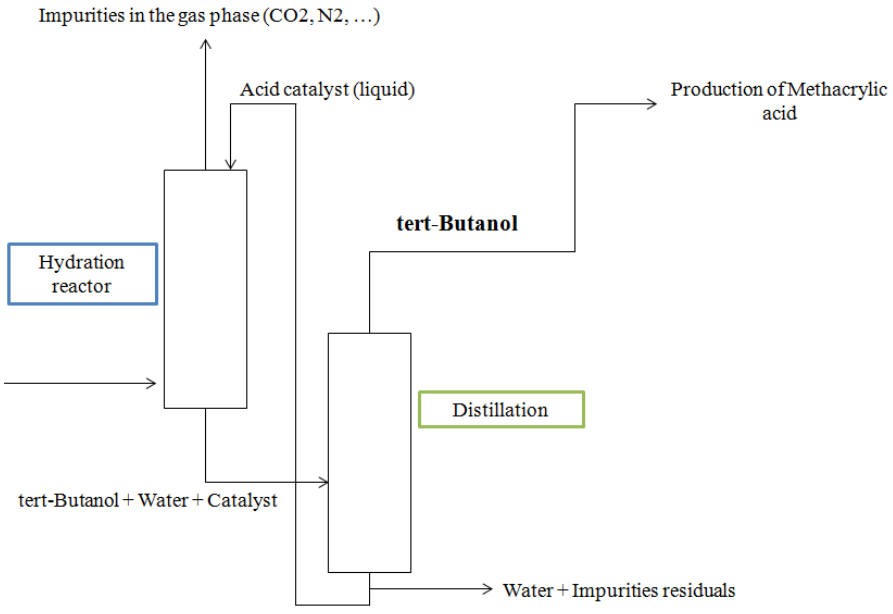

Figure A.1. IBN purification and transportation concept.

A.1. Bibliographic review.

General information

Isobutene is an alkene with four carbon atoms, which is one of the four butylene isomers. It is a colourless and highly flammable gas under standard temperature and pressure conditions. Conventionally, it is produced by petroleum refining units *via* processes such as atmospheric distillation, under vacuum, the Fluid Catalytic Cracking (FCC) and steam cracking. At the end of the production units of isobutene, the separation of the products is an important issue. Indeed, butenes (C4 alkenes) and butadienes (C4 dienes) are all present, and they are difficult to separate because of their relatively close boiling points. Separation by fractional distillation requires a fairly significant economic investment. This is why more efficient and selective physical processes, but also chemical processes are desired [1].

In the literature, three selective separation processes of isobutene from C4 are reported [2]:

- The reversible hydration of isobutene in the presence of an acid catalyst giving t-butanol as an easily separable intermediate, which can be subsequently dehydrated to pure isobutene.
- The irreversible oligomerization of isobutene in the presence of an acid catalyst, preferably giving di and tri-iso butenes.
- The irreversible polymerization of isobutene catalyzed by a Lewis acid affording poly-iso-butene.

The first method is the most effective one and thus the most common one in the industry. Therefore, a lot of studies are focused on the development/optimization of such technology.

Catalyst

Early studies have focused on the olefins hydration in general. These reactions were catalyzed by zeolites, silicates and zeolites which are modified in special way. Hereafter, we will focus only studies where the main product is tert-butanol. In the 90s, some studies have been carried out to replace Ethyl Ter Butyl Ether (ETBE) and Methyl Ter Butyl Ether (MTBE) by tertiary butanol. Micek-Ilnicka *et al.* [3,4] have worked on catalytic hydration of isobutene in order to perform then the alkylation with methanol . The tert-butanol synthesis reaction mechanism is shown in Figure A.2. Here, the chosen catalyst is $H_4SiW_{12}O_{40}$. This type of material belongs to the group heteropolyacids (HPA), which exhibit advantageous properties such as thermal stability, acidity and high oxidative capacity depending on the considered compound. The catalytic tests were performed in a continuous flow gas phase reactor using helium as a carrier gas. The operating conditions were chosen as follows: temperature between 50° and 80 °C, ratio isobutene / water between 2.1 and 8.2 and amount of catalyst between 0.2 and 0.4 g with a pretreatment at 60 °C for 15 hours under helium stream.

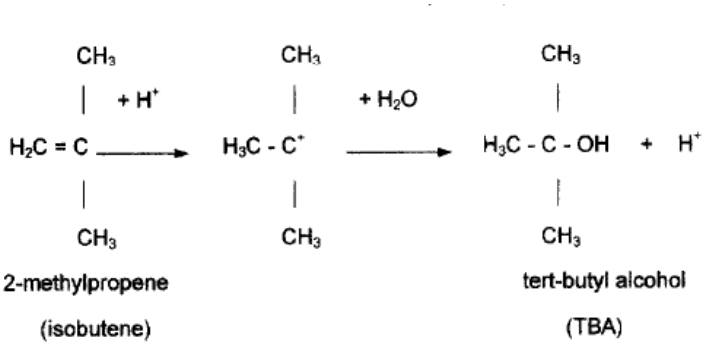

Figure A.2. Isobutene hydration mechanism over H4SiW12O40 [4].

Micek-Ilnicka *et al.* showed that an excess of IBN and a long contact time favour the secondary products formation (i.e., ethyl tert-butyl ether) what decreaseTBA selectivity. It is noteworthy that the ratio isobutene / water has no influence on the conversion, but rather on the selectivity. However, the conversion rate could not exceed 10% through reported experiments. Micek-Ilnicka [4] have worked on the water influence on ETBE favourable formation. The reaction was carried out as well in the gas phase over HPA $H_6P_2W_{18}O_{62}$ catalyst. The reaction kinetics study in the presence of water vapor showed that the isobutene partial pressure strongly affects the reaction rate. Further, Aoshima *et*

al. [5] reported studies made using a series of catalysts containing HPA of variable compositions. The main results are presented in **Table A.1**

Table A.1. IBN hydration results for different HPA catalysts (10 g IBN, 10 g but-*1*-ene, 50 g HPA, 100 g H_2O, 60 °C, 8.5 atm) [5].

Catalyst	Atomic Ratio		IBN conversion [%]	TBA Selectivity [%]
	Coordinate atom	Central atom		
12-Molybdophosphoric acid	12(Mo)	1(P)	89	100
12-Tungstophosphoric acid	12(W)	1(P)	77	100
12-Tungstosilicic acid	12(W)	1(Si)	79	100
12-Molybdosilic acid	12(Mo)	1(Si)	63	100
12-Tungstoboric acid	12(W)	1(B)	31	100
12-Tungstoarsenic acid	12(W)	1(As)	43	100
6-Molybdo-6-tungstophosphoric acid	[6(M)+6(W)]	1(P)	86	100
11-Molybdo-1-vanadophosphoric acid	[11(Mo)+1(V)]	1(P)	81	100

The selectivity to tert-butanol was 100% over all the HPA catalysts.

According to the literature review, we then decided to performed the reaction in the liquid phase over commercial $H_3PW_{12}O_{40}$.

A.2. Micro-test presentation.

Based on the above described bibliographic review, we built a set-up for the liquid-phase hydration of isobutene (IBN) under atmospheric pressure. The reactor (Figure A.3B) was made in glass and equipped with a propeller for stirring. Before each run, the HPA catalyst was dissolved in distilled water. In this system, the temperature was controlled by heating oil circulating in the mantle. The inlet mixture contained 10% IBN and 90% Helium introduced in the reactor with a gas distributor. The liquid reaction products were analysed by HPLC (liquid phase, determination of TBA quantity) Agilent 1200 equipped with a column REZEK ROA-Organic Acid H+ (300 x 7.8 mm) and a reflective index detector (RID). A H_2SO_4 (0.0024 M) solution was chosen as an eluent. The gas phase was controlled with online micro-GC (gas phase, determination of IBN conversion and formed CO_2 quantity) SRA3000 equipped with two columns – plot U and molecular

sieves and two TCD detectors. The schematic illustration of the prepared semi-batch system is presented inFigure A.3A.

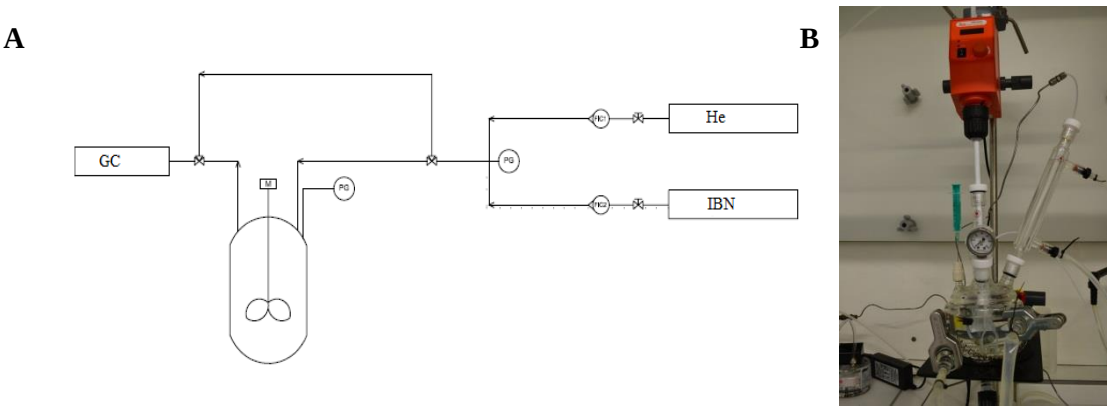

Figure A.3. A: Schematic diagram of the catalytic test rig built for IBN hydration to TBA; B: Photograph of the glass reactor used for the catalytic tests.

A.3. Preliminary studies.

During each run, two parameters were followed: *t*-butanol quantity measured by HPLC and *iso*butene conversion measured by micro gas chromatograph. The example of obtained data is presented at Figure A.4. In order to perform the studies of impurities influence, the catalytic system needs to be optimized. Three main factors are taken into account: temperature, stirrer speed and HPA concentration.

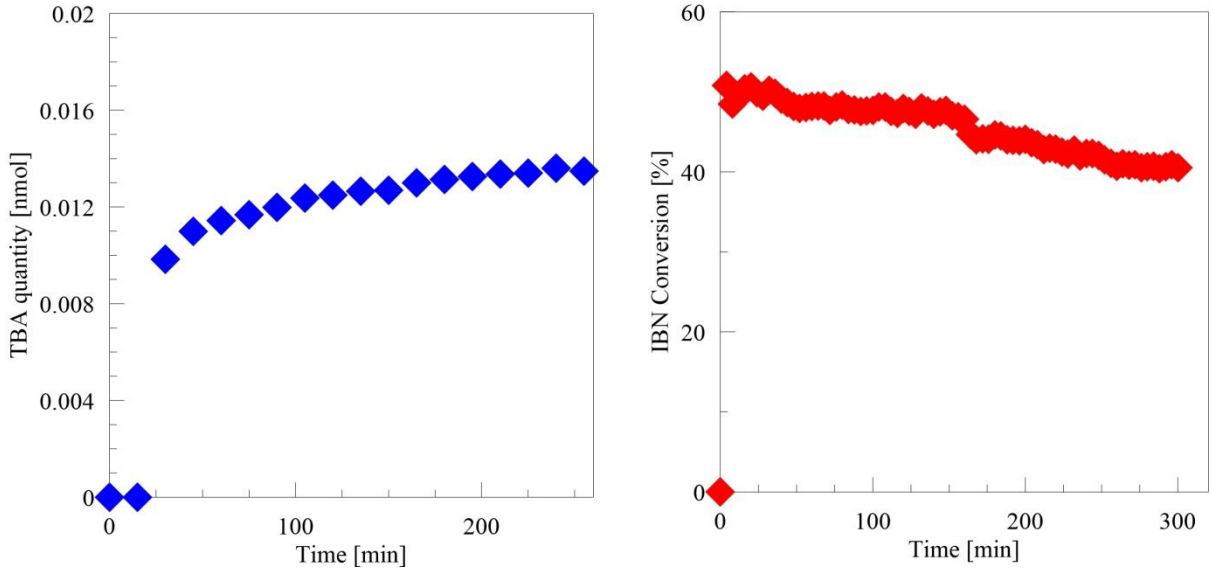

Figure A.4. Example data obtained during a run (32 wt.%HPA, 85°C, 320 rpm).

First, the influence of temperature and agitation speed was examined. During these tests, HPA concentration was fixed at 25 wt.% The obtained results are presented in Figure A.5A temperature increase caused an increase in IBN conversion and we accordingly chose to work at 85 °C, which is the TBA boiling point [6] Afterwards, we checked about the influence of the agitation speed (Figure A.5B). Here, we observe that the curve reaches the plateau at 320 rpm. This point reflects the moment when the gas-liquid transfer rate limit disappear and the process occurs only in chemical regime. That is why this agitation speed was chosen in following studies.

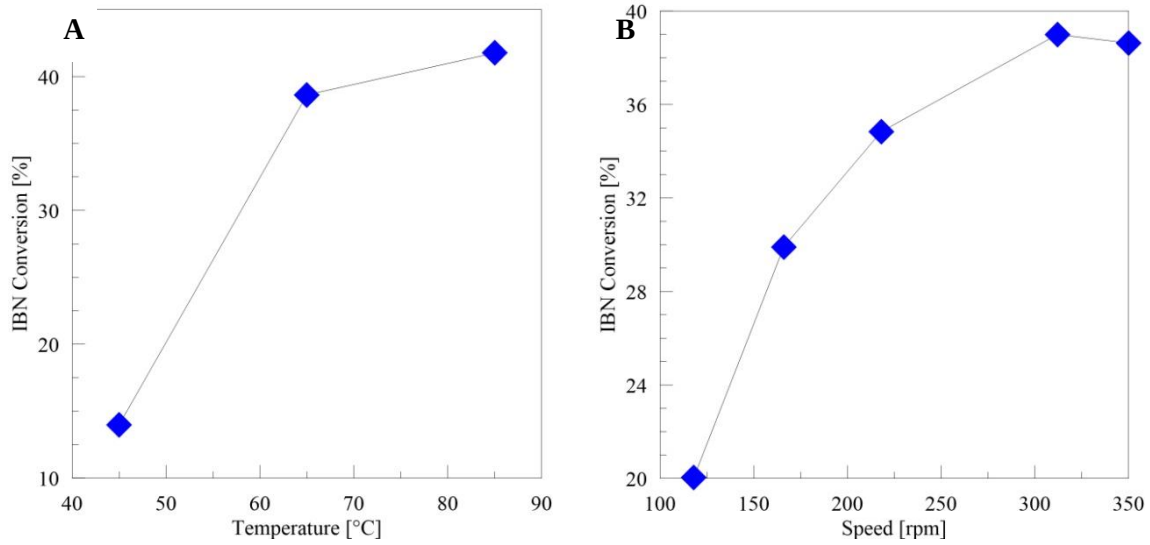

Figure A.5. A: Temperature influence on IBN conversion (25 wt.%HPA, 320 rpm) ; B: Agitation speed influence on IBN conversion (25 wt.%HPA, 65 °C).

The next factor we examined was the HPA concentration (Figure A.6). Three different catalyst quantities were used: 10 wt.%, 25 wt.% and 32 wt.%. The highest value was fixed by the solubility limit of the HPA experimentally verified (à 85 °C). It can be observed that, when increasing the catalyst concentration, the IBN conversion increases. This phenomenon was followed with pH measurement which shows a constant value from 15%$_{mass}$. Comparing to the catalytic results for 10%mass HPA, it can be concluded that for the isobutene hydration performance a defined pH is necessary. Thus, it was decided to use 32% concentration for following studies.

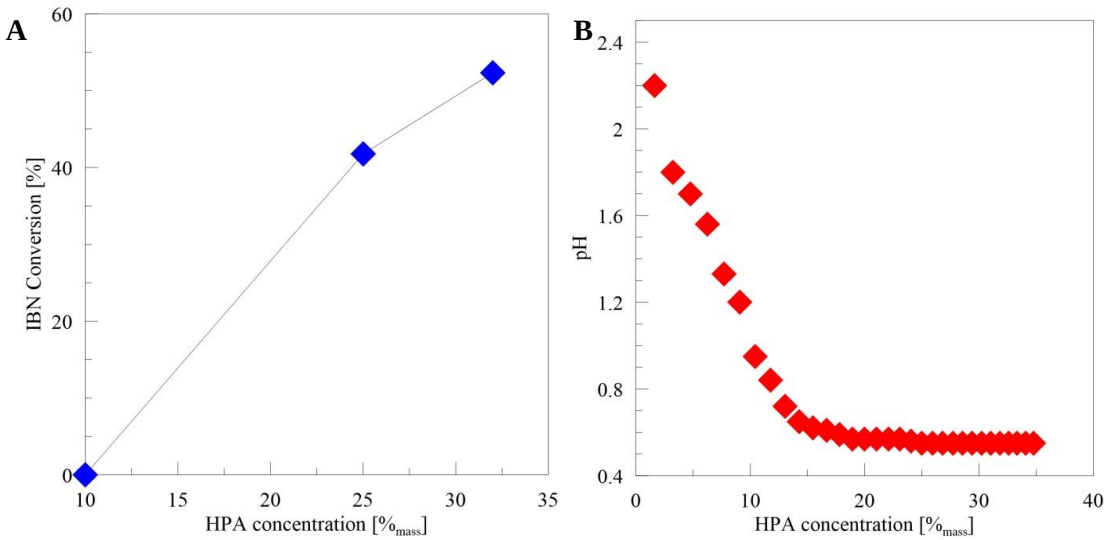

Figure A.6. A: HPA concentration influence on IBN conversion; B: HPA concentration influence on pH (320rpm, 85°C, 1h).

A.4. Bio-*iso*butene impurities influence.

The impurities effect (*e.g.*, CO_2, acetone and ammonia) was verified in following conditions chosen below:

- HPA concentration: 32%;
- Temperature: 85 °C;
- Agitation speed: 320 rpm.

The carbon dioxide influence was measured by changing the pure helium bottle with the 5%CO_2/95%He mixture. During the first 2 hours of reaction, no effect on the IBN conversion was detected and we considered that the carbon dioxide presence does not affect the considered reaction Due to CO2 dissolution in water and acid formation, the reactional mixture pH stays acid which is necessary for IBN hydration.

Afterwards, acetone was added in the reactional system at the concentration of 0.25 mol/L. Similarly, the presence of this molecule did not influence the IBN conversion. It should nevertheless be noted that the addition of acetone in the liquid medium creates acetone vapors in the gas phase *via* a stripping effect what can have a negative effect on experimental setup.

At last, the effect of NH_3 was studied. Firstly, its influence on the reactional mixture pH was checked. The obtained results are reported in Figure A.7B. This curve has two strokes: the first refers to the neutralization of HPA protons and the second corresponds to

the HPA degradation, which occurs in a basic environment to give WO_4^{2-} and PO_4^{3-} according to the following reaction (Eq.A.1):

$$PW_{12}O_{40}^{3-} + 24\ OH^- = PO_4^{3-} + 12\ WO_4^{2-} + 12\ H_2O \qquad (A.1)$$

It is noteworthy that the NH_3 addition induced a reactional mixture color change from transparent to intense white. This phenomenon usually reflects the HPA precipitation *via* a partial catalyst's protons replacement by NH_4^+ species. Afterwards, the evolution of IBN conversion was measured for different added quantities of ammonia (Figure A.7A). It can be remarked that the NH_3 presence had, as expected, a rapid effect on the reaction efficiency. The *iso*butene conversion reached 0% when the NH_3/HPA ratio reached 1.35. The ratio corresponds to a pH value of 2.5 which seems to be too low to perform isobutene conversion into tert-butanol.

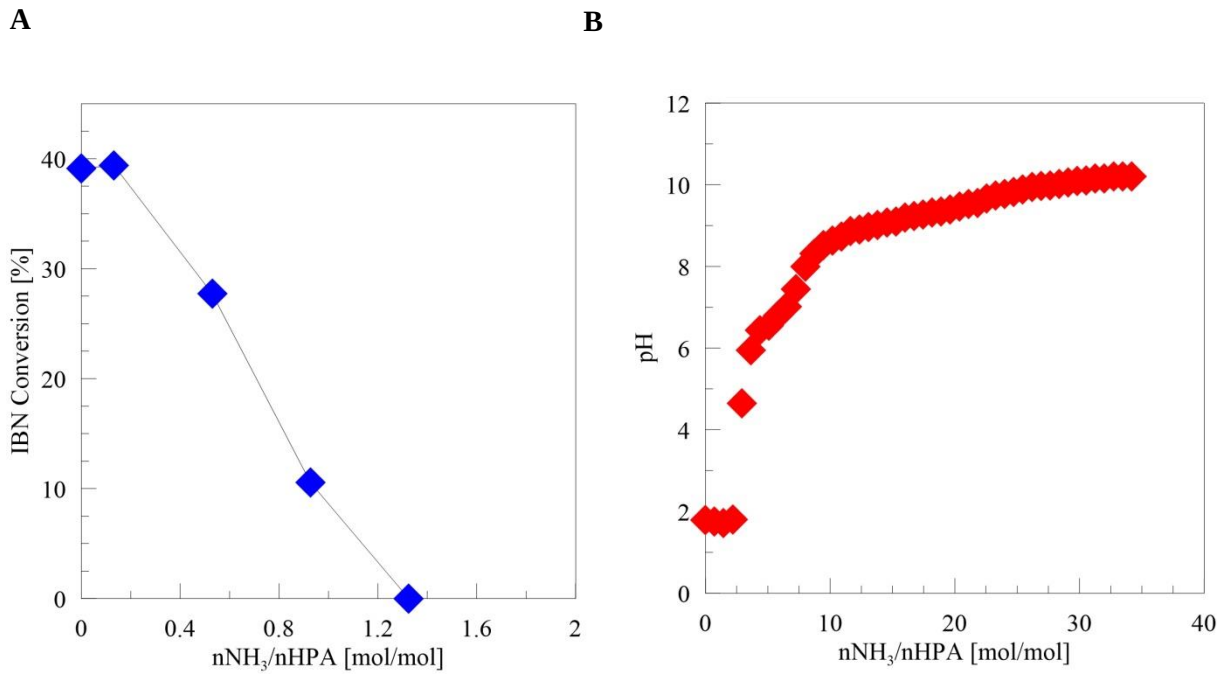

Figure A.7. A: NH3 addition influence on IBN conversion; B: NH3 addition influence on the pH (32 wt.%HPA, 320 rpm, 85 °C).

A.5. Conclusion.

Based on the data presented above, it can be concluded that carbon dioxide and acetone had not any influence on the *iso*butene hydration conversion. However, the NH_3 presence adversely affected the considered reaction efficiency. The IBN conversion diminution is observed after the the addition of 0.03 mol of NH_3, which means that the ammonia effect

on real streams will be limited. That is why, in the industrial scale the catalyst reacidification with the recycle can be proposed as solution.

A.6.References.

[1] *B. N. M. Leeuwen, A. M. Wulp, I. Duijnstee, A. J. A. Maris, and A. J. J. Straathof Applied Microbiology and Biotechnology*, vol. 93, no. 4 (2012) 1377.

[2] *H.-J. A. Klaus Weissermel Química orgánica industrial*. ed. Reverte (1981) 68–70.

[3] *Pozniczek, AA. Malecka-Lubanska, A. Micek-Ilnicka, A. Bielanski* Applied Catalysis A : General, 176 (1999) 101.

[4] A. *Micek-Ilnicka* Journal of Molecular Catalysis A: Chemical , 308 (2007) 252.

[5] *Aoshima et al.*, United States Patent, 4,236,034, Nov. 25, 1980.

[6] https://pubchem.ncbi.nlm.nih.gov/compound/tert-Butanol, verified 24 October 2016

B. TGA-DSC results for modified FeMo catalysts

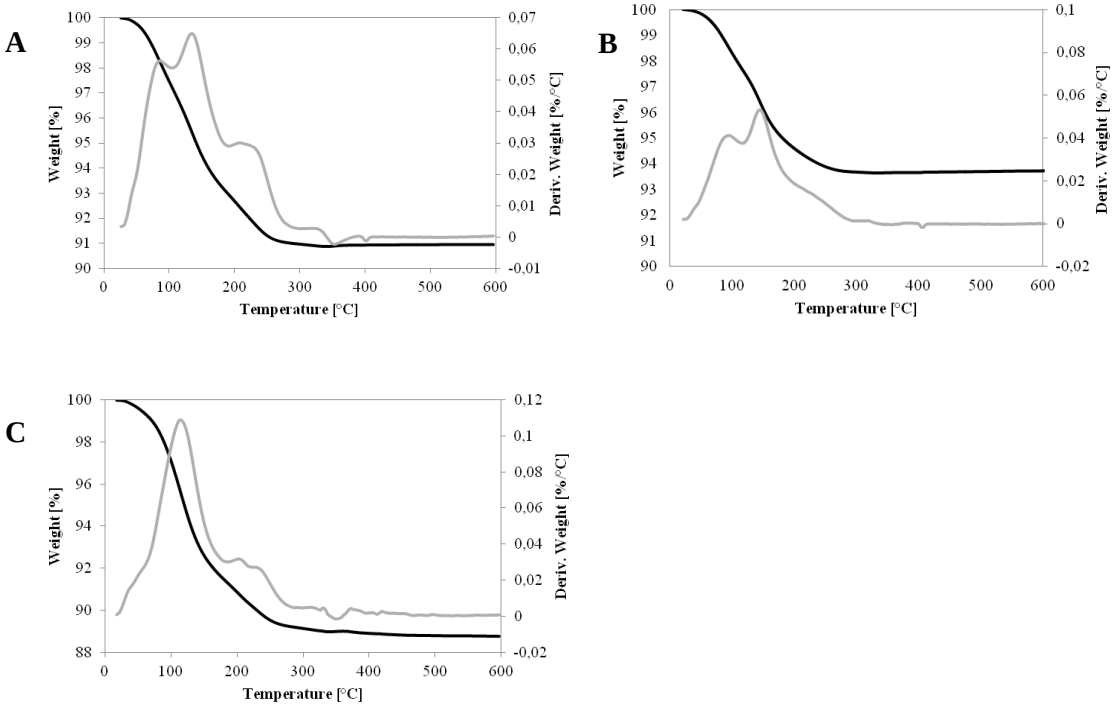

Figure B.1. TG(black) and DTG(grey) curves for A: FeMoCe1.5, B: FeMoCe2.0, C: FeMoCe2.5. The analysis was performed in the temperature range 20-600 °C with heating rate of 10 °C/min under air flow.

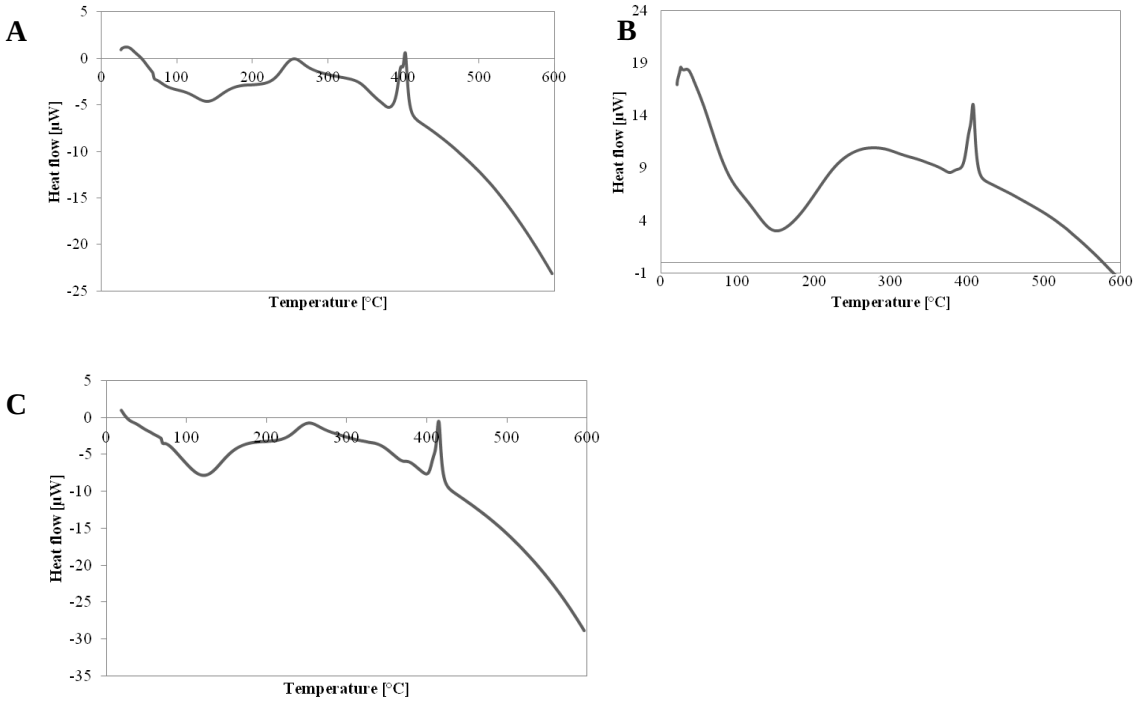

Figure B.2. DSC curves for A: FeMoCe1.5, B: FeMoCe2.0, C: FeMoCe2.5. The analysis was performed in the temperature range 20-600 °C with a heating rate of 10 °C/min under air flow.

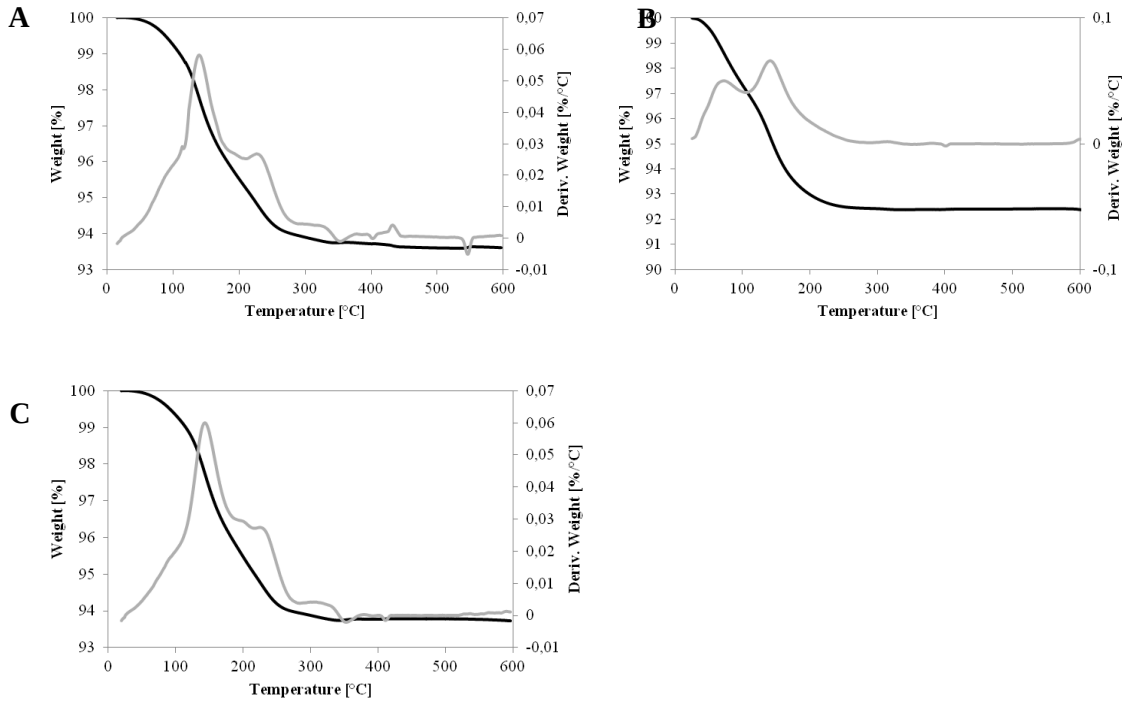

Figure B.3. TG(black) and DTG(grey) curves for A: FeMoLa1.5, B: FeMoLa2.0, C: FeMoLa2.5. The analysis was performed in the temperature range 20-600 °C with heating rate of 10 °C/min under air flow.

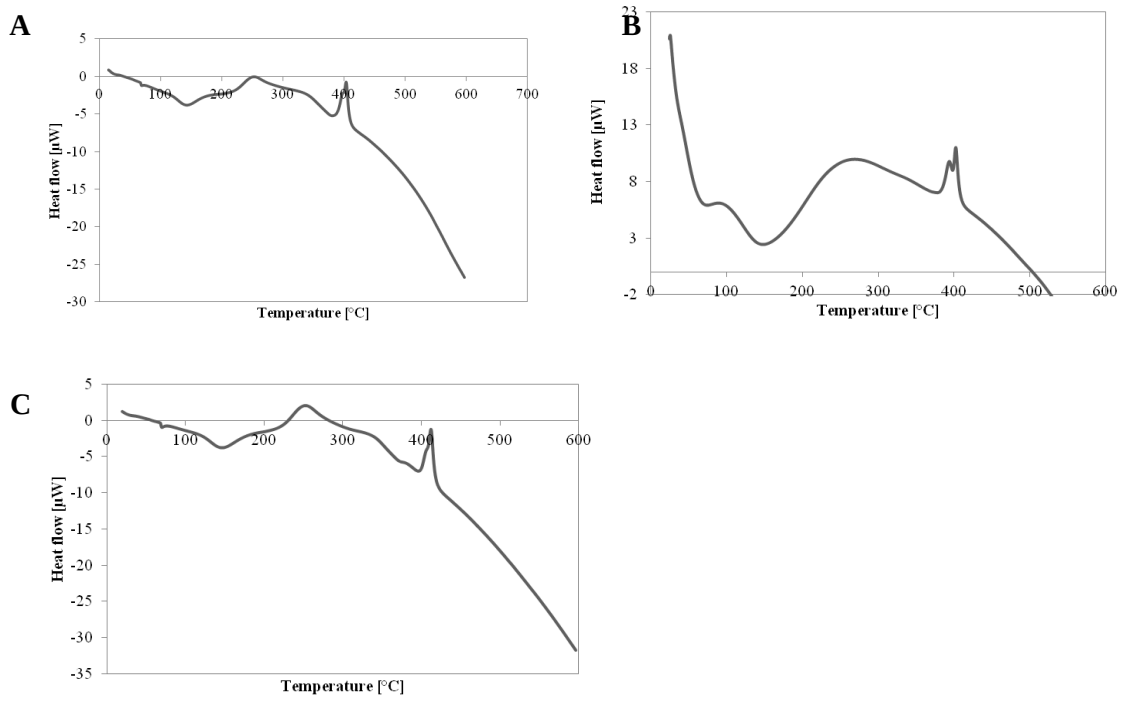

Figure B.4. DSC curves for A: FeMoLa1.5, B: FeMoLa2.0, C: FeMoLa2.5. The analysis was performed in the temperature range 20-600 °C with a heating rate of 10 °C/min under air flow.

C. XRD-HT results for FeMo catalysts.

A

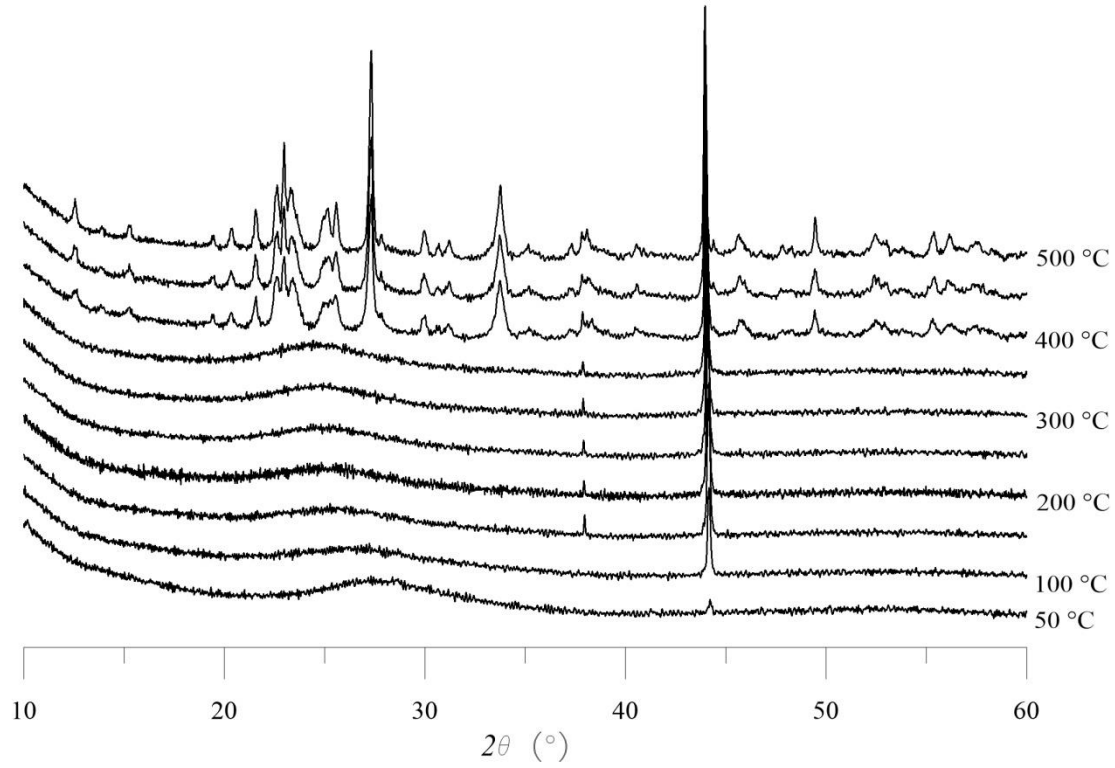

B

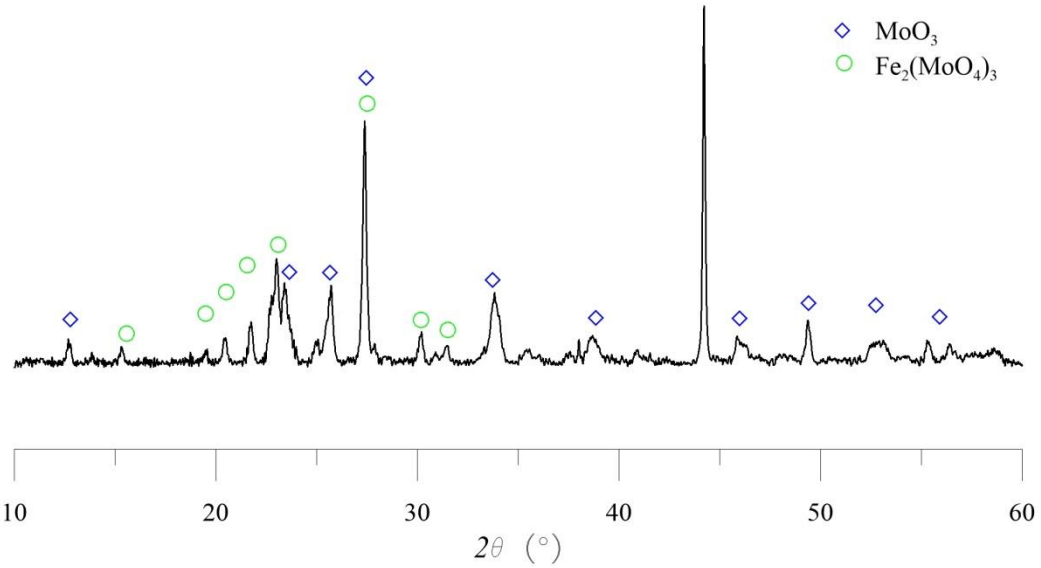

Figure C.1. A: XRD-HT diffractograms for FeMo1.5; B: XRD patterns at room temperature with phases matching for FeMo1.5.

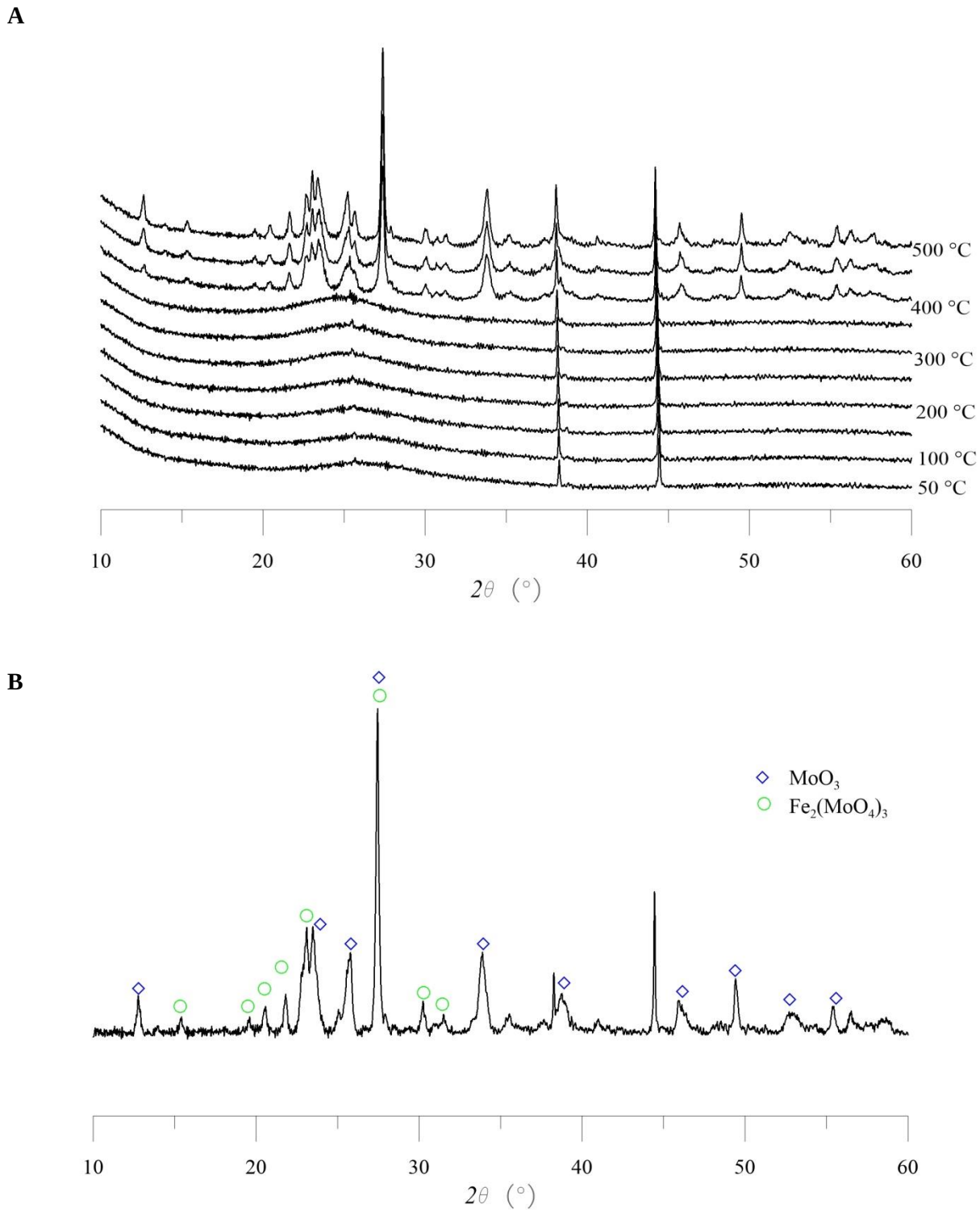

Figure C.2. A: XRD-HT diffractograms for FeMo2.5; B: XRD patterns at room temperature with phases matching for FeMo2.5.

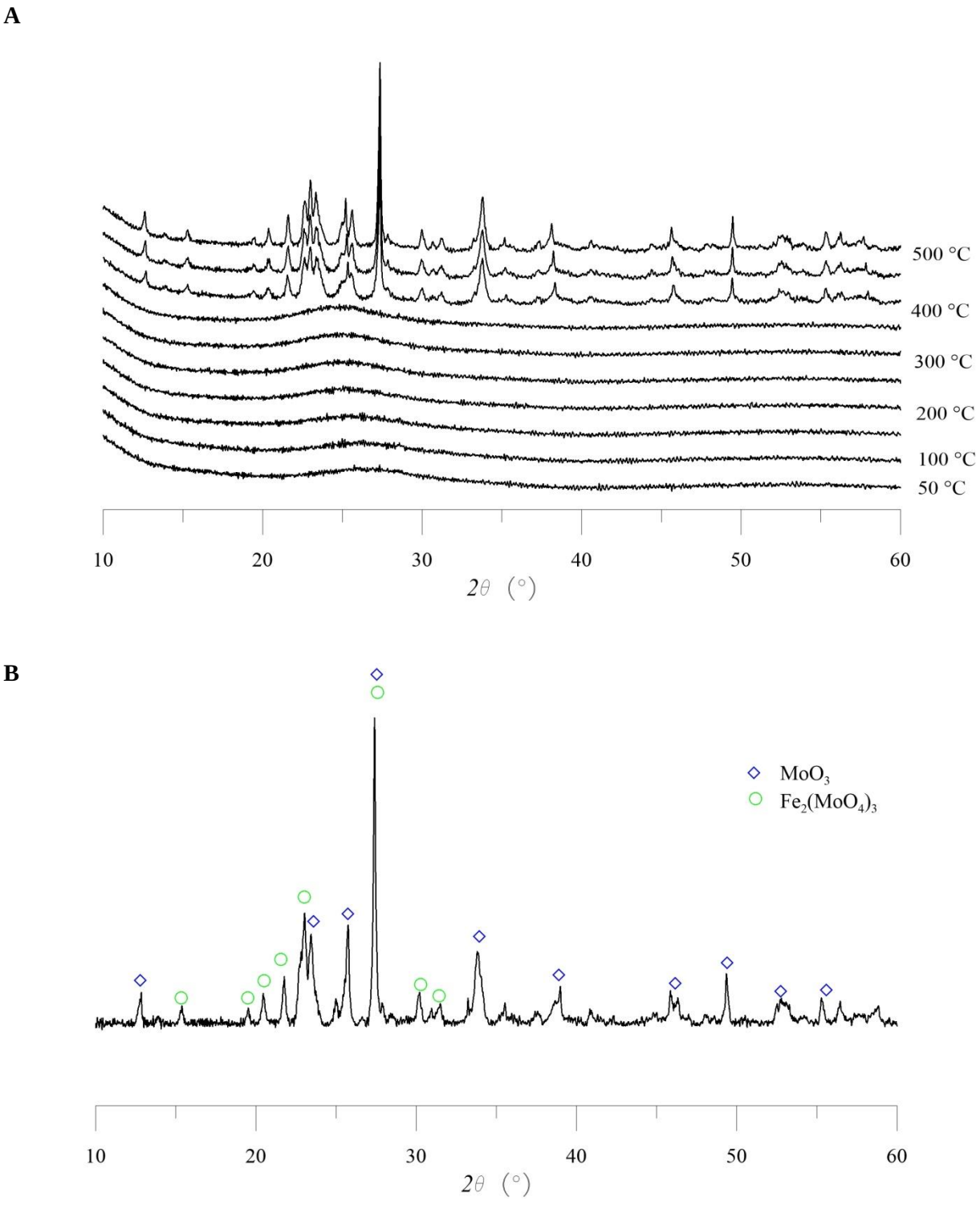

Figure C.3. A: XRD-HT diffractograms for FeMoLa2.0; B: XRD patterns at room temperature with phases matching for FeMoLa2.0.

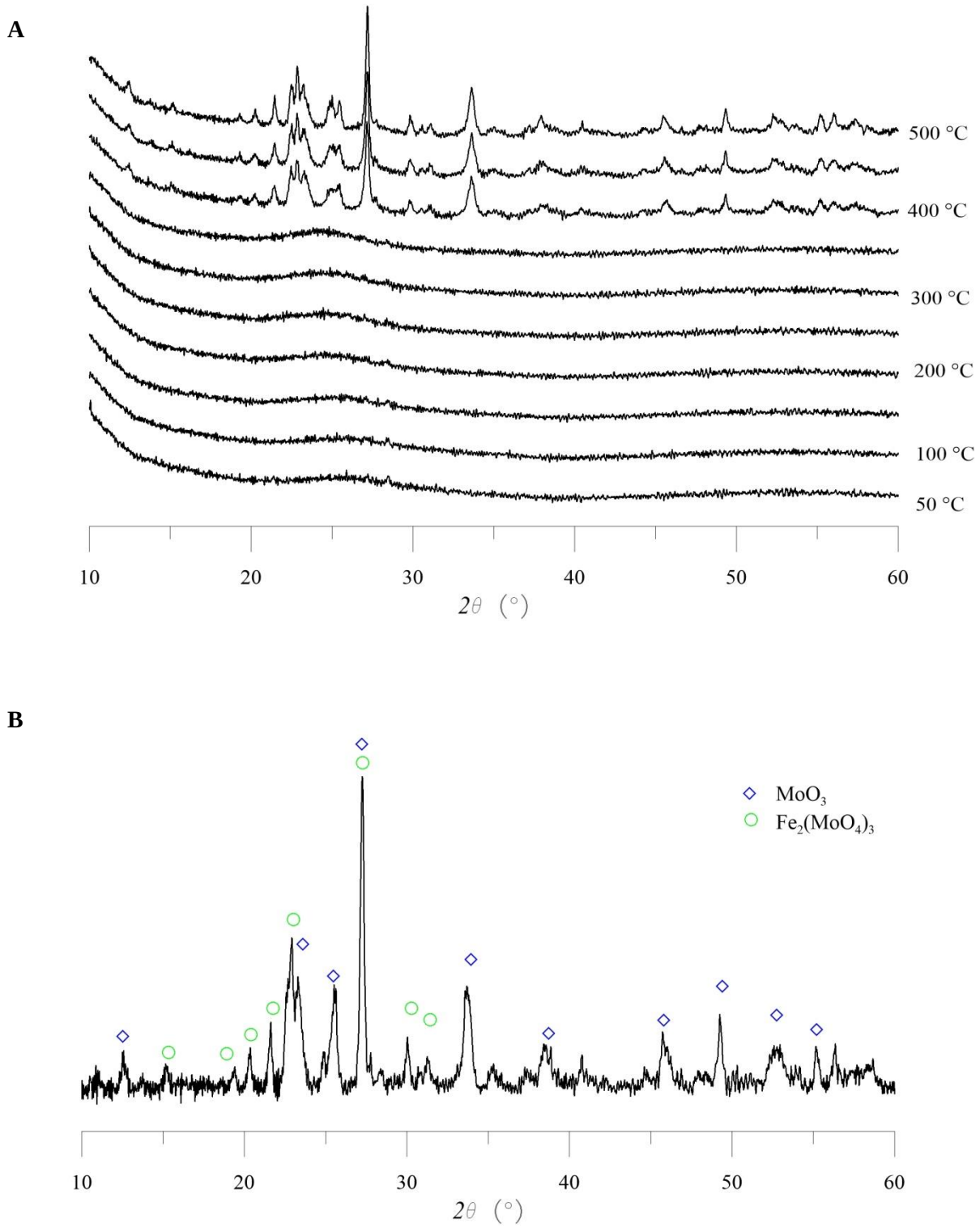

Figure C.4. A: XRD-HT diffractograms for FeMoCe2.0; B: XRD patterns at room temperature with phases matching for FeMoCe2.0.

D. Quasi *in situ* XPS results for FeMo catalysts.

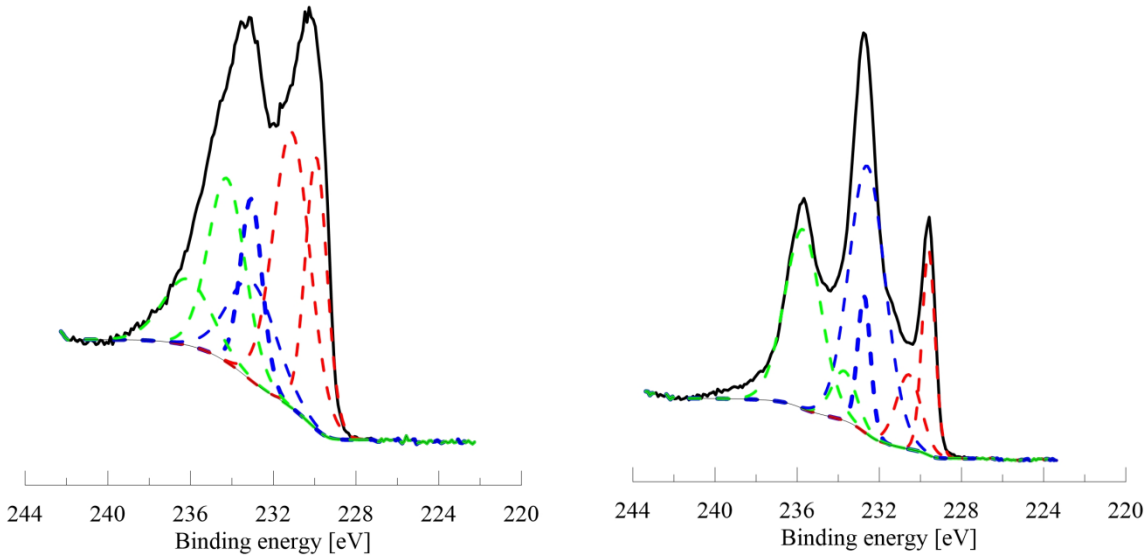

Figure D.1. FeMo1.5 calcined at 350 °C quasi in situ XPS results (320°C, MetOH/EtOH = 1, Alcohols = 13.2%, O_2 = 12%). A: under He + MetOH/EtOH flow; B: under He + MetOH/EtOH + O_2 flow.

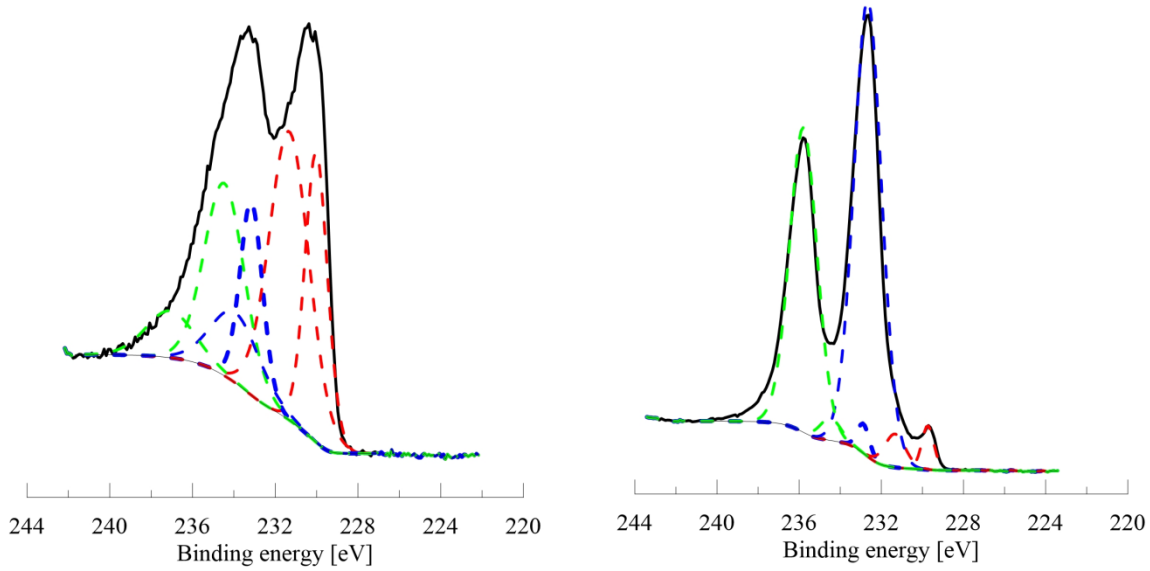

Figure D.2. FeMoCe2.0 calcined at 400 °C quasi in situ XPS results (320°C, MetOH/EtOH = 1, Alcohols = 13.2%, O_2 = 12%). A: under He + MetOH/EtOH flow; B: under He + MetOH/EtOH + O_2 flow.